Statens vegvesen

Norwegian Public Roads Administration

Compilation of 5 papers on (1) Electrical resistivity as a durability indicator and (2) Cracking tendency in hardening concrete

REPORT | Technology Department | No. 2482

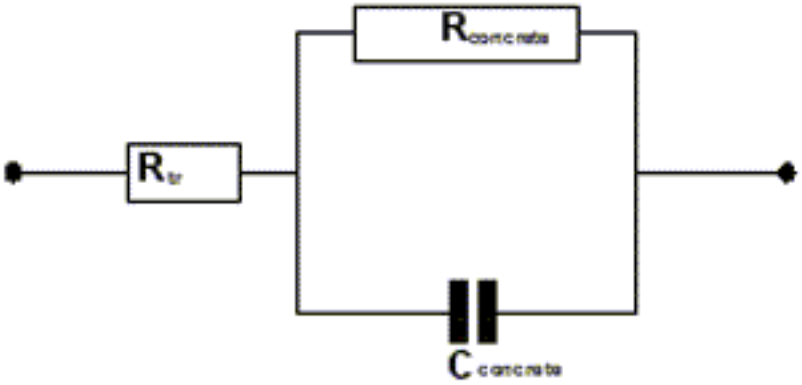

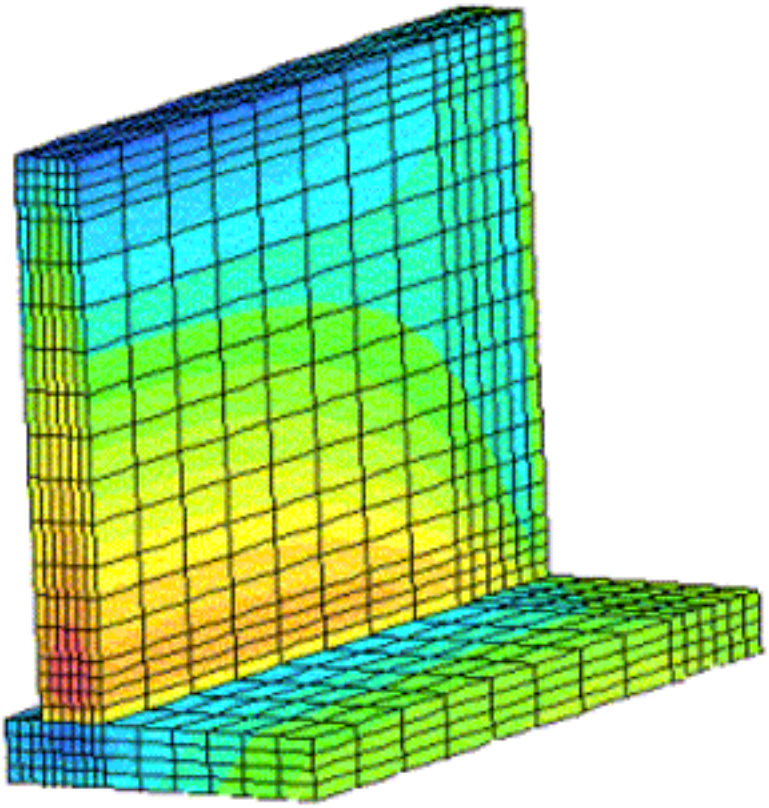

Date: 2007-02-08

Statens vegvesen

Norwegian Public Roads Administration
Directorate of Public Roads
Technology Department

Address: P.O.Box 8142 Dep
N-0033 Oslo
Telephone: +47 915 02030

www.vegvesen.no

TECHNOLOGY REPORT 2482

Title

Compilation of 5 papers on (1) Electrical resistivity as a durability indicator and (2) Cracking tendency in hardening concrete

Authors

Claus K. Larsen, Jan-Magnus Østvik, Øyvind Bjøntegaard

Date:	Executive officer	Project no.
2007-02-08	Ø.Bjøntegaard, J-M. Østvik, C.K. Larsen	
	Reviewed by	Number of pages
	Kjersti Kvalheim Dunham	67

Summary

The report contains 5 papers that were presented at the 2nd Int. symposium on Advances in Concrete through Science and Engineering 11-13 Sept. 2006, Quebec City, Canada (printed in the symposium proceedings RILEM PRO 51, ISBN 2-35158-003-06, Ed. by J.Marchand and B.Bissonnette). The first three papers deal with electrical resistivity as a durability parameter for concrete, while the two last papers deal with cracking tendency of hardening concrete.

Electrical resistivity (Paper 1-3): The parameter is very important as a durability indicator since high resistivity is beneficial as it means slow corrosion. Electrical resistivity (ER) has been studied with regard to electrical frequency range, concrete degree of saturation (DS), -temperature, -aging effect and -composition. The total investigation include lab. tests on lab.-made specimens and on field cores, as well as field measurements on long term sea exposed concrete elements using both automatic and manual monitoring systems. The ER (lab.and field tests) of water and atmospherically stored high performance concretes (HPC) increased clearly over time (years) due to aging effects, while sea water exposure (field cores) did not display any clear increase. In the latter condition the positive aging effect is believed to be counteracted by the intrusion of chlorides (more ions - lower ER). For water stored HPC even a small decrease in DS clearly increased the ER (indicating early discontinuity of the capillary water), while for traditional bridge concrete with higher w/b the resistivity was not so affected by DS. In the field measurements, over years, on sea exposed elements a beneficial aging effect was seen. The ER increases, not surprisingly, with concrete quality (especially for w/b-ratios below around 0.40); in the field tests this was particularly the case after longer times. Very high ER values were found for the concretes with fly-ash (both lab. and field), especially at longer times.

Cracking tendency in hardening concrete (Paper 4-5): Thermal (TD)- and autogenous (AD) deformations are the primary causes of self-induced stresses in hardening concrete structures subjected to restraint conditions. Much attention has been paid to AD during the last 10-15 years. This is seen, for instance, as the many conferences devoted exclusively to AD-aspects. In general, except for super HPC (w/b-ratios below 0.3), it appears that TD is greater than AD and it is therefore surprising that little attention has been paid to the coefficient of thermal expansion (CTE) in recent literature. Paper 4 presents an experimental strategy on how to separate TD and AD in tests and discusses the mechanisms behind the strong moisture dependence of the CTE. Paper 5 shows experimental results from a study on the effect of fly-ash (FA) on crack sensitivity. The given test series shows a beneficial effect of FA when an efficiency factor (k) of 1.0 is used for FA in the effective w/b-ratio calculation. The standards prescribes k=0.4 for FA added during mixing and k=1.0 when FA is part of a certified cement. The paper discusses this issue.

Key words

Concrete durability, electrical resistivity, laboratory tests, field measurements, hardening concrete, cracking tendency, fly-ash, slag

Summary

The report contains 5 papers that were presented at the 2nd Int. symposium on *Advances in Concrete through Science and Engineering* 11-13 Sept. 2006, Quebec City, Canada (printed in the symposium proceedings RILEM PRO 51, ISBN 2-35158-003-06, Ed. by J.Marchand and B.Bissonnette). The first three papers deal with electrical resistivity as a durability parameter for concrete, while the two last papers deal with cracking tendency of hardening concrete.

Electrical resistivity (Paper 1-3): The parameter is very important as a durability indicator since high resistivity is beneficial as it means slow corrosion. Electrical resistivity (ER) has been studied with regard to electrical frequency range, concrete degree of saturation (DS), -temperature, -aging effect and -composition. The total investigation include lab. tests on lab.-made specimens and on field cores, as well as field measurements on long term sea exposed concrete elements using both automatic and manual monitoring systems. The ER (lab.and field tests) of water and atmospherically stored high performance concretes (HPC) increased clearly over time (years) due to aging effects, while sea water exposure (field cores) did not display any clear increase. In the latter condition the positive aging effect is believed to be counteracted by the intrusion of chlorides (more ions – lower ER). For water stored HPC even a small decrease in DS clearly increased the ER (indicating early discontinuity of the capillary water), while for traditional bridge concrete with higher w/b the resistivity was not so affected by DS. In the field measurements, over years, on sea exposed elements a beneficial aging effect was seen. The ER increases, not surprisingly, with concrete quality (especially for w/b-ratios below around 0.40); in the field tests this was particularly the case after longer times. Very high ER values were found for the concretes with fly-ash (both lab. and field), especially at longer times.

Cracking tendency in hardening concrete (Paper 4-5): Thermal (TD)- and autogenous (AD) deformations are the primary causes of self-induced stresses in hardening concrete structures subjected to restraint conditions. Much attention has been paid to AD during the last 10-15 years. This is seen, for instance, as the many conferences devoted exclusively to AD-aspects. In general, except for super HPC (w/b-ratios below 0.3), it appears that TD is greater than AD and it is therefore surprising that little attention has been paid to the coefficient of thermal expansion (CTE) in recent literature. Paper 4 presents an experimental strategy on how to separate TD and AD in tests and discusses the mechanisms behind the strong moisture dependence of the CTE. Paper 5 discusses concrete proportioning with fly-ash (FA) and blast furnace slag (BFS) and shows experimental results from a FA-study. The given test series shows a beneficial effect of adding FA with regard to early crack sensitivity, but it is notable that, according to EN 206-1, the FA concrete should have been made with a w/b-ratio of 0.34 to be in the same “durability class” as the reference (the efficiency factor for FA is 0.4). Using w/b of 0.34 instead of 0.40 would likely be a less favourable situation for the FA-concrete. Consequently, the use of a certified CEM II (or CEM III for slag) cement is likely to be more beneficial to than adding FA (or BFS) directly during mixing since the efficiency factor is 1.0 for cements (w/b = 0.40 could then be used).

Sammendrag

Paper 1

Spesifikk elektrisk motstand i betong – Del I: Effekt av målefrekvens ved ulike fukt- og temperaturforhold

Spesifikk elektrisk motstand er en av de beste tilgjengelige metoder for å kunne vurdere en betongkonstruksjons levetid med tanke på armeringskorrosjon. Litteraturen viser at spesifikk elektrisk motstand varierer sterkt, i noen tilfeller flere ordensgrader. Fuktinnhold (betongens vannmetningsgrad), temperatur, sementinnhold og porevannskjemi samt ytre påvirkning (klorider etc.) er parametere som innvirker på betongens spesifikke elektriske motstand. Av disse er i særstilling fuktinnhold viktigst, og overskygger i mange tilfeller effekten av andre parametere. Temperatur er også sentral fordi den umiddelbart endrer betongens ledningsevne, og i tillegg fører til en redistribusjon mellom vannfasene i betongen (kapillært vann og gelvann).

Med utgangspunkt i dette ble det gjennomført en studie der målinger av spesifikk elektrisk motstand ble utført med Elektrokjemisk Impedans Spektroskopi (EIS) i frekvensområdet 100Hz til 40 MHz som referansemetode, og sammenlignet med andre AC (Alternerende strøm) målemetoder. Målingene ble utført på betongprismer med varierende fuktinnhold (kondisjonerte prøver) utsatt for varierende temperatur fra 20 °C ned til -28 °C.

Resultatene viser at målinger av spesifikk elektrisk i betong avhenger av målefrekvensen som benyttes. Hvor stor denne frekvensavhengigheten er henger sammen med både temperatur og fuktinnholdet i betongen. Størst variasjon fra reell DC (direkte strøm) ledningsevne får man ved lave temperaturer i kombinasjon med lavt fuktinnhold. Da ville en lav målefrekvens være optimalt. Ved høyere temperaturer og høye fuktinnhold er tendensen motsatt der en høyere målefrekvens er optimal, men her er variasjonene mye mindre. Innenfor det relevante frekvensintervallet, 100 Hz og 10 kHz, er variasjonene små ved høye fuktinnhold, og en 5 % variasjon dekker hele intervallet. Ved lave temperaturer og fuktinnhold kan variasjonen innenfor frekvensintervallet bli så stor som 30 %. Likevel er det grunn til å anta at i normalt Nordisk kystklima vil en målefrekvens mellom 100 Hz og 10 kHz representere den reelle spesifikke elektriske motstanden for våre betonger med tifresstillende nøyaktighet.

Paper 2

Spesifikk elektrisk motstand i betong – Del II: Effekt av fuktinnhold og temperatur

Spesifikk elektrisk motstand (resistivitet) varierer, som vist i Paper 1, i meget stor grad som funksjon av betongens fuktinnhold og temperatur. Dersom man skal kunne bruke resistivitet som en parameter eller egenskap for å vurdere risiko for eller hastighet av armeringskorrosjon, må en vite i detalj hvordan denne er påvirket av bl.a. fuktinnhold og temperatur.

Betonger med høy kvalitet (8 betonger), men varierende sammensetning, og referanse-betonger med høyt masseforhold uten silika (2 betonger) ble undersøkt i laboratoriet. En god del av resultatene er fra Masteroppgaven ved NTNU til Fritjof Askeland. Betongene er dels fra J-M.Østviks dr.grads arbeid (2 betonger – en høy- og en lavkvalitet) og dels fra Statens vegvesens prosjekt ”Utvikling av kloridbestandig betong” (8 betonger, inkl. 1 referansebetong tilsvarende brubetong før Pk2 i 1988). Disse 8 betongene har vært gjenstand for resistivitetsundersøkelser over en periode på 12 år, og gir således et godt grunnlag for å kunne si noen om en tidsutvikling.

Det ble laget skiver med tykkelse 20mm av betongene, og disse skivene ble så kondisjonert til samme fuktinnhold (vannmetningsgrad, DS) og deretter forseglet. Deretter ble

skivene utsatt for ulike temperaturer over en tidsperiode slik at (kvasi)likevekt kunne etableres, og resistiviteten ble så målt. For å kunne sammenligne resistivitetene ved ulike temperaturer og fuktinnhold, ble alle resistiviteter omregnet til resistivitet ved 10 °C ved hjelp av Arrhenius-ligningen med en aktiveringskonstant på 3000 K.

Resultatene viser at resistiviteten øker for alle betonger unntatt betonger med høy dosering av silika, der en faktisk kan få en reduksjon i resistivitet over tid. Betong med flyvaske er i en særstilling når det gjelder høye resistiviteter over tid. Betongs resistivitet øker markant ved kun en liten reduksjon i DS fra vannmettet tilstand (DS=100%) ned til 95%. Dette betyr at målinger av resistivitet på vannlagrede betonger ikke har relevans med tanke på korrosjonsvurdering for feltbetonger, som har en vannmetningsgrad på 80-90%. Temperaturavhengigheten til betongs resistivitet i området 1,5-40 °C kan karakteriseres ved Arrhenius-ligningen med en aktiveringskonstant på 3000-3500K (tilsvarer en aktiveringsenergi på ca 25-29 kJ/mol).

Paper 3

Spesifikk elektrisk motstand i betong – Del III: Langtidsmålinger på felteksponert betong i tidevannssonen

Det er utført feltmålinger, både manuelle og automatiske, av elektrisk motstand i betongbjelker over en periode på 8 år. Betongene, 14 i alt, har varierende kvalitet og sammensetning. Det er 1 referansebetong med høyt masseforhold uten silika, 7 betonger med m ca 0,40, 4 betonger med m ca 0,3 og 2 høyfaste lettbetonger. Alt er utført innenfor Statens vegvesens prosjekt ”Utvikling av kloridbestandig betong”. Bjelkene er armerte og instrumenterte, er 3m lange og henger i tidevannssonen på en kai utenfor Bergen.

Det er utført målinger i et automatisk loggesystem av betongtemperatur og elektrisk motstand, samt vannstanden og sjøens og luftens temperatur. Målingene utføres vanligvis hver time, men ved enkelte anledninger er det utført hyppige målinger hvert minutt for å få tak i variasjonene i elektrisk motstand med varierende sjøvannstand.

Resultatene viser at det er meget store variasjoner i elektrisk motstand med varierende vannstand. Dette har selvfølgelig stor betydning når en skal gjøre vurderinger av målinger utført innen en kort tidsperiode. Dersom en omregner motstand til resistivitet ved 10 °C, vil resistivitetsverdiene falle mer sammen og variasjonene er ikke så store. Dette viser at for å vurdere feltmålinger må en vurdere resistivitet ved samme temperatur (motstand må omregnes til resistivitet og det må gjøres en temperaturkompensering).

Videre viser resultatene at resistiviteten øker til dels meget med lengden på eksponeringen. Denne effekten er mer tydelig for betong som ikke er neddykket i sjøvann eller som står i tidevannssonen. Betonger med flyveaske viser en økning i resistivitet på mer en 10 ganger over en 8 års periode, og har også i denne undersøkelsen i særklasse høyest resistivitet. En vurdering av bestandighet/levetid for armerte betongkonstruksjoner ved hjelp av resistivitet, gir meget klare signaler om at flyveaske er særdeles gunstig.

Paper 4 (keynote)

Drivkreftene til opprissing i betongens herdefase: Termiske- og autogene deformasjoner

Artikkelen gir en state-of-the-art på termisk dilatasjon og autogent svinn (selvuttørkingssvinn), som er drivkreftene bak opprissing i herdnende betong utsatt for (indre og/eller ytre) fastholding. Artikkelen diskuterer også ulike strategier for å separere virkning av de to drivkreftene ved laboratorieforsøk.

Effekten av autogent svinn kan være betydelig i betonger med lave v/b-forhold (<0.45) og mye selvuttørking. Det har vært mye oppmerksomhet rundt dette de siste 10-15 årene, noe

som blant annet kan ses av de mange konferansene internasjonalt som har hatt autogent svinn som hovedtema. Effekten av herdetemperatur (termisk dilatasjon) er imidlertid av størst betydning i de fleste betonger/situasjoner og artikkelen tar opp det paradoksale i at såpass lite er gjort internasjonalt for å øke vår forståelse av termisk dilatasjon.

I tillegg til at varmeutviklingen er svært avhengig av betongsammensetningen er utvidelseskoeffisienten også svært fuktavhengig. Fuktavhengigheten forklares ved en mekanisme som kan kalles "termisk indusert relativ fuktighetsendring". Fenomenet skyldes porevannets termodynamiske egenskaper og er målt eksperimentelt (absorbsjonsentalpi). Grovt sett går dette ut på at når et lukket system (betongens poresystem) med en gitt relativ fuktighet (RF) gis en temperaturøkning vil RF øke i systemet (rundt 0.2% pr. ^{o}C) og konsekvensen er en svelling. Svellingen kommer da i tillegg til den "rene" termiske utvidelsen av betongen (det motsatte skjer ved avkjøling). Mekanismen er størst ved "middels" RF (50-70%) og eksisterer ikke i betong som er vannmettet eller helt uttørket. For en betong som støpes ut (dvs. har ca. 100% RF) og deretter selvuttørker på grunn av hydratasjonsreaksjonene (RF reduseres) medfører dette at utvidelseskoeffisienten øker over tid. En betong med lavt v/b-forhold kan derfor forventes å ha et betydelig autogent svinn, den vil avgi mye herdevarme (høyt sementinnhold) og, sist men ikke minst, den vil utvikle en høy utvidelseskoeffisient. Alt disse komponentene bidrar til stor voluminstabilitet i betong med lave v/b-forhold og dermed til høy opprissingstendens.

En interessant konsekvens av kunnskapen er at en betong som holdes fuktig gjennom herdefasen vil få svært gunstige herdeforhold idet den vil ha lav utvidelseskoeffisient samt at den vil få sitt autogene svinn eliminert. I praksis er det imidlertid umulig å holde tett høykvalitetsbetong fuktig innvendig ved vanning fra utsiden, men det arbeides faktisk på forskningsfronten med strategier for å sikre høyt internt fuktnivå (såkalt "internal curing").

Paper 5

Risstendens i herdefasen for lavvarmebetong med flyveaske- og slagginnblanding

Artikkelen presenterer eksperimentelle målinger og spenningsberegninger og det vises en klart gunstig effekt av flyveaske (FA) på risstendensen når den tilsettes på erstatningsbasis med sement i forholdet en-til-en i en betong med v/b = 0,40. Den gunstige effekten skyldes hovedsakelig redusert herdevarme i FA-betongen. v/b-forholdet ble altså holdt konstant i undersøkelsen og FA behandlet som sement i beregning av masseforholdet (*k*-faktor lik 1.0 for FA).

NS-EN 206-1 angir imidlertid $k = 0.4$ for tilsatt FA. For praktisk proporsjonering betyr dette at økt tilsetning av FA innebærer en reduksjon av v/b-forhold for å opprettholde et masseforhold på 0,40. Det er derfor grunn til å tro at FA-tilsetning i henhold til standarden ville gitt noe mindre gunstig effekt enn resultatene som framkom i undersøkelsen (lavere v/b-forhold betyr generelt mer herdevarme og mer autogent svinn). For en sertifisert FA-sement er situasjonen imidlertid en helt annen, her er *k*-faktoren lik 1.0 for hele sementen (dvs. inkludert FA). Dette er aspekter man kan legge på minne ved parameterstudier på FA (og eventuelt slagg som har $k = 0.6$ i hht. NS-EN 206-1).

Contents

Paper 1 ELECTRICAL RESISTIVITY OF CONCRETE. PART I: FREQUENCY DEPENDENCE AT VARIOUS MOISTURE CONTENTS AND TEMPERATURES

J-M. Østvik [(1)], C.K. Larsen [(1)], Ø. Vennesland [(2)], E.J. Sellevold [(2)] and M.C. Andrade [(3)]

[(1)] Norwegian Public Roads Administration, Technology Dept., Oslo, Norway
[(2)] Norwegian Univ. of Science and Technology, Dept. for Engineering Science, Trondheim, Norway
[(3)] Instituto Eduardo Torroja (IETcc – CSIC) Madrid, Spain

Abstract

The electrical resistivity of concrete is probably the best available parameter to predict the durability of concrete structures in terms of corrosion. Measurements of resistivity have been carried out with electrochemical impedance spectroscopy at high frequencies (100 Hz – 40 MHz) as the main method compared to other AC methods at various frequencies. The results demonstrate frequency dependence of the resistivity. This frequency dependence is a function of the moisture content and temperature of the concrete. However, it appears that measurements of the resistivity of concrete exposed to normal Nordic climatic conditions can be performed at a fixed frequency in the interval 100 Hz to 10 kHz and with them represent the relevant DC resistivity with acceptable accuracy.

1. INTRODUCTION

The range of resistivity (ρ) in concrete varies over several orders of magnitude. The resistivity of saturated concrete is determined by both the magnitude and the degree of continuity of the concrete pore structure, as well as the conductivity of the pore water. Both these factors are strongly influenced by the concrete binder components and mix proportions. The water to binder ratio is the primary factor with respect to porosity, but pore structure and continuity of the capillary pores are strongly influenced by pozzolanic additions such as silica fume and fly-ash. The pore water ionic content determines its conductivity; consequently pozzolana has strong effects also on this factor since they reduce the pore water pH. Chloride intrusion also increases the conductivity. For a given concrete the main determining factor is the moisture content, here expressed in terms of the degree of saturation (DS) in %. DS is related to a water stored state, i.e. air voids are not included. A water stored state is of course somewhat uncertain since it can vary with specimen dimensions, initial moisture contents, etc. A dry concrete may act more or less as an insulator ($\rho > 10^6$ Ωm) while a wet one may act as a semi – conductor ($\rho \approx$ 10-500 Ωm). This large difference in electrical resistivity has been verified by several authors, and reviewed in [1].

Temperature has strong influence on concrete resistivity, both directly and immediately, and over time since a temperature change leads to redistribution of pore water between its various phases (gel-capillary) and to changes in the ionic concentrations.

The resistivity also varies with the degree of hydration, and the semi-conductor behaviour implies that ρ is frequency dependent, for instance [2].

Part I of this III paper sequence takes up measurement techniques and in particular the question on how to determine the DC resistivity at various temperatures and moisture states. Experiences from dynamic experiments considering the frequency dependence at these different stages are reported. This is based on the PhD thesis of Østvik [5]. Part II reports on resistivity of old concrete tested in different moisture (DS) conditions and temperatures. Part III concerns in-situ resistivity of field exposed concrete beams using embedded electrodes.

Our interest in concrete resistivity is at least twofold:

1. Corrosion of reinforcement in the coastal infrastructure is the major durability problem in Norway. The rate of corrosion above the seawater is primarily determined by the resistivity, local and/or bulk, depending on the corrosion process. It is consequently of inherent interest to know how the overall bulk resistivity of the concrete (which is the one that is readily accessible and measurable) varies with temperature and DS, and, in particular how it develops over time under field conditions.
2. The resistivity can in principle be used to monitor the DS in a structure [5]. DS is regarded as particularly important since every durability issue involves the moisture content. DS in concrete bridges has been determined by sample taking [3, 4], but this is a very costly and cumbersome process. Monitoring resistivity is technically much easier, and more reliable, than the notoriously unreliable relative humidity probes. The challenge is to interpret the resistivity data in terms of DS, since temperature, aging effects and chloride intrusion has significant effects and must be compensated for. The present data may hopefully be useful as a starting point in this respect.

Figure 1 shows a number of data sets (ρ vs. DS) from the literature [3, 5 – 9]. The w/c – ratio for these concretes varies from 0.40 to 0.60, and some of the 0.40 concretes contains fly-ash and or silica fume. The differences are very large indeed, even for nominally equal concretes. The data, and our experience, indicates strongly that resistivity measurements are

sensitive to the technique employed, and in particular to the concrete -electrode contact in partly dried states. This will be further discussed in the present part of this paper sequence. The figure gives two clear indications; as w/c – ratio decreases the resistivity increases as does the moisture sensitivity very strongly. This trend is further supported by the results in Part II. Part III will highlight the difficulties of application of these findings in the field.

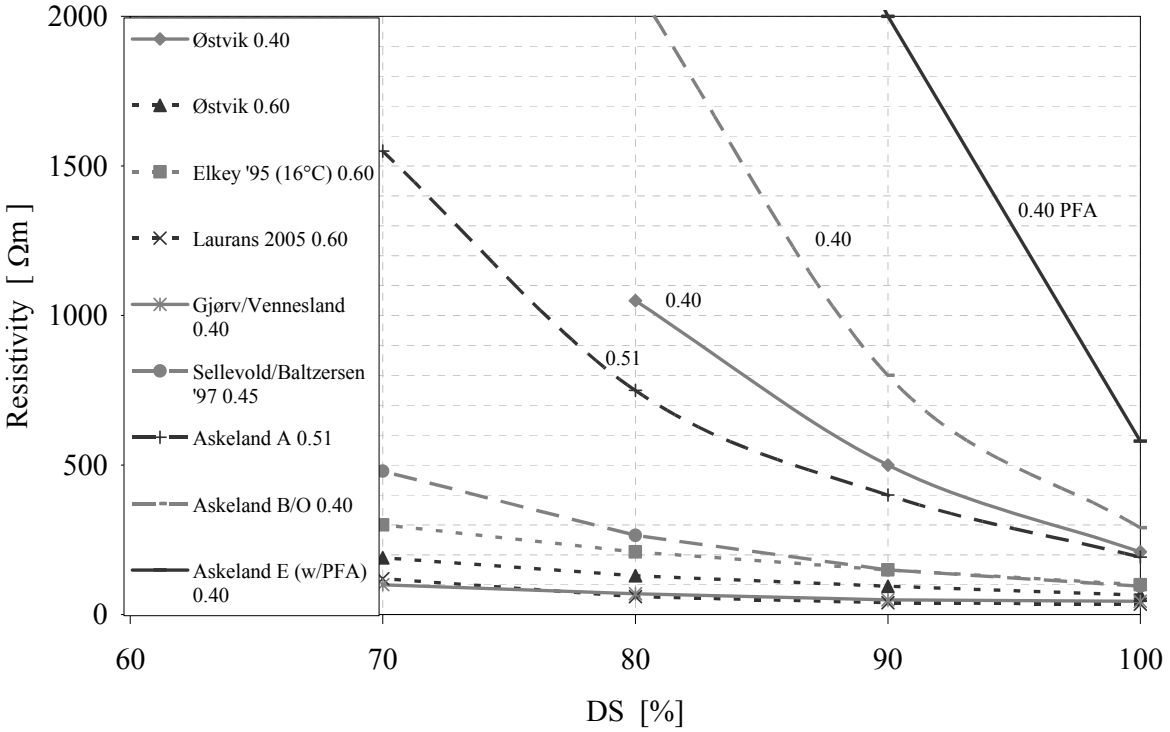

Figure 1 Literature data on moisture/resistivity relationships

2. EXPERIMENTAL

The concrete mixes used in the present experiments are one mix with a w/b-ratio of 0.40 that represents a high performance concrete, and a reference concrete with a w/b of 0.60. Specifications for the mixes are given in Table 1.

Table 1 Mix proportions of the concrete mixes

Materials	**w/b 0.4**	**w/b 0.6**
	[kg/m^3]	[kg/m^3]
Cement: HSOPC, CEM I 52.5 LA (Norcem Anlegg)	444	340
Micro silica (Elkem)	35.5	
Free water	182	191
Adsorbed water	11.3	12.0
Aggregate fraction 0-8 mm (Årdal natural)	993	705
Aggregate fraction 0-2 mm (Årdal natural washed)	0	352
Aggregate fraction 8-11mm (Årdal)	662	705
Super plasticizer (Sikament 92)	4.44	0.68
Air entrainment (Sika AER)	0.13	0.02
Proportioned Concrete density (kg/m^3)	2328	2306
Average compressive strength (after 28 days curing in water)	*85 MPa*	*55 MPa*

Test specimens were concrete slices cut from cast beams 100x100x1500mm with embedded electrodes in the form of stainless steel grids. A principle drawing of the specimens is given in Figure 2.

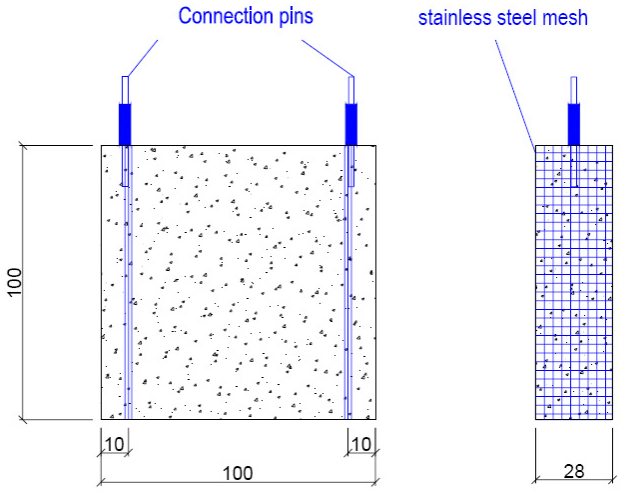

Figure 2 Principle drawing of the concrete specimen

The slices were conditioned to various moisture contents prior to the measurements. The concrete were between 100 and 300 days old when the tests were conducted in order to exclude hydration effects. The measurements were primarily carried out by Electrochemical Impedance Spectroscopy (EIS) as the reference method. The results were additionally compared to resistivities found by positive feedback on a potentiostat and potential square pulse (chronoamperometry at fixed frequencies).

Experimental scope:

Measurement techniques:	
Electrochemical Impedance Spectroscopy	(100 Hz – 40 MHz)
Positive Feedback	(range dependent frequencies)
Potential Square Pulse	(Fixed frequencies 120 Hz and 1 kHz)
Temperature (constant):	20°C, 2°C, -14°C and -28°C
Moisture content*:	30% ≤ DS ≤ 100%

*) The moisture contents are calculated from weights in situ, saturated and dry states.

3. RESULTS AND DISCUSSION

The EIS measurements were mathematically modelled and interpreted using a single Randles Circuit (RC), given in Figure 3, and the results were regarded as the "true" resistivities. The value, $R_{concrete}$, represents the DC resistivity of the concrete, which is the relevant quantity for corrosion purposes.

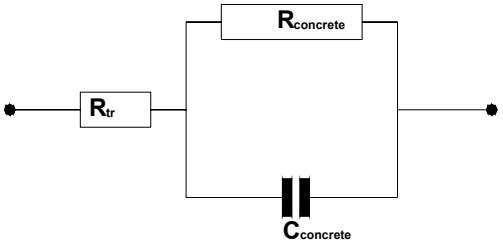

Figure 3 The single RC used for fitting of the EIS measurements

The concrete impedance to form a suppressed single arc is commonly observed in a Nyquist diagram (Figure 4). In order to verify the single RC modelled results, a small selection of measurements were interpreted by 2 and 3 serial connected RC without giving large variations from the single RC. We also found that the transition resistor (R_{tr}) was for nearly all cases insignificantly small, which is a good indication that the electrode setup (embedded mesh) and the cabling was functioning well.

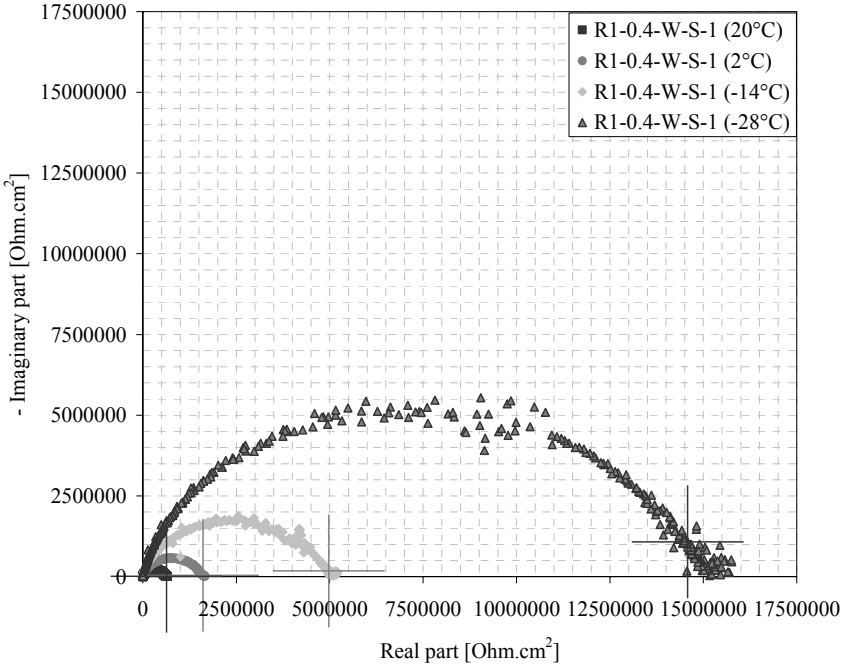

Figure 4 Nyquist diagram for the w/b 0.4 concrete specimens at the four tested temperatures (DS ≈ 90%). The large crosses show the impedance at 1 kHz.

In Figure 4 examples of the measured impedances are shown in a Nyquist diagram. The letters following the w/b ratio gives the curing and handling conditions, explained in [5], but not necessary here since the only variable here was temperature. The measurements were performed in the frequency range 100 Hz to 40 MHz, with the low frequency on the right side of the arc and increasing to the left. In Figure4 the 1 kHz impedances are highlighted as large crosses. It can be seen that the measured impedance at this frequency has a capacitive contribution (most apparent at -28 °C), but small. Considering the same results as given in Figure 4 in a BODE plot (Figure 5) the frequency dependence becomes more explicit.

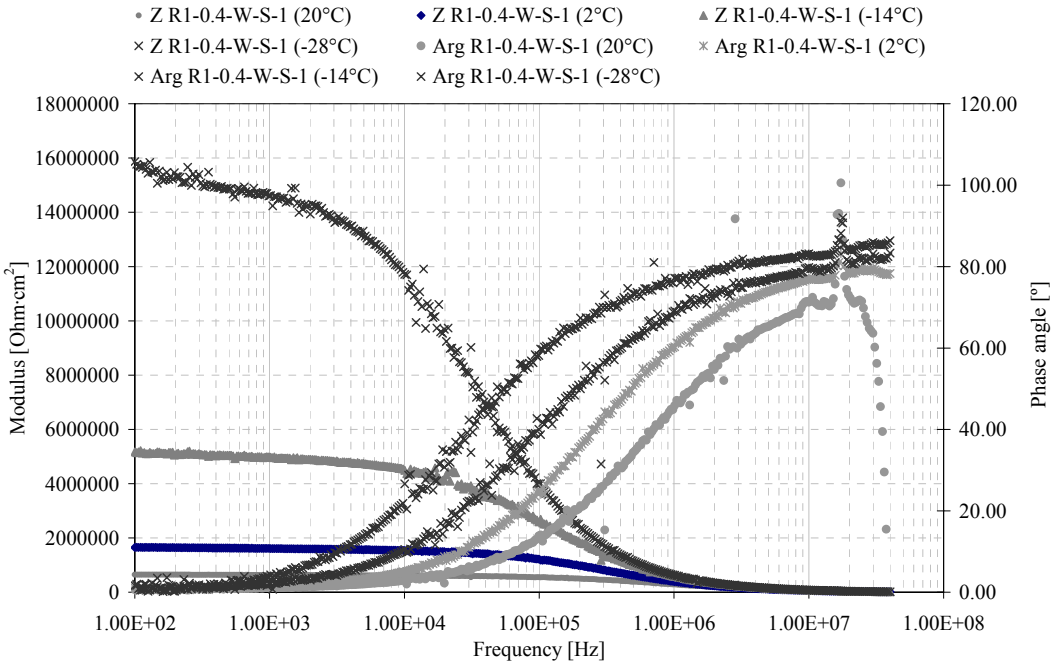

Figure 5 *Bode Plots for the w/b 0.40 concrete specimens high moisture contents (DS ≈ 90%).*

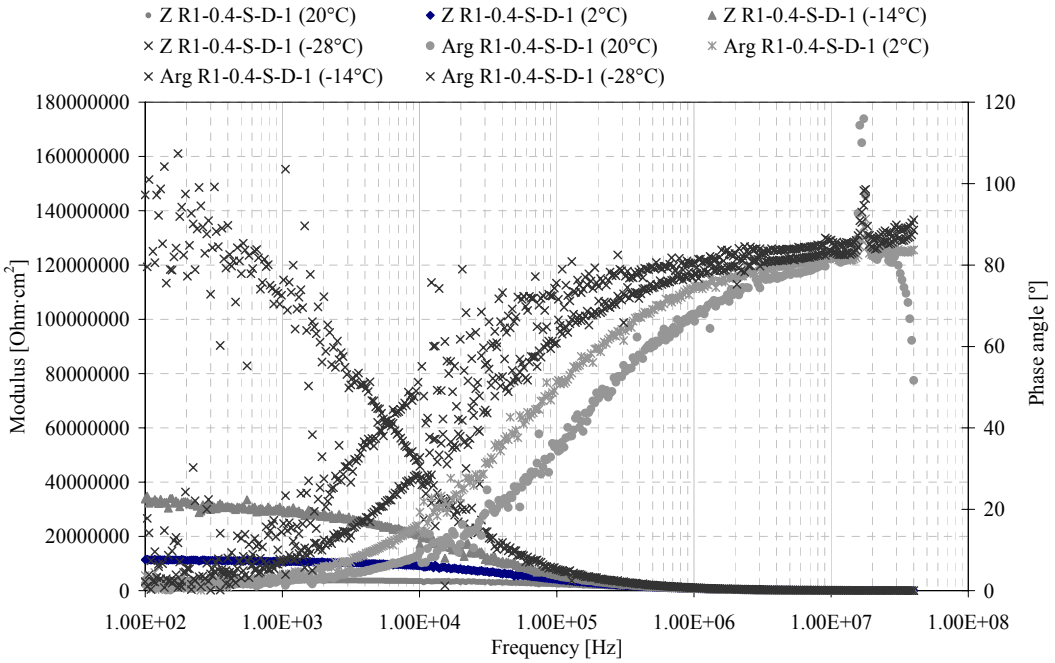

Figure 6 *Bode Plots for the w/b 0.4 concrete specimens at low moisture contents (DS ≈ 55%).*

One can see that the modulus (absolute value of the impedance) is nearly unchanged between 100 Hz and 10 kHz, i.e. it is relatively close to the value of the real component and also the DC value, for the higher temperatures. At lower temperatures, hence high resistivities, the slope of the line increases, demonstrating stronger frequency dependency.

In order to detect the effect of moisture on the frequency dependence a series of dry concrete specimens were tested at the same temperature conditions. The results are given in Figure 6.

By comparing the results in Figures 5 and 6, one can clearly see that moisture plays a profound role for the frequency dependence of measurements, and that it is also clearly temperature sensitive, shown as the scattered sloping line at the figure top left side.

The modelled DC resistivities ($R_{concrete}$) found by EIS was compared to results found by the positive feedback on an AMEL potentiostat and potential square pulse equipment. Some deviations were found, supporting our assumptions on frequency dependence. Significant deviations were found at high resistivities (dry and cold concrete), especially for the positive feedback measurements, however, these were attributed to limitations in the internal resistor in the equipment.

When the raw data from the impedance measurements was examined more closely we found that the DC component of the impedance showed small deviations from the modelled resistivity for all frequencies between 100 Hz and 10 kHz. The data is given in Tables 2 and 3.

Table 2 Deviation between measured and modelled resistivity at various frequencies for a wet concrete

	Moisture content DS [%]	Temperature [oC]	Modeled DC [Ωm]	Frequency [Hz]		
				100	1000	10000
R1-0.4-W-S-1 (20°C)	93.8 %	20	756	804	790	766
Deviation vs modeled				6.4 %	4.5 %	1.4 %
R1-0.4-W-S-1 (2°C)	91.8 %	2	1955	2061	2011	1914
Deviation vs modeled				5.4 %	2.9 %	-2.1 %
R1-0.4-W-S-1 (-14°C)	89.8 %	-14	6170	6460	6215	5516
Deviation vs modeled				4.7 %	0.7 %	-10.6 %
R1-0.4-W-S-1 (-28°C)	87.8 %	-28	18500	19823	18220	13092
Deviation vs modeled				7.2 %	-1.5 %	-29.2 %

Table 3 Deviation between measured and resistivity at various frequencies for a dry concrete

	Moisture content DS [%]	Temperature [oC]	Modeled DC [Ωm]	Frequency [Hz]		
				100	1000	10000
R1-0.4-S-D-1 (20oC)	55.5 %	20	4630	4983	4784	4308
Deviation vs modeled				7.6 %	3.3 %	-7.0 %
R1-0.4-S-D-1 (2oC)	55.3 %	2	13500	14155	13381	10820
Deviation vs modeled				4.9 %	-0.9 %	-19.9 %
R1-0.4-S-D-1 (-14oC)	55.1 %	-14	38000	42144	36740	18905
Deviation vs modeled				10.9 %	-3.3 %	-50.3 %
R1-0.4-S-D-1 (-28oC)	54.9 %	-28	152500	182154	137270	48146
Deviation vs modeled				19.4 %	-10.0 %	-68.4 %

In Tables 2 and 3 the range of deviation for between measured impedances at three selected frequencies and the modelled DC resistivity is shown. It appears to be a substantial moisture effect as well as a clear temperature effect. The results indicate that to obtain the most correct DC resistivity one needs to perform measurements at increasing frequency as the moisture content and temperature increases in the selected frequency interval. This correlation becomes apparent if viewed graphically, as shown in figures 7 and 8. The EIS results as a whole demonstrate that the measured impedance at positive temperatures and

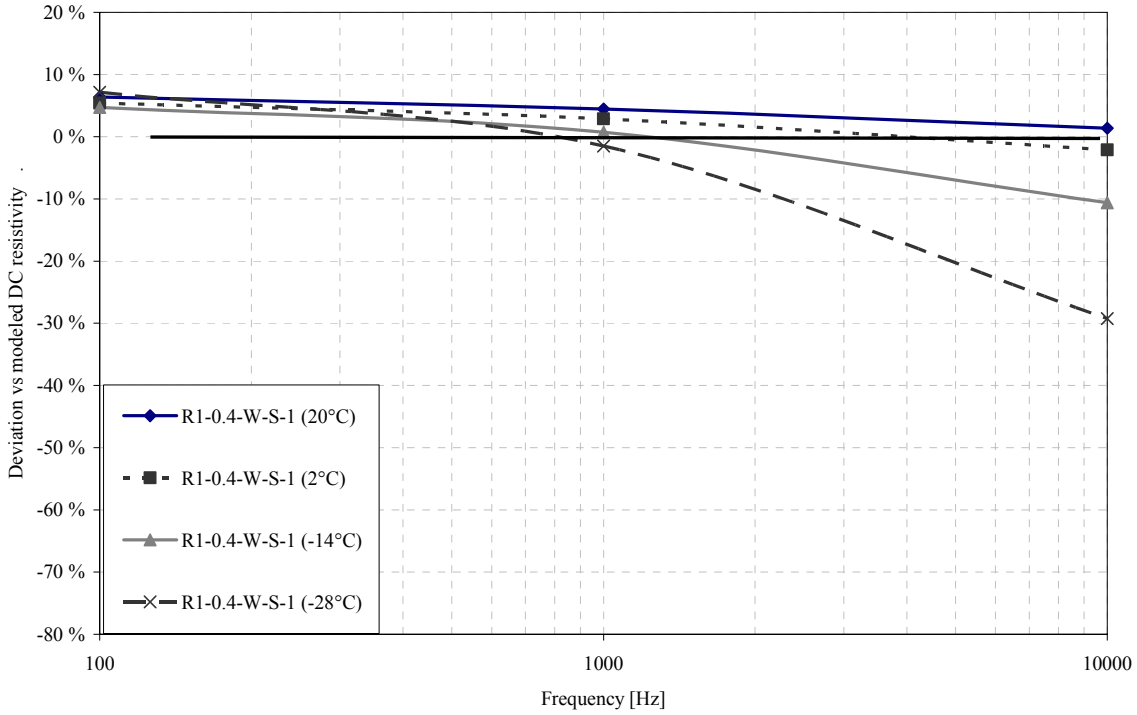

Figure 7 *Deviation from modelled resistivity at various frequencies for a wet concrete*

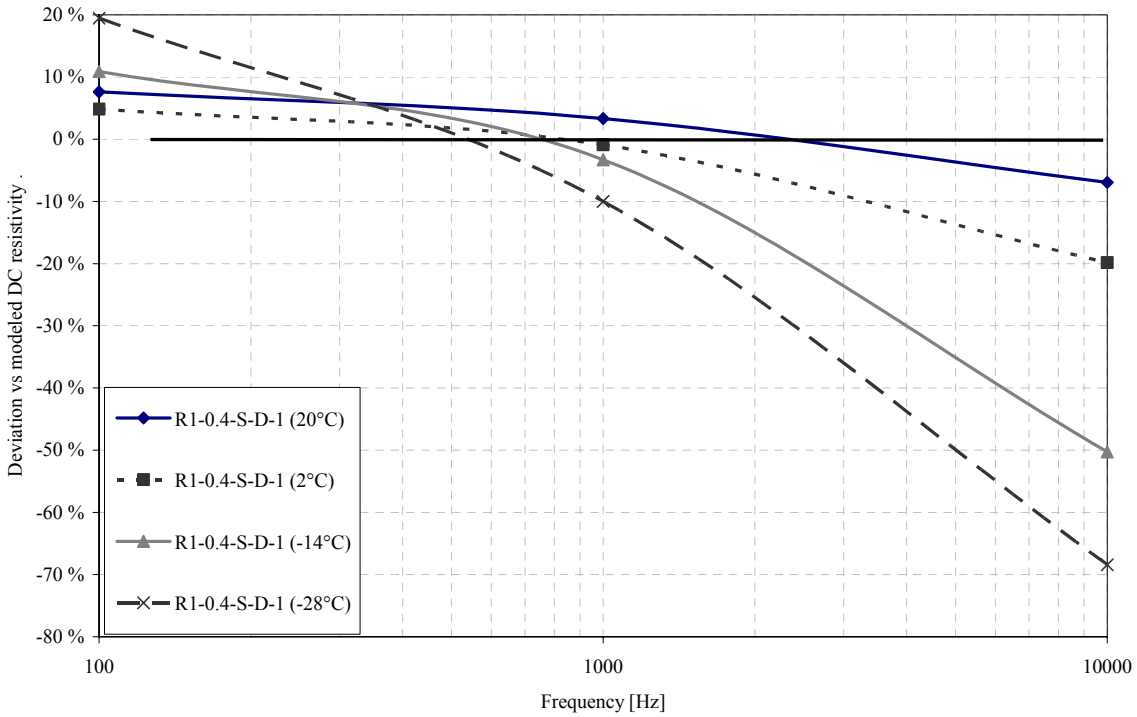

Figure 8 *Deviation from modelled resistivity at various frequencies for a dry concrete*

moisture contents above about 60 % degree of capillary saturation did not depend very much on the frequency in the range 100-10 kHz.

Measurements of the electrical resistivity of concrete structures is normally performed using easy-to-handle equipment based on either a 2 electrode system on drilled cores or in field using embedded electrodes. This type of equipment normally operates on fixed frequencies in the range 100 – 1000 Hz. It is known from the literature that a temperature change of 1°C changes the resistivity 3-5 %, and normally the temperature accuracy is less than 1°C, especially for field measurements. The effect of the frequency dependence if viewed in this perspective will therefore be acceptably small for normal moisture contents for normal structural concrete in the Nordic climate. However, figures 7 and 8 states that if measurements are to be performed on concrete that is drier than approximately DS ≈ 60 % the matter is very different, especially if the temperature drops below 0°C.

The complex structure of concrete with local variations in both solid and liquid phases and even local variations in the chemical composition, results in large variations of the electrical resistivity over a concrete section. Seen in a corrosion perspective, information on these local changes would be helpful in detection and localisation of e.g. corrosion pits. However, at present the only option available is measurements of the bulk electrical properties, and most importantly the bulk electrical resistivity. The literature suggests a limit of 1 kΩm [10] for the electrical resistivity, where resistivities above this limit rarely allows significant corrosion activity. If the effect of the frequency dependence of measurements is viewed in this perspective, the effect is merely of academic interest.

Weiss et al. [2] states that measurements at a fixed frequency may show measurable differences between different specimens; however, these differences are likely to include other features of the system than DC resistivity. We agree in principle with their statement, however, for normal field conditions, it is likely that the effect of other electrical properties is negligible. Consequently the use of a fixed frequency of 1 kHz for resistivity measurements in concrete yields close to the relevant DC value for high and intermediate moisture contents and temperatures. For low moisture contents and low temperature the situation is quite different.

4. CONCLUSIONS

The frequency dependence of the electrical resistivity of concrete has been measured. The frequency dependence is most marked at low moisture contents and low temperatures. For normally exposed concrete structures in Nordic climate the effect of frequency appears to be relatively small in the range 100 Hz – 10 kHz. This allows measurements to be made at fixed frequencies in this range, and to interpret this as the DC resistivity directly with acceptable accuracy.

ACKNOWLEDGEMENTS

The authors greatly acknowledge the Norwegian Public Roads Administration and the Norwegian Research Council for funding this work. Furthermore we wish to thank the colleagues at Instituto Eduardo Torroja in Madrid for allowing the use of their expertise and equipment.

REFERENCES

[1] Whiting, D.A, Nagi, M.A., *"Electrical Resistivity of Concrete – A Literature Review"*, R&D Serial No.2457, Portland Cement Association, Skokie, Illonois, USA, 57 pages, 2003.

[2] Weiss, W.J., Shane, J.D., Mieses, A., Mason, T.O. and Shah, S.P. "Aspects of Monitoring Moisture Changes using Electrochemical Impedance Spectroscopy" Report TVBM-3085, Lund University, Sweden. June 1999.

[3] Sellevold, E.J. 1997. Resistivity and humidity measurements of repaired and non-repaired are in Gimsøystraumen bridge. Proceedings of the International Conference Repair of Concrete Structures. From Theory to Practice in a Marine Environment: Svolvær, Norway, 28-30 May 1997: Norwegian Road Research Laboratory.

[4] Relling, R.H. and Sellevold, E.J. "In Situ Moisture State of Coastal Concrete Bridges" Proceedings "Concrete Repair, Rehabilitation and Retro fitting", Cape Town, Nov. 2005.

[5] Østvik, J.M. "Thermal Aspects of Corrosion of Steel in Concrete", Doctoral Thesis at NTNU, Trondheim 2005:5. ISBN 82-471-6868-5 (Electronic Version).

[6] Elkey, W. and Sellevold, E.J., *Electrical Resistivity of Concrete*, Norwegian Road Research Laboratory, Publication No. 80, Oslo, July 1995.

[7] Gjørv, O.E., Vennesland, Ø , and El-Busiady, A.H.S., "Electrical Resistivity of Concrete in the Oceans," *Proceedings – 9th Annual Offshore Technology Conference, Houston*, Texas, pages 581 to 588, May 2-5, 1977.

[8] Laurens, S., Balayssac, J.P., Rhazi, J., Klysz, G and Arliguie, G. "Non-destructive Evaluation of Concrete Moisture by GPR", *Materials and Structures 38*, Nov. 2005.

[9] Askeland, F. "Elektrisk Motstand på Betong ved forskjellig DS og Temperatur". MSc-thesis, Dept.of Structural Eng., NTNU, Trondheim, June 2005.

[10] Andrade, C, Alonso, C, "Corrosion rate monitoring in the laboratory and on-site". *Construction and Building Materials*. Elsevier Science Ltd., London, pp 315-328, 1995.

Paper 2 ELECTRICAL RESISTIVITY OF CONCRETE. PART II: INFLUENCE OF MOISTURE CONTENT AND TEMPERATURE

C.K. Larsen [(1)], E.J. Sellevold [(2)], F. Askeland [(2)], J-M. Østvik [(1)] and Ø.Vennesland [(2)]

[(1)] Norwegian Public Roads Administration, Technology Dept., Oslo, Norway

[(2)] Norwegian University for Science and Technology, Dept. for Engineering Science, Trondheim, Norway

Abstract

Resistivity of concrete in a structure can be measured relatively easily, and is important with respect to steel corrosion rate. Further interpretation of such data is not easy, since the resistivity for a given concrete varies strongly with temperature, water content and conductivity of the pore water. Resistivity for a number of 12 year old high performance concretes were measured in the laboratory as functions of water content and temperature. Such data is essential to obtain more information from field monitoring, for example the moisture variations which are central to all durability related issues for concrete structures.

1. INTRODUCTION

Part II of this 3 paper sequence concerns resistivity measurements in a variety of high performance concretes over a 12 year period, as well as results on the effects of degree of saturation and temperature on small disc samples cut from water stored specimens at 12 years age. The data is from the Norwegian Public Roads Administration (NPRA) project "Development of Chloride Resistant Concrete" started in 1993 and continuing today. The project is documented in a number of internal reports [1] and papers [2, 3, 4]. The data on the disc specimens (from the NPRA concretes) presented here is from a M.Sc. thesis at NTNU (2005) by F. Askeland [5]. Some data are also presented from the PhD thesis of J.-M. Østvik [6].

2. MATERIALS

The compositions for the concretes used by Østvik are given in Part I of this paper sequence. The NPRA concretes are characterized in Table 1. Note that the concretes were proportioned to produce practically useful mixes, i.e. the idea was not systematic parameter variation. Mix A was a traditional reference concrete, B, O, D and E were typical new generation bridge concretes with different binder types, while F, G and J contained more silica fume (SF). These 7 concretes are all considered high performance concretes. The 1 year strength listed is for 100 mm cubes after water storage.

The air contents listed are measured on hardened concrete using the PF-method [7]. The binder volume values are calculated from the recipes and do not include the air contents.

Table 1 NPRA concretes

Symbol	Concrete characteristics	1 year cube strength
A	Reference concrete with Norcem STD cem. w/c = 0.51, Air = 2.3%, Binder vol. = 29% Represents earlier bridge concrete	60 MPa
B	Norcem STD cem. w/b = 0.38, 4% SF, Air = 4.2%, Binder vol. = 30% Typical new generation bridge concrete	90 MPa
O	w/b = 0.40, 4% SF, Norcem Anl. Cem. Air = 4.1 %, Binder vol. = 30%	94 MPa
D	w/b = 0.39, 7% SF, Norcem Sulf. Res. Cem. Air = 1.8%, Binder vol. = 31%	84 MPa
E	w/b = 0.39, 4% SF, Norcem FA (20% fly ash) Air = 1.8%, Binder vol. = 30%	87 MPa
F	w/b = 0.42, 11% SF, Norcem STD cem. Paste rich mix, Binder vol. = 35%, Air = 1.2%	97 Mpa
G	w/b = 0.46, 9% SF, Norcem STD cem. Air = 1.7%, Bind vol. = 30%	89 MPa
J	w/b = 0.34, 6% SF, Norcem STD cem. Air = 1.6%, Binder vol. = 32%	107 MPa

The 8 NPRA concretes discussed here were also used to produce beams (150x300x3000mm) in 1993. These were subsequently suspended from a pier in Northern Norway in a way that kept the bottom 0.5 m always immersed, the middle 2m in the tidal zone and the top 0.5 m in the splash zone above the top water level. Electrochemical measurements and chloride profiles have been made periodically, and reported [2, 4]. The general trend is that concrete A has significantly higher chloride ingress in terms of chloride diffusion coefficient, compared to the other concretes. The chloride diffusion coefficient for

concrete E has gradually decreased over the last 7-8 years, presumably due to the slow pozzolanic reaction of fly ash [4].

3. EXPERIMENTAL

Table 2 lists resistivity values measured in different ways over the 12 year period. The initial data (1993) were taken on 45 mm thick discs in the electrical migration cell. The 100 mm cube values are made using wetted mats and metal plates pressed together on opposite sides. The 12 year data on field cores (150 mm long) were taken after sawing 50 mm discs, and then using the same method as for the cubes. Both outer discs contained exposed surfaces that were removed by grinding about 2 mm before testing. The cores were taken from the bottom parts of the beams suspended from the pier.

The 12 year measurements at different degrees of saturation (DS) and temperatures were done on 20 mm discs cut from water stored cylinders [5]. These were conditioned by removing water by careful drying at 30-35 °C to make DS values of roughly 88%, 77% and 66%. Each specimen was then applied conductive paint as electrodes on 50 mm opposite sections of the circumference, and then tightly wrapped to avoid moisture loss. These sealed samples were stored 7 weeks at 20.5°C to homogenize the moisture content. Periodic resistance measurements indicated that this was sufficient. The resistance measurements were carried out at 1000 Hz (see Part I for justification) at temperatures of 20.5°C, 1.5°C (7 day storage) and 40°C (3 day storage).

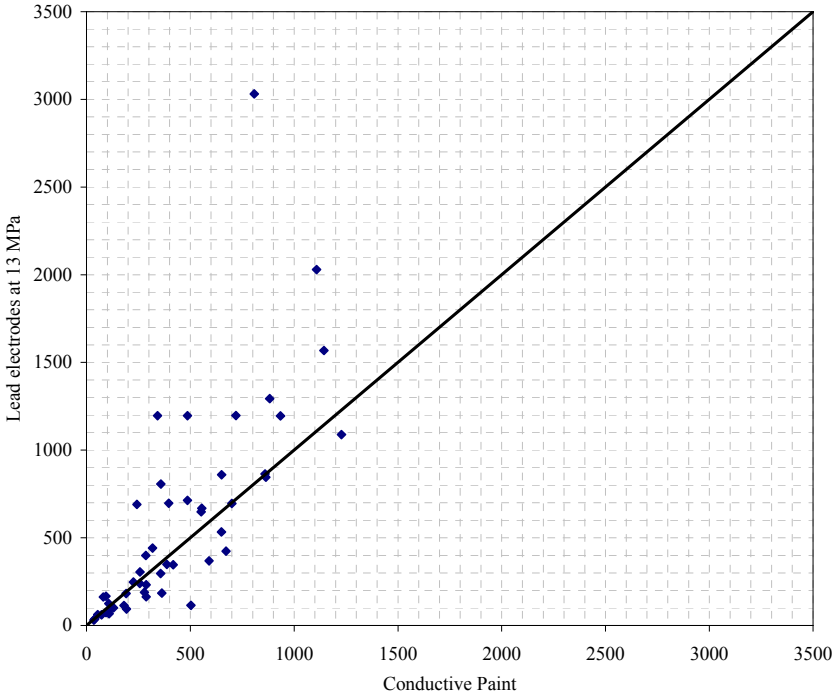

Figure 1 Comparison of resistivity [Ωm] measured by two methods

As already shown in Part 1 of this paper, both the magnitude and DS sensitivity of concrete resistivity varies greatly in the literature. We believe this variation to be mainly caused by test method, and particularly the electrode-concrete contact, which is very difficult to ensure when the concrete is partly dried. A number of controls on the 20 mm discs were therefore carried out by using two lead plates as electrodes pressed against the two opposite flat sides of the discs with, applying about 13 MPa. The results compared to the paint electrodes are shown in

Figure 1, for a number of specimens. Further details are given in [5]. There is large scatter, which clearly increases as resistivity increases, i.e. DS decreases. Thus as stated above, the uncertainty also for the present data increases as DS decreases.

Table 2 Resistivity over time for water stored concrete (Ωm at 10°C)*

CONCRETE		A	B	O	D	E	F	G	J
1993 Measured at 22°C LAB 90 days Factor = 1.54 Cyl.		69	179	233	487	323	588	390	367
1995 Measured at 13°C LAB 2 years Factor = 1.12 Cubes		116	267	286	404	750	486	410	426
1999 Measured at 17°C LAB 6 years Factor = 1.30 Cubes		140	316	324	415	1062	481	441	480
2005 Measured at 24°C LAB 12 years Factor = 1.64 Discs		280	438	410	507	850	418	472	425
Measured at 5°C 2005 Factor = 0.82 12 years in sea water. Cores from test elements.	50-100mm from surface	54	149	230	410	905	457	357	344
	0-50 mm from surface	107	293	398	517	1023	617	576	517

*Adjusted using Arrhenius eq. with activation constant = 3000°K = Activation energy divided with the Gas constant. The resulting adjustment factor is given in the table.

4. RESULTS AND DISCUSSION

Table 2 shows resistivity values for the water stored NPRA concretes over the 12 year period. Note that different sample geometries and electrode types have been used at different temperatures. The values are listed as 10°C values, i.e. they are adjusted from the original values using the Arrhenius equation with an activation constant of 3000°K, which correspond to activation energy of about 25 kJ/mole. This value of activation energy is discussed later.

The data for the water stored concretes (4 first rows) are not entirely consistent. In general there is an increase over time as we expect, but the 20% fly ash mix (E) is in a class by itself. Conversely, the mix with 11% silica fume (F) shows a consistent decrease – but from a very high initial value. This phenomenon has been seen also in Phase II of the NPRA-project and will be discussed later.

For the higher w/c-ratio mix (0.51, concrete A) the resistivity increased with time, but lags well behind all the high performance concretes.

The samples taken from the field exposed elements behave unexpectedly in some ways, as one would expect the surface part of the core to be more saturated than the inner part, thus leading to lower resistivity. The surface parts (0-50mm) have much higher resistivities than their inner cores (50-100mm) in all cases. Thus, the ageing effects when exposed to sea water are greater in the cover zone than in the bulk concrete.

The silica fume reduction (F) is absent for the field samples. The data background is too small to draw any conclusions on this question of long term resistivity of concrete with more than 10% silica fume, but it will be followed up in field samples of Phase II of the NPRA project.

4.1 Variable Degree of Saturation (DS)

Table 3 gives the resistivity data at 4 DS values and 3 temperatures. Note that the 15 saturated discs per set were measured at 20.5°C only. They were subsequently split into sets of 5 and desorbed to desired DS. The mean DS values for the 8 sets are as given in the table (88, 77 and 66%), but the mean values for each set of 5 discs varied as follows: 87.7–89.0 %, 75.7 – 77.8 % and 63.9 – 67.5 %. This variation is small, and justifies the use of the overall average values.

Table 3 Resistivity [Ω m] for sets of 5 discs (and CV in % of mean)

DS= 100% 20.5°C (sets of 15 discs)		DS = 88%			DS = 77%			DS = 66%			POROSITY VOL %	
		20.5°C	1.5°C	40°C	20.5°C	1.5°C	40°C	20.5°C	1.5°C	40°C	1993	2005
A	192 41%	390 50%	738 51%	212 45%	889 39%	1873 42%	426 33%	2169 78%	5169 81%	970 70%	12.1	12.4
B	299 12%	1088 32%	2482 30%	481 31%	2600 30%	6674 42%	1185 39%	8671 34%	18363 40%	3945 30%	11.4	9.8
O	280 11%	787 16%	1699 14%	370 14%	2791 10%	6257 11%	1123 10%	5596 18%	11843 13%	2580 23%	10.3	10.7
D	346 8%	975 35%	1967 34%	492 36%	2401 30%	5237 28%	1103 38%	5086 17%	11074 19%	2442 18%	12.1	11.5
E	580 8%	2237 19%	4280 22%	1001 21%	4263 20%	9734 19%	1967 11%	9214 20%	19880 22%	4150 15%	11.9	10.4
F	286 7%	1140 14%	2516 14%	492 12%	2711 10%	6112 9%	1195 13%	5790 20%	12360 32%	2670 20%	14.7	12.4
G	323 11%	1047 29%	2133 27%	520 27%	2635 25%	5912 19%	1227 29%	7166 22%	16152 22%	3182 21%	12.5	12.2
J	290 20%	872 21%	2030 19%	370 24%	2464 9%	5721 8%	1065 10%	4561 46%	11263 42%	2081 42%	11.1	9.9

Porosity does not include air content

The values given below the resistivity value in each box gives the CV (coefficient of variation), i.e. the standard deviation as % of the mean value for each set. The CV is particularly high for mix A, and in general tends to increase with decreasing DS-values. The relatively high CV values is, in our opinion, probably caused by the small sample thickness (20 mm) relative to d_{max}= 16 mm. This is supported by the results on cubes from the same concretes (Table 2), where the CV values all were below 10% for the sets of 5 to 7 100 mm cubes.

Table 3 also gives porosity values, excluding air content [7], for the concretes measured at 90 days (1993) and 12 years (2005). The 1993 values are mean values for 6 samples (45 mm thick discs), 3 from a molded cylinder and 3 from a core. The 2005 values are mean values for the 15 discs (20 mm) for each concrete. The overall mean values were 12.0 vol % in 1993 and 11.2 vol. % in 2005. Thus, a decrease due to long term hydration is indicated, but the trend is too unsystematic to be given much weight for individual mixes.

Figure 2 shows the data at 20.5°C in two ways: As resistivity vs. DS directly and as conductivity (inverse of resistivity) vs. DS. The data from Østvik [6] are shown in parallel graphs in the figure – in order to facilitate the comparison. Note that the Østvik data extends to below DS = 30%, while Askeland [5] only goes to DS = 66%.

From the point of view of practical use we consider the conductivity plots most relevant; assuming sufficient access to oxygen the rate of corrosion is directly related to conductivity but inversely to resistivity. In Norway the most severe durability problem for the marine infrastructure is undoubtedly reinforcement corrosion. The moisture content in Norwegian coastal bridges has been found to vary little over time and position in the bridge above the splash zone, and was in the range 80 – 90 % DS [9]. Thus concrete conductivity in this range is of particular practical interest.

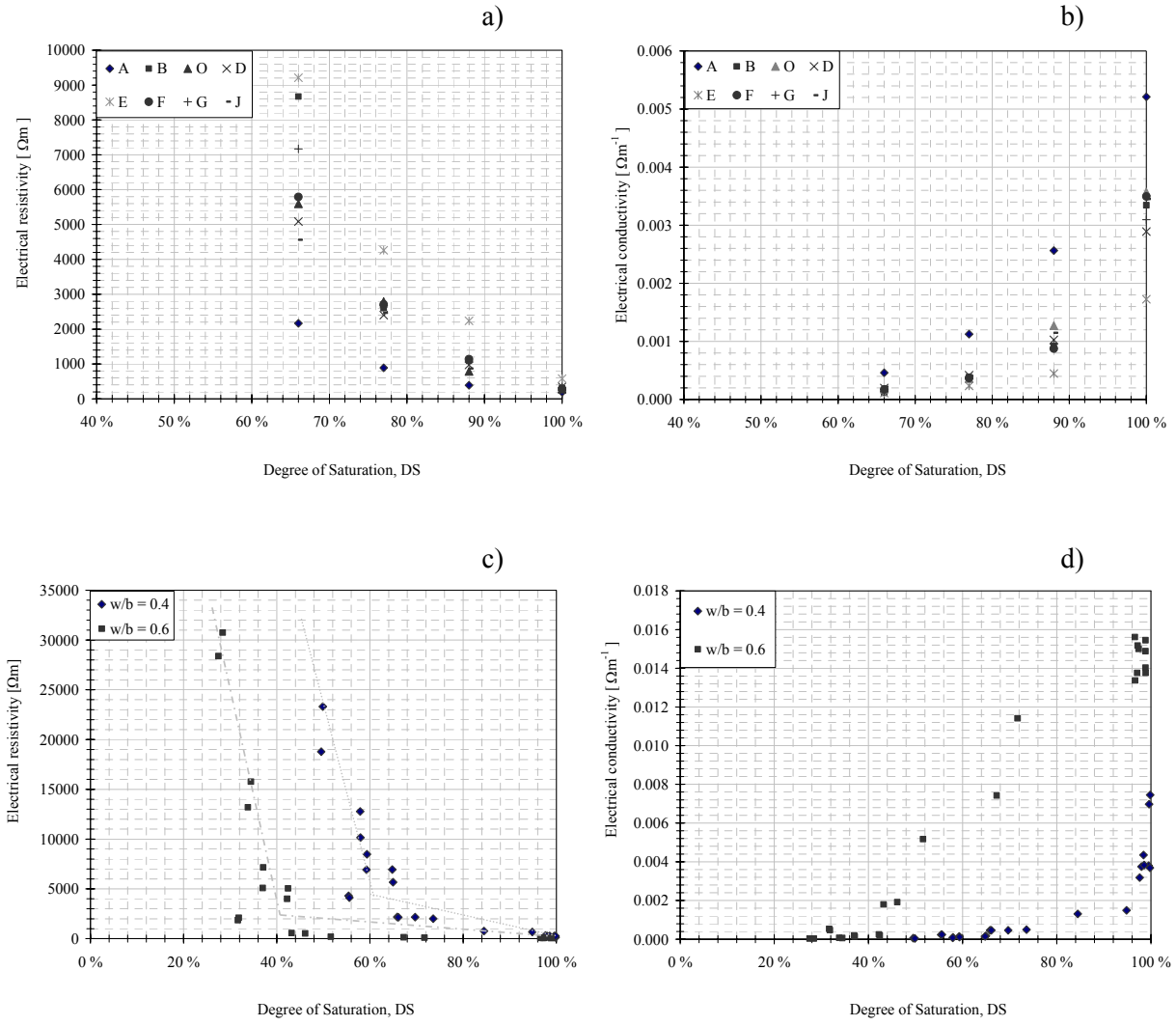

Figure 2 Resistivity and conductivity vs. degree of saturation. a) and b) represent NPRA concretes, c) and d) represent Østvik [6] concretes.

The conductivity data in Figure 2b show quite different behavior for the traditional bridge concrete (A) and the high performance varieties; with the fly ash variety (E) in a class by itself with very low conductivity. Concrete A retains relatively high conductivity values (resistivity under 1000 Ω·m) down to about DS = 75% while the other 7 fall below this value around DS = 85 – 90%. The experimental points are only at DS = 100 % and 88 %, thus it cannot be seen how fast the drop is from saturation. Figure 2d, however, has more points in the high range, and the w/c = 0.40 sample displays a sharp drops in conductivity already at DS = 96%. We take this to indicate that the drop in conductivity is greater than predicted by straight lines from DS = 100 to 88 % in Figure 2b. For the 0.60 concrete the behavior is much more gradual (Figure 2d). Apparently, increased concrete quality (reduced capillary porosity) leads to a greater sensitivity of the conductivity to DS. This we consider natural, since the (continuous) capillary pores are the most efficient transporter of current, and very little (if any) water loss will interrupt their continuity. The very resistive fly ash concrete (E) may reach a level of 1000 Ω·m after a water loss of only a few % DS.

Note that the conductivity values in Figure 2d are well above those in Figure 2b. Presumably this is a result of the age difference between the concretes, about 1 year versus 12 years.

We note that this physical interpretation of the data ignores the effects of pore water chemistry. It is well known that silica fume both produces less capillary pores, and reduced pH in the pore water. Both these effects increase the resistivity at a given DS. At dosages around 10% all the silica fume has reacted in a few months [8]. Consider the large effects of fly ash at long times in this light: When silica fume has reacted its effects on pore water pH gradually diminishes resulting in reduced resistivity. Fly ash, on the other hand, continues to react, maintaining lower pH and high resistivity. This hypothesis is at present just that, but is a warning not to interpret resistivity data only in terms of pore structure. Figure 2c shows very marked features, with sharp transition points at about DS = 40 and 60% for w/c=ratios of 0.60 and 0.40 respectively. Østvik [6] discusses these in terms of gel and capillary porosity. Presumably, at the transition points, all capillary water is removed, and further drying removes gel/interlayer water producing solid like behavior with very high resistivity.

Consequently, the two types of plots (resistivity and conductivity) illustrate different phenomena.

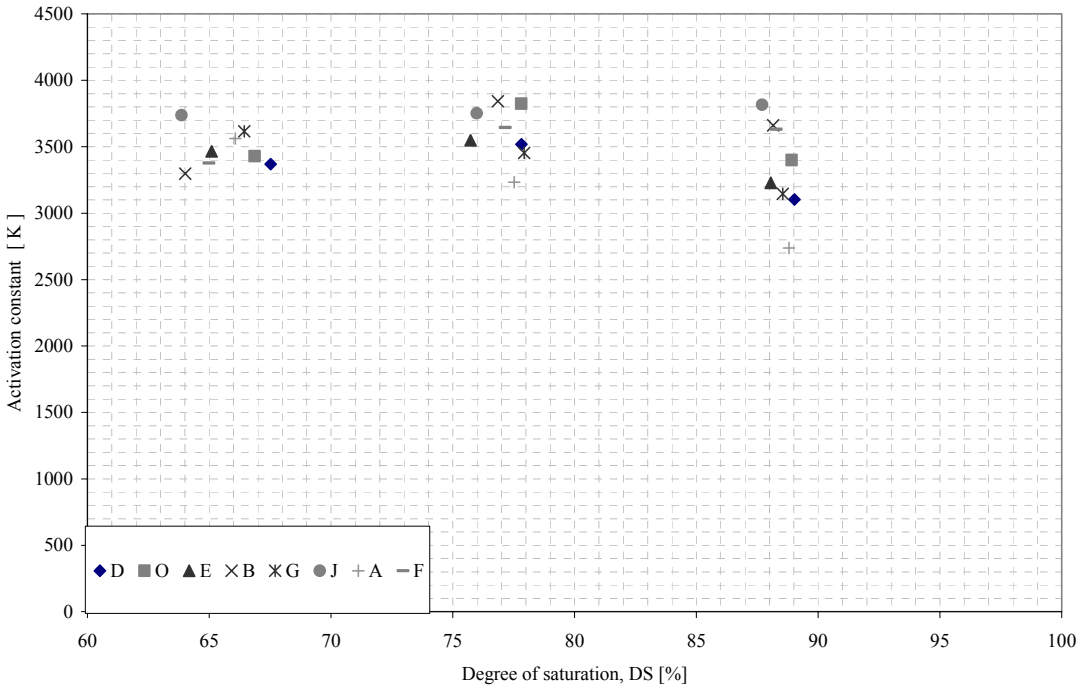

Figure 3 Temperature sensitivity of the resistivity. Activation constant vs. degree of saturation for mean values of all concretes.

4.2 Effects of temperature

After water removal to reach the desired DS, the discs were stored 7 weeks before the measurements were made at 20.5°C, with periodic controls underway to ascertain the closeness to equilibrium values. The next step was 1 week storage at 1.5°C before measurements and then 3 days at 40°C and measurements. Finally, all discs were dried at 105°C to calculate the actual DS for each at the time of the measurements.

We consider the 20,5°C values good, and representative of a first dried state. Experience in the NPRA project and extensive work on pore water composition after moisture/temperature

changes by Larsen [10], has indicated that the resistivity is by no means a unique function of DS and T, but depends on the entire moisture and temperature histories. The same is true for the physical (pore) structure [11]. Consequently the values at 1.5°C and 40°C are less "fundamental", since they follow a certain arbitrary conditioning cycle.

Figure 3 gives the temperature effect on the mean value of each concrete in the form of the activation constant vs. DS. The activation constant defines the temperature sensitivity; higher values mean greater sensitivity. The mean of all the mean values for each set is the same at both DS = 66% and 77%, with a tendency to decrease as DS further increases. Extrapolation to DS = 100% gives a value of about 3000°K, which has been used in Table 2 to adjust the data sets to a common temperature of 10°C. Note that this activation constant is somewhat higher than earlier data on water stored concrete [6].

5. CONCLUSIONS

- The resistivity of high performance concretes stored in water generally increases over time in the 12 year period covered. Fly ash containing concrete increases slowly but very strongly, while concrete with silica fume reaches very high resistivity early, but over years it may decrease somewhat. It is suggested that this is a consequence of the fact that silica fume is consumed early, leading to a subsequent gradual increase in pore water pH and thereby increased conductivity.
- Exposure to sea water for 10 years did not cause reduced resistivity for any concrete. Thus, the positive aging effects more than compensate for the intrusion of chlorides. For concretes more than 50 mm from the exposed surface the chloride content was insignificant, but the resistivity clearly lower than near the surface
- 12 years water cured high performance concrete was desorbed to 88%, 77% and 66% degree of saturation. The measured conductivity for the high performance concretes dropped sharply from DS = 100% to perhaps DS = 95% , indicating that very little water removal is needed to interrupt the continuity of the capillary pores responsible for the most effective charge transport. For Norwegian coastal concrete structures the level of the reinforcement generally has a degree of saturation in the range 80 – 90% (above the splash zone). Therefore, when assessing corrosion rates the relevant resistivity value is not the one measured after water storage.
- Traditional bridge concrete with w/c greater than 0.5 displays a more gradual drop in conductivity as water is removed, as expected because of the higher content of continuous (capillary) pores.
- The temperature sensitivity of the resistivity in the range 1.5 – 40°C is characterized by the Arrhenius equation with an activation constant in the range of 3500 – 3000 °K, the latter value being reached near saturation.

ACKNOWLEDGEMENTS

The authors greatly acknowledge the Norwegian Public Roads Administration and the Norwegian University for Science and Technology for their support. Furthermore we wish to thank F. Askeland for allowing us to use some of his results.

REFERENCES

[1] Liestøl, G, Kompen, R., Sellevold, E.J. and Isaksen, H.R. "Development of Chloride Resistant Concrete", Norwegian Road Directorate (Bridge Section) Reports 95-07 (199), 96-08 (1996) and 98-10 (1998). Oslo, Norway. In Norwegian.

[2] Isaksen, H.R. "Development of Chloride Resistent Concrete", Norsk Betongdag 1997, Proceedings, Norwegian Concrete Association, Oslo. In Norwegian.

[3] Sellevold, E.J. 1997. Resistivity and humidity measurements of repaired and non-repaired are in Gimsøystraumen bridge. Proceedings of the International Conference Repair of Concrete Structures. From Theory to Practice in a Marine Environment: Svolvær, Norway, 28-30 May 1997: Norwegian Road Research Laboratory.

[4] Larsen, C.K., "Influence of concrete composition on long term chloride ingress," Proceedings - International Conference on Bridges 2006, Dubrovnik, Croatia, May 2006.

[5] Askeland, F. "Elektrisk Motstand på Betong ved forskjellig DS og Temperatur". MSc-thesis, Dept.of Structural Eng., NTNU, Trondheim, June 2005.

[6] Østvik, J.M. "Thermal Aspects of Corrosion of Steel in Concrete", Doctoral Thesis at NTNU, Trondheim 2005:5. ISBN 82-471-6868-5 (Electronic Version).

[7] Sellevold, E.J. and Farstad, T. 2005: The PF-method – A Simple Way to Estimated he w/c-ratio and Air content of Hardened Concrete". Proceedings of Con. Mat'05 and Mindess Symposium, UBC, Vancouver 2005.

[8] Justnes, H., Sellevold, E.J. and Lundevall, G. "High Strength Concrete Binders, Parts A and B", CANMET/ACI Proceedings, Istanbul 1992, ACI SP 132-47.

[9] Relling, R.H. and Sellevold, E.J. "In Situ Moisture State of Coastal Concrete Bridges" Proceedings "Concrete Repair, Rehabilitation and Retro fitting", Cape Town, Nov. 2005.

[10] Larsen, C.K. "Chloride Binding in Concrete. Effect of Surrounding Environment and Concrete Composition", Dr.ing. Thesis, NTNU, Trondheim, 1998:95. ISBN 82-471-0 337-0.

[11] Sellevold, E.J. and Bager, D.H. "Low Temperature Calorimetry as a Pose Structure Probe", Proceeding 7th Int. Conf. on the Chem. Of Cem., Vol. 4, Paris 1980.

Paper 3 ELECTRICAL RESISTIVITY OF CONCRETE. PART III: LONG TERM FIELD MEASUREMENTS ON CONCRETE ELEMENTS IN THE TIDAL ZONE

C.K. Larsen [(1)], J-M. Østvik [(1)], E.J. Sellevold [(2)] and Ø. Vennesland [(2)]

[(1)] Norwegian Public Roads Administration, Technology Dept., Oslo, Norway

[(2)] Norwegian University for Science and Technology, Dept. for Engineering Science, Trondheim, Norway

Abstract

Beams made with a variety of high performance concretes, and with embedded electrodes to measure resistivity, were produced in a full scale plant. The beams were exposed on the West-coast of Norway so that one electrode pair was in a part of the beam always submerged in sea-water, one pair in the tidal zone and one pair always above the sea-water.

The resistivity of all concretes was measured periodically over an eight year period, either by an automatic monitoring system at 100Hz or manually with a hand-held device at 1000Hz. The interplay of temperature- and water-level variations in a typical 24 hour period is analyzed with a view to eliminate the two effects on long term data. The goal is to determine the true resistivity development which is believed to be the main factor influencing on the rate of reinforcement corrosion.

The eight year development for the different concretes, each with the three different exposure conditions is discussed.

1. INTRODUCTION

The Norwegian Public Roads Administration (NPRA), as the owner of several hundred large concrete bridges in harsh marine environment, initiated a large research project focusing on deterioration and durability of reinforced concrete, "Development of chloride resistant concretes", in 1993. The project, still running today, involved extensive laboratory investigations in addition to field exposure of various types of reinforced concrete elements made from 31 different concrete types. Phase I (started in 1993) of the project involved 17 different concretes, whereas Phase II (started in 1997) involved another 14 different concretes. More information on the project and some chloride ingress results can be found in [1, 2, 3].

In Phase II monitoring of some corrosion parameters were initiated in 1999. This involved automatic measurements of the electrical resistance (converted to resistivity by calculation) of concrete and the rate of oxygen reduction (cathodic effectiveness) for the various concrete types.

As stated in Part I, our interest in concrete resistivity is at least two-fold. For this project emphasis has been put on resistivity as a corrosion parameter and how it is influenced by concrete composition (concrete quality) and variation over time and different exposure conditions. This paper reports some results from the monitoring of the electrical resistivity of concrete over a period of eight years.

2. EXPERIMENTAL

2.1 Concrete types and elements

The concretes in Phase II were designed to represent both past, present and future concretes used in Norwegian coastal bridges. Note that all concretes were full scale mixed at a concrete factory and cast under realistic conditions to represent "real-crete" and not "lab-crete". Also note that the experimental setup does not involve a systematic variation of parameters, but is more based on producing workable concretes expected to achieve good durability properties by means of different binder compositions.

The concrete qualities span from a pure OPC concrete with w/c-ratio 0.56 to an OPC concrete with 9% silica fume and a w/b-ratio of 0.32. There are six concretes with various three-powder mixes (OPC/PFA/CSF; OPC/BFS/CSF). Table 1 shows the mix proportions of all 14 concretes without additives. All concretes were mixed using the same plastizers, super-plastizers and air-entraining additives in varying amounts in order to produce concretes with good workability.

For each concrete type, three different types of reinforced elements were made: 3m long beams, 15 x 30 cm in cross-section; 1m high pillars, 30 x 30 cm in cross-section; and 1.5 x 0.75 m big slabs, 20 cm thick. The beams, which are the subject of this paper, have been exposed in the tidal zone in the western part of Norway since 1998. Six beams were made of each concrete type: two beams were exposed un-cracked, cover depth 25mm; two were cracked in the middle section and exposed to sea water with the cracks left open (tensioned by bending), cover depth 25mm; and two un-cracked beams with cover depth 60mm. One beam of each type was produced with cast-in electrodes, i.e. three beams of each concrete type have cast-in electrodes. The electrodes are simply reinforcement steel bars 40cm long with diameter 12mm. The placement of both beams, and electrodes in the beams, is such that the three electrodes in each beam are situated in a) purely atmospheric; b) tidal; and c) purely submerged conditions, respectively. Figure 1 shows the details of beams and electrodes.

Table 1 Mix proportion of the concretes, constituents in kg/m^3

Concrete	*Cement*	*PFA*	*BFS*	*CSF*	*Water #*	*Sand*	*Gravel*	*w/b*	*Cement type*
1	326	-	-	-	181	939	886	0.56	CEM I
2	365	-	-	15	180	932	880	0.47	CEM I
3	374	-	-	34	192	861	881	0.47	CEM I
4	378	-	-	34	181	872	898	0.44	CEM I
5	312 *	79	-	16	175	885	918	0.43	CEM II/A-V
6	389 **	-	-	35	186	827	932	0.44	CEM I
7	139 ***	-	254	16	165	889	920	0.40	CEM III/A
8	338	84	-	17	186	795	926	0.42	CEM I
9	443	-	-	40	153	823	913	0.32	CEM I
10	360 *	90	-	40	165	814	928	0.34	CEM II/A-V
11	406	101	-	20	173	742	922	0.33	CEM I
12	384	95	-	19	169	798	926	0.34	CEM I
13	435	-	-	25	185	738	587 ¤	0.40	CEM I
14	406	-	-	34	188	707	591 ¤	0.43	CEM I

\# Free water content (total water minus absorbed water in the aggregate)

* PFA blended OPC; 20% PFA/80% OPC

** Sulphate resistant OPC

*** BFS blended OPC; 65% BFS/35% OPC

¤ Light weight aggregate (high strength)

2.2 Measurements

The electrical resistance was measured between the electrode at each of the three positions (a-c) and the main reinforcement in two different ways:

- Continuously, with an automatic monitoring system with data logging capabilities.
- Manually, with a hand-held device from time to time over the exposure period.

The data logging equipment has capacity to continuously monitor all three beams (i.e. nine resistances) of one concrete type at the same time. This means that over the same period of time only one concrete type is monitored, i.e. a direct comparison between different concrete types over the same period of time is not possible. However, with this setup we get a lot of good data for the chosen concrete to evaluate different exposure conditions (position) and the influence of cover depth. To measure all concretes almost at the same time, one has to switch from one concrete to the other consecutively. This has to be done by physically un-plugging and re-plugging the measurement cable from the DSUBs that connects the nine electrodes in each concrete type (one DSUB for each concrete type). This has been done several times in different seasons with different temperatures to get comparable data from all concrete types. The monitoring system is measuring the resistance at 100Hz ("ResMes" device from Protector AS in Norway), and the logging interval can be adjusted to any given interval down to one measurement every second ("Camur" data logger from Protector AS). Normally the

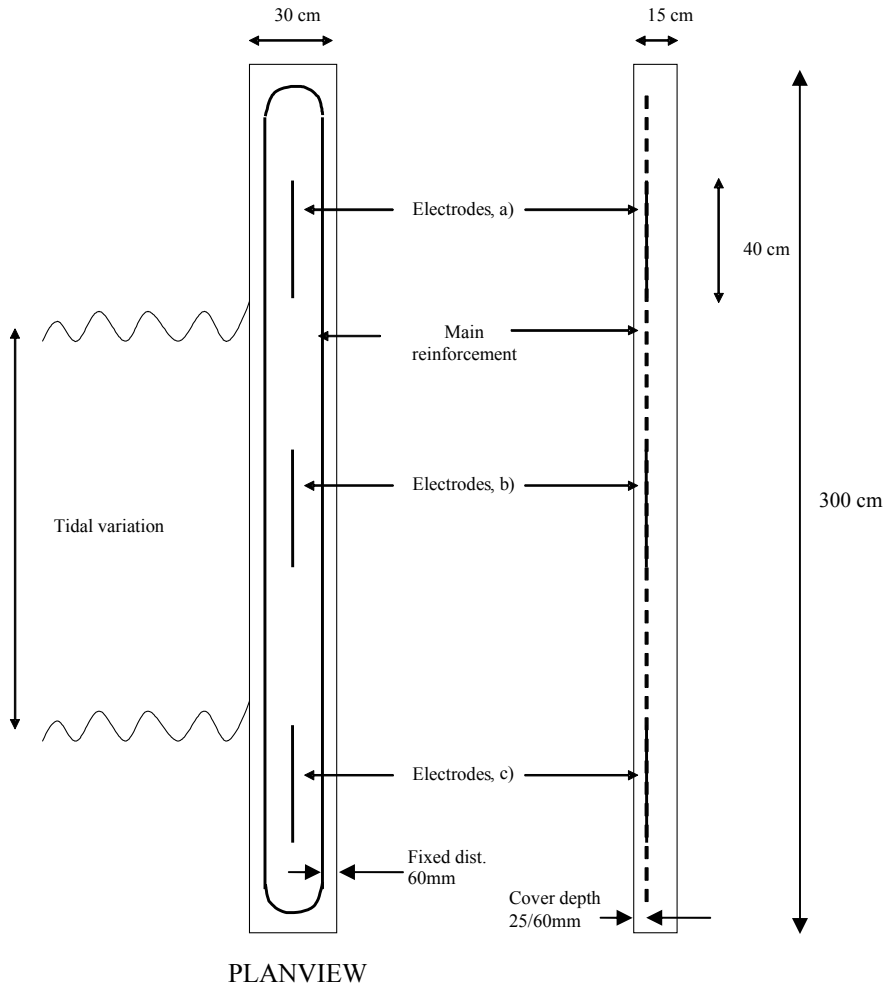

Figure 1 Reinforced beams with electrodes at three positions

logging interval is one measurement every hour. Data is downloaded to a desktop computer in the office using a modem and lately via Internet.

The manual measurements were done at 1000 Hz with a hand-held LCR-meter (potential square pulse), type Escort ELC-131D. This has been done occasionally to control the measurements made by the monitoring system. As concluded in Part I, there is practically no difference between measurements taken at 100Hz and 1000Hz in relatively wet concrete. To verify this, a systematic comparison between the "ResMes" device and the hand-held device, which has the ability to measure at both 120Hz and 1000Hz was carried out.

In addition to the resistance measurements, air, sea-water and concrete temperatures at positions a) - c) (at 25mm depth) were automatically monitored (thermocouple type T) along with the tidal variation (high precision water-pressure sensor).

2.3 Converting from resistance to resistivity

To convert from resistance, the measured value, which depends on the electrode configuration, to resistivity, which is a material parameter (dependant of moisture content and temperature, among other factors), one can use two parallel electrodes in a homogenous media as a model:

$$\rho = \frac{\pi \cdot L}{\cosh^{-1}\left(\frac{d}{2r}\right)} \cdot R = k \cdot R \qquad (1)$$

where	ρ	=	resistivity	[Ωm]
	L	=	length of the electrodes	[m]
	d	=	distance between the two electrodes	[m]
	r	=	radius of the electrodes	[m]
	R	=	measured resistance between the two electrodes	[Ω]
	k	=	conversion factor	[m]

In this case:

L	=	0.400 m
d	=	0.090 m
r	=	0.006 m

which gives $k = 0.464$ (unit: m).

The electrode configuration implies that there are two equal concrete resistances in parallel, which leads to a total resistance, R_{tot}, which is the actual measured resistance in this investigation:

$$R_{tot} = \frac{1}{2} \cdot R \qquad (2)$$

The concrete resistivity is therefore:

$$\rho = k \cdot R = 2 \cdot k \cdot R_{tot} = 0.93m \cdot R_{tot} \qquad (3)$$

In other words, all reported concrete resistivities in this paper are the measured resistances multiplied with 0.93m.

It must be emphasized that eq. (3) is most likely not correct in the sense that the conductive path (the current distribution) does not exactly follow the length of the shortest electrode (one of the three electrodes in pos. a)-c)). The main reinforcement is much longer than the three electrodes and acts as the “counter electrode”. Thus, the effective L in (1) is probably longer leading to a bigger conversion factor than 0.93m. It is also possible that the increase in L depends on the resistivity of the concrete. A higher resistivity will most likely tend to narrow the current distribution, i.e. the higher the resistivity the lower conversion factor. In the extreme, with a current distribution at an angle of 45°, the conversion factor will be doubled. Nevertheless, for any given concrete this conversion factor is assumed to be constant, thereby justifying a comparison over time and between exposure conditions. A detailed comparison between the various concrete types will, however, be affected by this uncertainty.

3. RESULTS AND DISCUSSION

3.1 Comparison of measurements at 100Hz, 120Hz and 1000Hz

As can be seen from Table 2, measurements at 1000Hz ("Escort") yield a somewhat lower concrete resistivity compared to measurements at 100Hz ("ResMes"), as verified by the laboratory findings in Part I. The resistivity was on average 4% lower at 1000Hz compared to 100Hz, nearly the same as found in Part I for wet concrete (se Table 2 in Part I). Thus, measurements from the monitoring system and the hand-held device are comparable. Furthermore, there is no reason to question the measurements done with the "ResMes" device at 100Hz as measurements done with the hand-held device were in good agreement with EIS (Electrochemical Impedance Spectroscopy) as indicated in Part I, as long as the concrete is relatively wet (as the field concrete is) and the temperature is not too low (as it seldom is along the West-coast of Norway and never in the submerged condition!).

Table 2 Comparison of concrete resistivities ("as-measured") at various frequencies, unit Ωm. Measurements taken August 18th 1999 on beam 3

Concrete	*Position a)*			*Position b)*			*Position c)*		
	100Hz	120Hz	1000Hz	100Hz	120Hz	1000Hz	100Hz	120Hz	1000Hz
1	90	90	88	77	77	75	58	58	56
10	1497	1535	1482	849	802	769	738	731	705
14	652	649	638	374	372	361	399	396	384

Water level and concrete temperature not measured
100Hz: "ResMes"@ 100Hz; 120Hz: "Escort"@ 120Hz; 1000Hz: "Escort"@ 1000Hz

3.2 Tidal effects on resistivity measurements

In order to investigate the effect of the tidal variation the data logger was periodically programmed to make frequent measurements during a few days. Typically, measurements of resistivity, temperature and water-level were taken every five minutes. The following results were taken in March 2006 on concrete no. 1 (the one with highest w/c-ratio and no pozzolanic materials).

Figure 2 shows the temperature variation for the three electrode positions a)-c), together with the air- and sea-water temperatures. The corresponding resistivities ("as-measured" without any compensation except the transition from resistance to resistivity, according to (1)) are given in Figure 3 and 4 for beam 1 (cover depth 25mm) and beam 5 (cover depth 60mm), respectively.

It is clear from Fig. 2 that the sea-water strongly influences the concrete temperature in position b), i.e. the electrode position within the tidal variation. The concrete temperature in pos. b) drops markedly when the sea-water drops below the measuring point at pos. b) (exactly at height 1.50m, see Fig. 3), then gradually decreases in this case towards the air-temperature (or the concrete temperature at pos. a), whichever is the "nearest") until the sea-water again reaches the measuring point with an instant rise in concrete temperature as a result. The concrete temperature in the submerged part (pos. c)) is stable at a temperature about 1°C lower in this case than the sea-water temperature. The concrete temperature in pos. a) (atmospheric) follows more or less exactly the time variation of the air-temperature. However, there is a time-lag of between about 30 and about 90 minutes before the concrete temperature responds to a change in the air-temperature. This is of course attributed to the much higher heat-capacity of concrete compared to air.

Keep in mind, when evaluating the temperature variation in Fig. 2 that the absolute accuracy of the temperature measurements (thermocouple type T) is about ± 0.5°C, thus the 1°C difference between pos. c) and sea-water is probably not real.

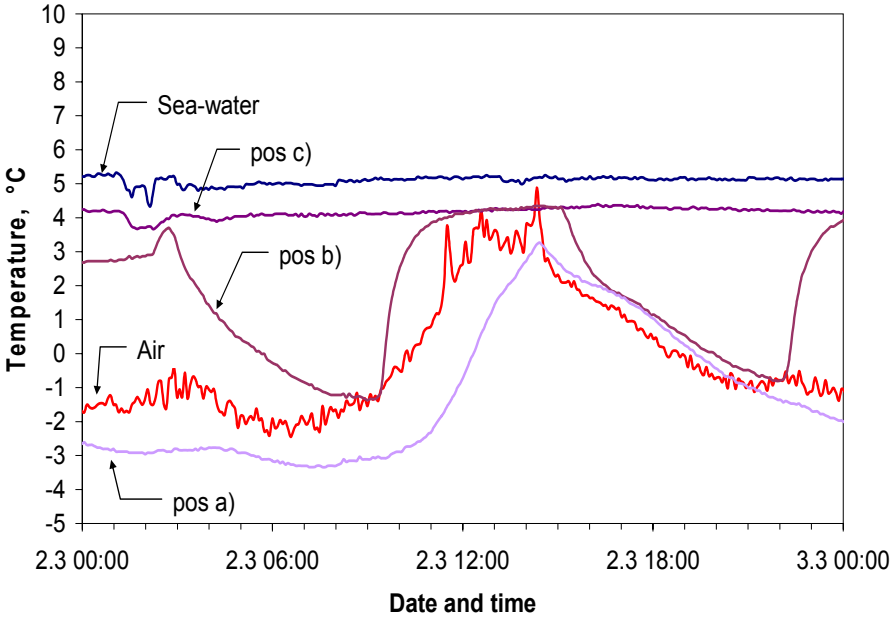

Figure 2 Temperature variations during a 24h period in March 2006

It is quite obvious from Figs. 3 and 4 that the "as-measured" resistivities are influenced by changing exposure conditions, i.e. temperature, position, and tidal variation (water level). The first thing needed to be done with the "as-measured" resistivities is of course a temperature compensation, as the temperature varies relatively much during the 24h period, as seen from Fig. 2. In order to compare the various resistivities, as functions of concrete composition, time and exposure condition (which influences the degree of saturation of concrete (DS) and the chloride content), the "as-measured" values have been adjusted from the original temperature (the concrete temperature at the corresponding position at the time of measurement) to a value that represents 10°C using the Arhenius equation with an activation energy constant of 3500K (corresponding to an activation energy of 28.5 kJ/mole). This value will be discussed later.

Figures 5 and 6 show the temperature compensated resistivities @10°C for beam 1 and 5, respectively.

Looking at Figs. 5 and 6 reveals at least three important observations: 1) the level of the measured resistivities for beam 1 is reasonable and within the expected range compared to similar concrete in Part II, and manual measurements (see later); 2) the resistivities in beam 5 is about twice as high as the resistivities in beam 1; and 3) most of the "tidal influence" in Figs. 3 and 4 was apparently due to temperature effects as the temperature compensated resistivities became more stable with time. The first observation justifies the use of Eq. (3) to calculate resistivity from resistance, i.e. the uncertainty connected to the value of the conversion factor is small, and will not be further discussed in this paper. The second observation must be real as the three electrodes in each beam verify each other. The reason why beam 5 yields twice the resistivity of beam 1 is difficult to explain. The obvious explanation is perhaps connected to electrode depth, as the cover in beams 1 and 5 are 25mm and 60mm, respectively. Concrete 1 is the only concrete made purely of OPC. McCarter et.al [4] found large variation in the conductivity with depth within the cover zone (5-50mm) for a concrete made of purely OPC. The conductivity at the outer part was about 2.5 times higher

than the inner part. In terms of resistivity, this means that the inner part of that OPC concrete had about 2.5 time's higher resistivity than the outer part, i.e. in good agreement with the second observation stated above. The third observation, however, has two major implications: I) the temperature compensation is basically successful; and II) there are obviously some effects left to explain as the curves are not horizontal nor perfectly smooth, as one should expect if no other effect than temperature is dominant over the 24h period. Possible explanations and their implications will be discussed in the following:

One explanation might be that the chosen activation constant is not correct or that the activation energy changes with changing exposure condition, as found in [5] and as stated in Part II. Looking at Fig. 5, pos. a) at about noon the 2nd March there is a sudden and rather big increase in resistivity over a period of about three hours. In that period, the concrete temperature in pos. a) increases rapidly from about -3°C up to about +3°C. It might be possible that the activation energy changes as a result of the rapid change in temperature and the fact that the change takes place around the freezing point of water. To compensate for this, the activation constant has to be gradually changed from 3500K up to about 5000K and then down to 3500K again. It is hard to believe that this is the case, but it must be admitted that the variation in activation constant from 3500K to 5000K is not unreasonable, and within the range as found in [5].

This sensitivity to the activation constant may have significant influence on the usefulness of resistivity measurements to estimate changes in moisture content and ionic strength in the pore solution. The reason for this is simple: using an activation constant of about 5000K on the whole 24h period will lead to practically overlapping curves for positions a), b), and c) at 10°C, i.e. there are no other effects than temperature. However, a lower activation constant, e.g. 3000K (or even lower) will lead to a higher resistivity at 10°C in pos. a) than in pos. c), which we then could interpret as lower moisture content in pos. a). The point is: without knowing the correct activation constant when compensating for temperature, erroneous conclusions can be drawn.

Assuming that the correct activation constant has been used, one could explain the resulting variation as changes in DS or even changes of the ionic strength of the concrete pore solution. However, bearing in mind that the moisture state in concrete changes very slowly [6,7] and that the ionic strength, especially the OH^- concentration, is so high that any change due to the moderate change in temperature in this case [8], will likely not significantly influence the resistivity (or more precisely, the conductivity of the pore solution).

A different explanation for the variation in the temperature compensated resistivities might be that the electrode configuration involves geometrical effects as the water-level changes and thereby affects the conductive path. Keep in mind that the distance between the electrodes is 90mm, whereas the distance from the electrodes to the surface (and thereby to the sea-water) is only 50mm (two times 25mm) for beam 1 (and 120mm (2*60mm) for beam 5). The point is not followed up further in this paper.

Finally, a possible explanation could be that the measured temperature (it was measured in one point at the middle of the electrode length) and the concrete temperature along the electrode are not equal, i.e. the observed anomalies may be attributed to temperature gradients in the system.

To summarize: even though there are a few uncertainties connected to the resistivity monitoring results, and a full interpretation of any deviation from the expected smooth behavior of the temperature compensated resistivities is not given, it is concluded that the monitoring system provides us with resistivity levels. These levels are accurate enough to be used to evaluate this important durability parameter as a function of concrete composition and exposure condition over time in field concrete.

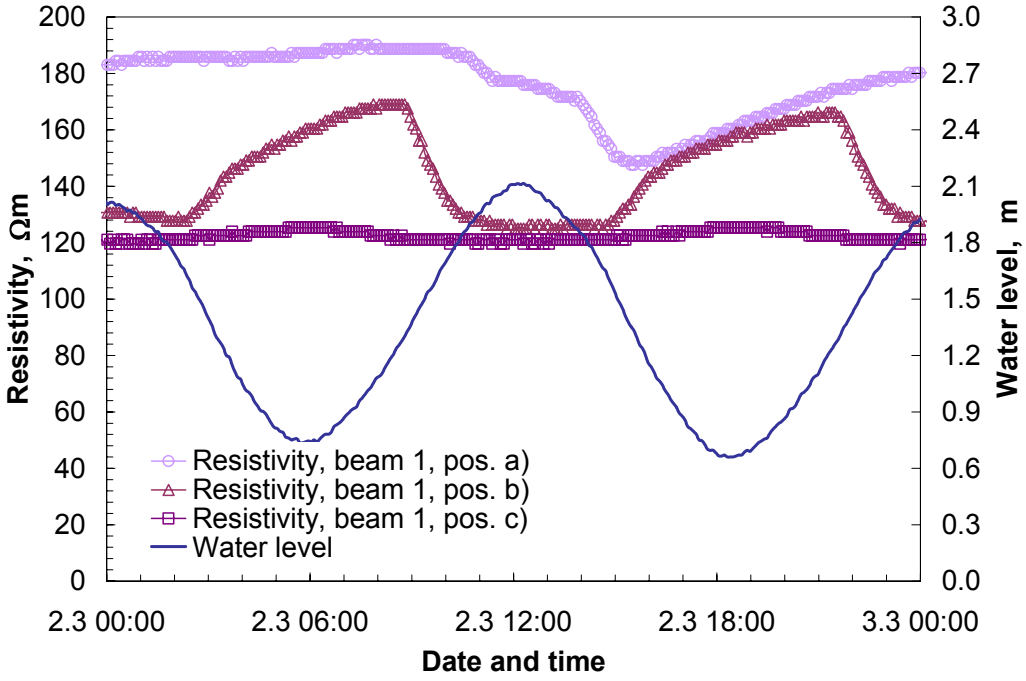

Figure 3 Variation of the "as-measured" resistivity during a 24h period. Beam 1 (depth 25mm); concrete 1.

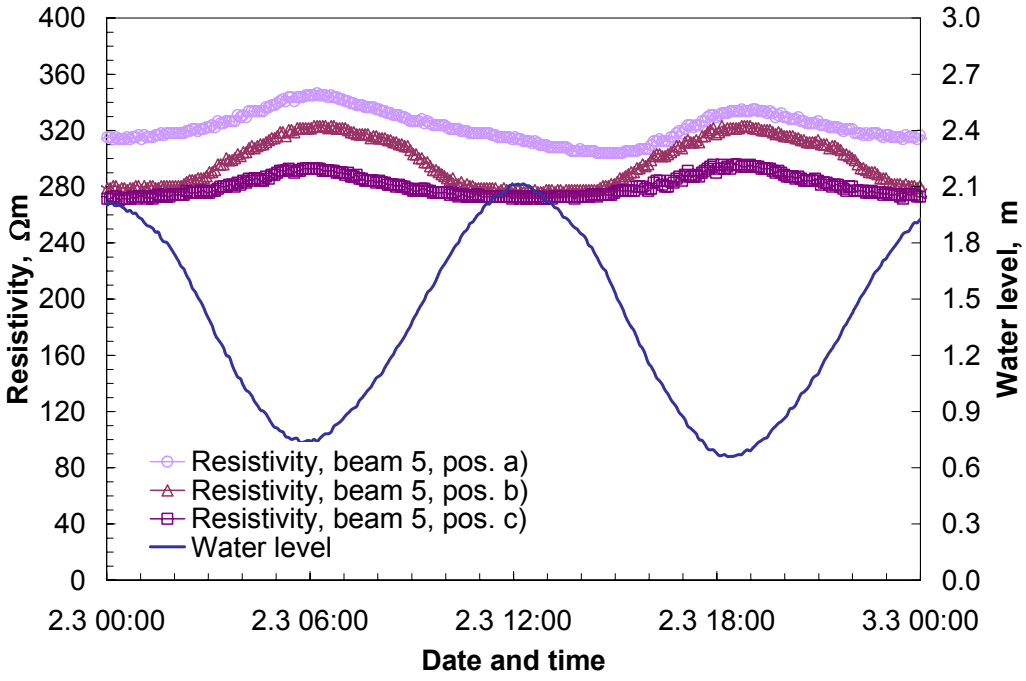

Figure 4 Variation of the "as-measured" resistivity during a 24h period. Beam 5 (depth 60mm); concrete 1.

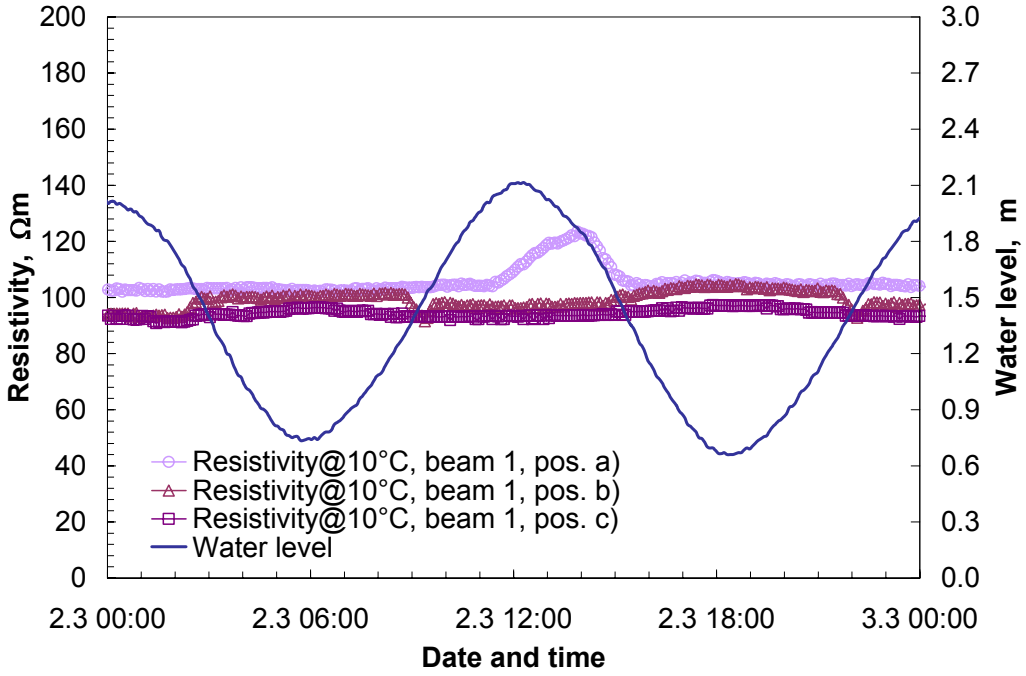

Figure 5 Variation of the resistivity @10°C during a 24h period. Beam 1 (depth 25mm); concrete 1.

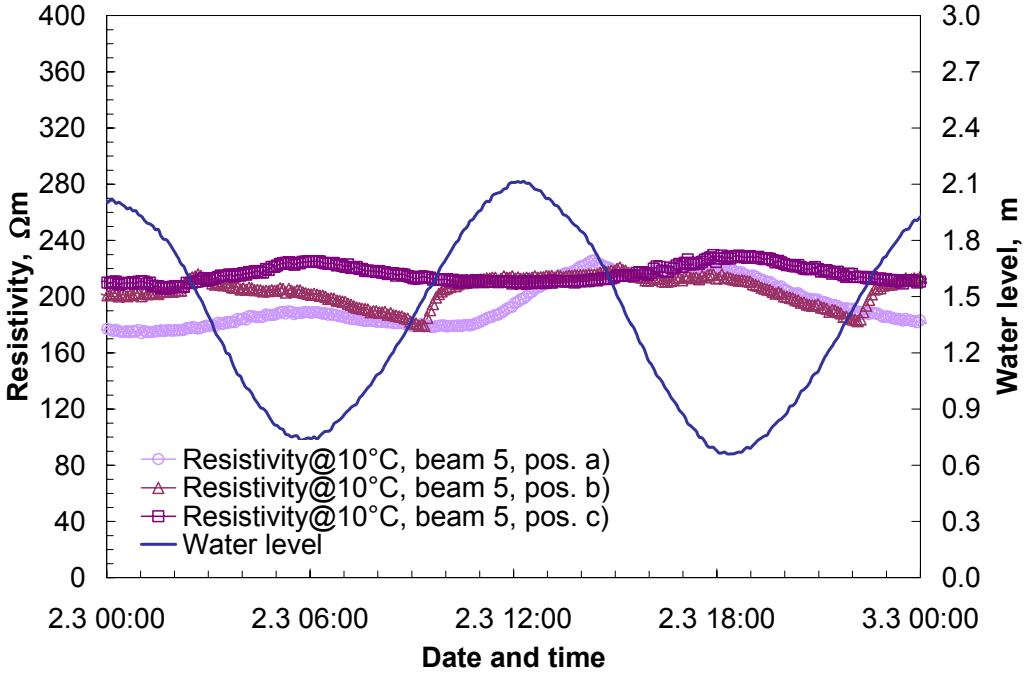

Figure 6 Variation of the resistivity @10°C during a 24h period. Beam 5 (depth 60mm); concrete 1.

3.3 Variation of resistivities over time

Tables 3 and 4 give the field resistivities for the various concretes and electrode position for all beams initially and after about eight years of exposure, respectively.

Looking at Tables 3 and 4 reveal interesting data on the magnitude of concrete resistivity over time. To sort out significant effects, average values for position, concrete quality (binder composition) and time were calculated. Average values are given in Tables 5 and 6. Note that the given averages, for clarity, only include resistivities from the nine concretes that have complete data sets (concretes 2, 3, 4, 6, 9, 10, 12, 13, 14).

Table 5 reveals that the concrete resistivity generally increases over time, and that the increase is influenced by exposure condition. For the atmospherically exposed concrete (pos. a)) the resistivity after 8 years exposure is 2.8 times higher, whereas for the submerged concrete (pos. c)) the factor is only 1.8. The aging effect is more pronounced for the atmospherically exposed concrete. The aging effect is most likely a combined effect of changes in DS, pore water composition, and refinement of the pore structure. A similar aging effect was also found by McCarter et.al [4]. Another important observation from Tab. 5 is the overall averages for the various beams. Both initially and after 8 years of exposure, there is no significant difference in resistivity measured in beam 1 compared to beam 5. This might contradict the differences found for concrete 1 as seen in Figs. 5 and 6. However, concrete 1 is the only pure OPC concrete investigated (and also the one with highest w/c-ratio). The findings of McCarter et.al [4] for field exposed concrete support this in that they found that their OPC concrete was significantly more influenced by cover depth than their GGBS and PFA blended concretes.

One of the most significant finding, and at least the most interesting with respect to durability and service life, is clearly shown in Table 6. Initially, the PFA-blended concretes have relatively low resistivity compared to the CSF-blended concretes. However, after 8 years the picture is totally different. The resistivity of the PFA-blended concretes has increased with a factor of more than one order of magnitude (11.3) for position a), whereas the corresponding factor for the CSF-blended concretes is 2.3. For position c) the factors are 6.9 and 1.6, respectively. These results are expected when considering that CSF is practically fully reacted after a few months of hardening [9], while PFA reacts much slower. However, the magnitude of the difference between CFS and PFA concretes is greater than expected.

The increase in resistivity over time for the PFA-blended concretes is attributed to the slow pozzolanic reaction of PFA, producing refinement of the pore structure and possibly also changes in the pore solution chemistry. Both the significant increase over time and the magnitude of the resistivity values, strongly indicate that the long-term durability properties related to reinforcement corrosion are significantly better for PFA-blended concretes. With resistivity values above 1000Ωm the corrosion rate is supposed to be insignificant [10], i.e. it is likely, in the event of reinforcement corrosion initiation, that the corrosion rate in PFA-blended concretes is negligible. This is of course of great importance for any owner of concrete structures in marine environments.

Table 3 Initial concrete resistivities @10°C, unit Ωm. Measurements on exposed elements taken June 1998 at 1000Hz (hand-held device). Concrete age: about 8 months.

Concrete	*Beam 1*			*Beam 3*			*Beam 5*		
	a)	b)	c)	a)	b)	c)	a)	b)	c)
1	64	63	65	61	64	60	58	62	59
2	150	140	137	145	120	130	127	138	135
3	216	203	190	226	174	196	201	202	194
4	392	354	321	401	256	336	396	422	393
5	227	214	184	221	145	178	203	196	199
6	335	288	265	326	229	260	294	321	279
7	215	184	180	208	149	175	179	170	180
8	299	286	241	308	238	245	285	271	252
9	882	867	716	840	485	721	836	881	875
10	744	763	509	739	505	551	738	764	684
11	401	438	342	421	352	354	422	438	406
12	373	381	286	345	289	276	308	308	284
13	338	365	319	354	311	322	283	322	330
14	353	305	321	391	248	349	259	271	289

Water level: not measured, but estimated to be about 1.4m
Concrete temperature at pos. a): ~14°C b): ~11°C c): ~11°C

Table 4 Concrete resistivities @10°C after 8 years exposure, unit Ωm. Measurements on exposed elements taken January 2006 at 1000Hz (hand-held device).

Concrete	*Beam 1*			*Beam 3 **			*Beam 5*		
	a)	b)	c)	a)	b)	c)	a)	b)	c)
1	106	101	88	81	119	167	n/a	n/a	n/a
2	264	216	165	147	271	199	198	288	129
3	426	363	278	486	402	353	362	301	236
4	953	709	450	979	878	592	861	700	485
5	1446	1020	581	1335	538	819	1164	916	n/a
6	619	517	350	578	513	443	485	443	301
7	n/a	n/a	n/a	732	607	483	n/a	n/a	n/a
8	1494	1044	683	1410	1210	901	1495	1092	n/a
9	1609	1215	722	1543	1399	1049	1441	1239	807
10	3068	2136	1099	2567	2542	1593	2632	2157	1334
11	2127	1614	910	1934	1827	1313	2042	1438	n/a
12	2396	1716	901	1912	1757	1213	2107	1424	1019
13	750	665	553	819	788	750	652	595	563
14	780	594	470	714	579	717	642	548	526

Water level: 1.2m
Concrete temperature at pos. a): ~0.5°C b): ~2.0°C c): ~5.5°C
* Beams were measured on land, 2 days after removal from sea-water, air temperature about 2.5°C
n/a: unstable measurements (unknown reason)

Table 5 Average concrete resistivities @10°C as function of time and position, Ωm. Measurements on exposed elements at 1000Hz (hand-held device).

Exposure time	*All beams*			*All positions*		
	Pos. a)	Pos. b)	Pos. c)	Beam 1	Beam 3	Beam 5
Initially	407	367	358	389	353	390
8 years	1111	924	641	888	955	832

Table 6 Average concrete resistivities @10°C as function of binder composition, Ωm. Measurements on exposed elements at 1000Hz (hand-held device).

Binder comp.	*All beams initially*			*All beams after 8 years*		
	Pos. a)	Pos. b)	Pos. c)	Pos. a)	Pos. b)	Pos. c)
PFA blended	216	201	173	2447	1955	1193
CSF blended	323	288	295	729	630	483

4. CONCLUSIONS

The electrical resistivity of field exposed concrete elements has been measured over a period of eight years. Measurements were made at 100Hz with an automatic monitoring system, and at 1000Hz with a hand-held LCR-meter. For field measured resistivities it is important to compensate for temperature in order to evaluate effects of time and of exposure condition.

Temperature compensation using the Arhenius equation with an activation constant of 3500K gave reasonable values. However, the value of the activation constant has a significant influence when attempting to evaluate effects other than temperature (e.g. moisture content, ionic concentration, and aging).

The concrete resistivity increases significantly over time due to various aging effects. The increase is influenced by exposure condition and concrete composition. For atmospherically exposed concrete the aging effect is more pronounced than for concrete in submerged conditions. For PFA-blended concretes the increase in resistivity is more than one order of magnitude after eight years exposure in the atmospherically exposed concrete. The corresponding increase for CFS-blended concretes is a bit more than a factor two.

Using resistivity as a durability parameter related to corrosion rate puts PFA-blended concretes in a very beneficial light. Any corrosion being initiated in the PFA-blended concretes is supposed to be insignificant due to the very high resistivities over time.

ACKNOWLEDGEMENTS

The authors greatly acknowledge the Norwegian Public Roads Administration for their financial support of this work.

REFERENCES

[1] Liestøl, G, Kompen, R., Sellevold, E.J. and Isaksen, H.R. “Development of Chloride Resistant Concrete”, Norwegian Road Directorate (Bridge Section) Reports 95-07 (199), 96-08 (1996) and 98-10 (1998). Oslo, Norway. In Norwegian.

[2] Isaksen, H.R.; Liestøl, G.; Giæver, N.A.; Kompen, R.; Sellevold, E.J. 1998. Development of a chloride-resistant concrete. Part 1, Laboratory tests and concrete properties. *Concrete under severe conditions 2*. Gjørv, O.E., Sakai, K. and Banthia, N. (eds), Tromsø, E&FN Spon.

[3] Larsen, C.K., "Influence of concrete composition on long term chloride ingress," Proceedings - International Conference on Bridges 2006, Dubrovnik, Croatia, May 2006.

[4] McCarter, W.J., Chrisp, T.M., Starrs, G., Basheer, P.A.M., and Blewett, J., "Field monitoring of electrical conductivity of cover-zone concrete," *Cement & Concrete Composites* 27, pp. 809-817, 2005

[5] Østvik, J.M. "Thermal Aspects of Corrosion of Steel in Concrete", Doctoral Thesis at NTNU, Trondheim 2005:5. ISBN 82-471-6868-5

[6] Sellevold, E.J. 1997. Resistivity and humidity measurements of repaired and non-repaired are in Gimsøystraumen bridge. Proceedings of the International Conference Repair of Concrete Structures. From Theory to Practice in a Marine Environment: Svolvær, Norway, 28-30 May 1997: Norwegian Road Research Laboratory.

[7] Relling, R.H. and Sellevold, E.J. "In Situ Moisture State of Coastal Concrete Bridges" Proceedings "Concrete Repair, Rehabilitation and Retro fitting", Cape Town, Nov. 2005.

[8] Larsen, C.K. "Chloride Binding in Concrete. Effect of Surrounding Environment and Concrete Composition", Dr.ing. Thesis, NTNU, Trondheim, 1998:95. ISBN 82-471-0 337-0.

[9] Justnes, H., Sellevold, E.J. and Lundevall, G. "High Strength Concrete Binders, Parts A and B", CANMET/ACI Proceedings, Istanbul 1992, ACI SP 132-47.

[10] Andrade, C. & Alonso, C., "Corrosion rate monitoring in the laboratory and on-site", *Construction and Building Materials*, Elsevier Science Ltd., London, 1995, pp 315-328.

Paper 4 DRIVING FORCES TO CRACKING IN HARDENING CONCRETE: THERMAL AND AUTOGENOUS DEFORMATIONS

E. J. Sellevold and Ø. Bjøntegaard

The Norwegian University of Science and Technology, Department of Structural Engineering, Trondheim, Norway

Abstract
Thermal- and autogenous deformations are the primary causes of self-induced stresses in hardening concrete structures. Both types of deformations, and their interactions, are discussed and illustrated with examples from tests on different concrete compositions subjected to isothermal and realistic temperature developments.

For practical calculations of cracking risk in concrete structures, mathematical models for both types of deformations are needed. A strategy to develop such models is presented.

1. INTRODUCTION, BACKGROUND AND SCOPE

There is currently worldwide interest in early age cracking problems in high performance concrete (HPC) structures. HPC contain more binder producing more heat during hydration, and the low w/b-ratios imply finer pore structure resulting in strong self desiccation (low RH = relative humidity and high capillary tension). Both factors produce increased self-induced deformations relative to normal strength concrete – and also increased vulnerability to early cracking.

The widespread interest in early cracking has resulted in much research, and many conferences devoted exclusively to aspects of the topic since the RILEM conferences in München 1994 [1] and Paris 1982 [2], with proceedings: Trondheim 1996 [3], Hiroshima 1998 [4], Lund 1997, 1999 and 2002 [5,6,7], Paris 2000 [8], Sendai 2000 [9], Haifa 2001 [10]. Conferences with special sessions on the topic is the trend recently, for instance Phoenix 2002 [11], Colorado 2003 [12] and Evanston 2004 [13]. RILEM has had several committees on the topic; two completed TC 119-TCE München [1] and TC 181-EAS [10], and two currently working, TC 195-DTD and TC 196-ICC.

Much new information is therefore available on all the factors involved. The major factors in early cracking are illustrated in Figure 1a. Crack risk is assessed by comparing self-induced stress with the tensile strength during the hardening period. In FEM calculations the temperature and stress development over time at critical positions in structures are mapped out, based on concrete properties, structural configuration and environmental conditions. The important concrete properties (in addition to the heat development) are listed in the boxes: AD = autogenous deformation, CTE = coefficient of thermal expansion, E = elastic modulus, R/C = relaxation/creep and R = degree of restraint. The relaxation effect reduces the stresses generated (the product of the deformations and E), it is denoted R/C since it is generally based on creep experiments and models, which are converted to relaxation using linear viscoelasticity with aging effects. The restraint (R) is of course a result of structural geometry, restraint from adjoining structures and friction against ground.

The plot in Figure 1b illustrates stress developments for a simple case of a beam under uniaxial stress (i.e. the conditions in a typical TSTM-machine), t_0 [14] separates the hardening period from the initial period, and marks the time when the particular concrete has sufficient rigidity for the self-induced deformations to generate measurable stresses (about 0.10 MPa in a TSTM-machine, corresponding to t_0 = 8-12 hrs for a typical HPC at 20^{o}C. The figure illustrates both the initial heating producing compression and the subsequent tension as cooling occurs, for different degrees of restraint. Note that during heating the AD and the thermal effects tend to compensate, but during cooling both produce tension. Note that during cooling the temperature effect is of course always contraction, whereas AD may be both contraction and expansion, see later.

The stress generation during the hardening period can today be predicted quite well by calculations; since we are dealing with quite solid concrete whose properties can be measured and modeled. The initial period up to t_0, in contrast, is much less well understood since we are dealing with a complex liquid-semisolid-solid transition. However, the period is very important from a practical point of view since cracking often occurs here. The initial period is clearly a difficult, but important topic for research.

The accuracy of the hardening period calculations depends primarily on the quality of the input data on materials properties. Good data requires extensive and expensive testing. Lack of such data is today the biggest hurdle to full utilization of the many available FEM-programs. Possibly in the future the problem will be solved by establishing regional data bases using systematic sets of test.

This paper will not give any comprehensive review of the large literature now available. Interested readers are referred to the proceedings cited above as well as the periodic journals.

We will focus on the two deformation factors AD and CTE based on our own experiences since 1992, and extensive international cooperative programs; bilateral, RILEM and EU-based.

The two factors are of great importance since they are the very sources of stress generation. We will discuss the nature and characteristics of the two types of deformations – and, in particular, give a strategy on how to determine the two for practical use in calculation programs.

We note that Figure 1b and the following Figures 3 - 8 are based on a number of tests on the very same concrete; the concrete is denoted *Concrete 1* from this point. The concrete is made with CEM I (OPC), water-to-binder (w/b) ratio of 0.42, 5% silica fume of cement weight, paste volume=28% and 0-16 mm gneiss/granite aggregate. *Concrete 1* results are also part of Figure 9 and 11.

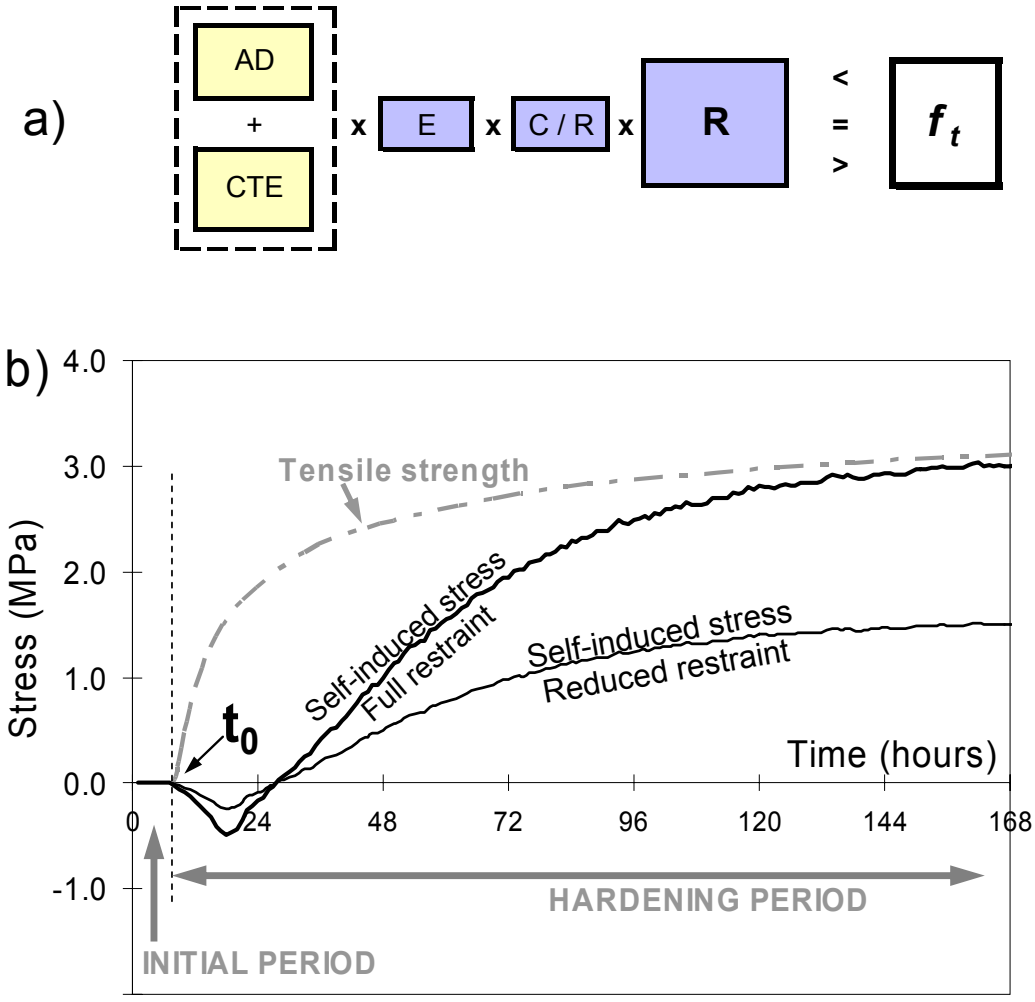

Figure 1: Principle of stress generation (a) and stress/strength development (b) in hardening concrete during a realistic temperature history (T_{max}=40 ^{o}C). Note that the self-induced stress at full restraint and the tensile strength are both from measurements on a typical HPC (*Concrete 1*, see later). Note also that the high stress development at full restraint generated failure in tension after 8 days (192 hours) [16].

2. AUTOGENOUS- AND THERMAL DEFORMATIONS

Figure 2 shows isothermal volumetric changes in cement paste from mixing – and illustrates clearly the concepts we are dealing with. The chemical shrinkage is the total volume change associated with the hydration reactions, while the volumetric AD is the external manifestation, for instance measured as the volume change of a rubber balloon filled with cement paste. The two curves coincide until the paste has built up sufficient rigidity to allow empty pores to form. From then on AD is much smaller than the chemical shrinkage. Note that the departure point is between initial and final set [15], while t_0 is well beyond final set. There appears to be general agreement that the basic cause of AD is the chemical shrinkage - and that the mechanism is capillary tension in the pore water generated by the air-water menisci in the partly empty pores. The process is geometry controlled, i.e. finer pores $\rightarrow$ smaller meniscus radius $\rightarrow$ larger capillary tension $\rightarrow$ lower relative humidity (RH) $\rightarrow$ generally more AD. This simple model explains the effects of w/c-ratio, silica fume, cement fineness etc. in a very satisfactory way.

For concrete AD is generally measured linearly. Typical 20 ^{o}C isothermal results are shown in Figure 3, where also the parallel self-induced stresses under full restraint are shown [4,16]. AD shows early strong contraction followed by expansion; the contraction we consider (at least partly) an artifact of the measuring system, but the expansion is real, caused by reabsorbtion of bleed water, and produces compressive stress as expected.

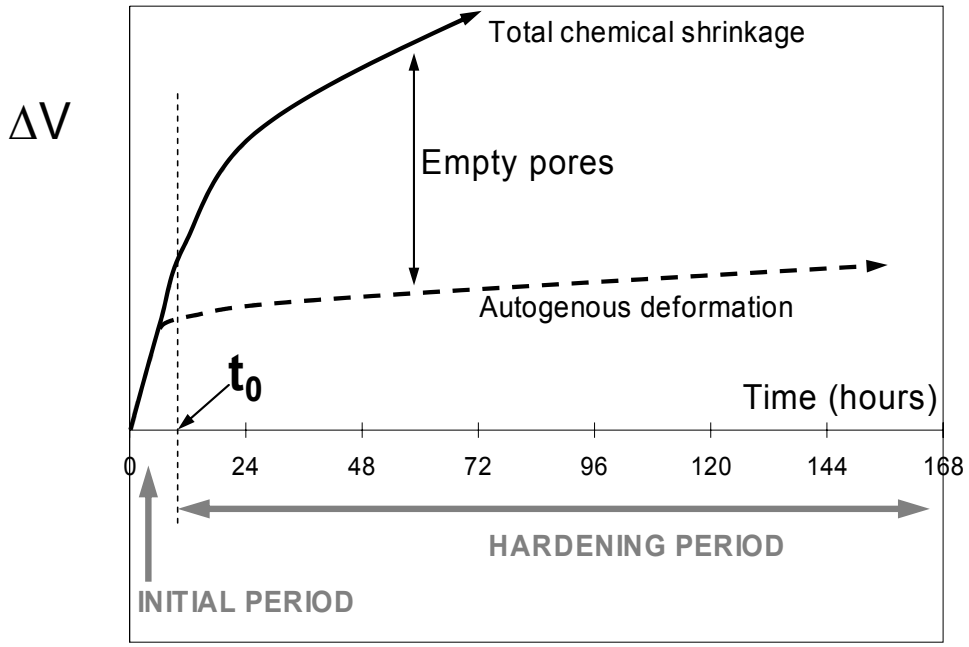

Figure 2: Total chemical shrinkage and volumetric autogenous deformation (shrinkage), isothermal conditions. Principle sketch.

The whole question of measurement system is very important – as evidenced by the large differences found on AD in the literature and from Round-Robin tests [22]. RILEM TC-195-DTD is currently working on the problem and will produce recommendations.

Concrete structures are of course subjected to elevated temperatures during hydration – typically with maximum around 24-48 hrs (up to 60-70^{o}C) followed by cooling. AD must therefore be known at various temperatures. Isothermal test are convenient in order to avoid thermal contributions. One set of such data is shown in Figure 4 [4,16]. Clearly the curves are unsystematic with respect to temperature variations – and no basis for predicting AD during variable realistic temperature conditions. The concretes were mixed and maintained at their

different temperatures. In order to give more realistic conditions in a new series, the concrete was kept at 20 °C for 6 hrs and then heated to different elevated levels. A series started at 13 °C was also done. Both results are given in Figure 5, after compensating for the thermal deformations during the early heating. The variation is much more systematic, but attempts to apply the maturity principle to produce common curves does not work very well [4,16].

Consequently we conclude that isothermal AD data is of little use in predicting AD under realistic temperature conditions.

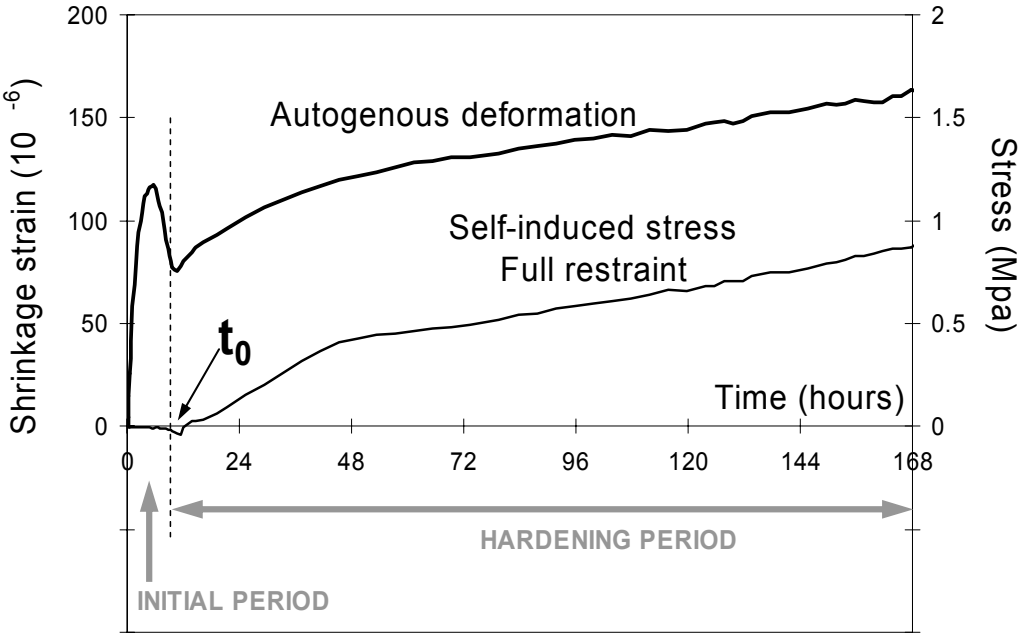

Figure 3: Autogenous deformation (linear) and self-induced stress at full restraint for *Concrete 1* during 20 °C isothermal conditions. [4,16]

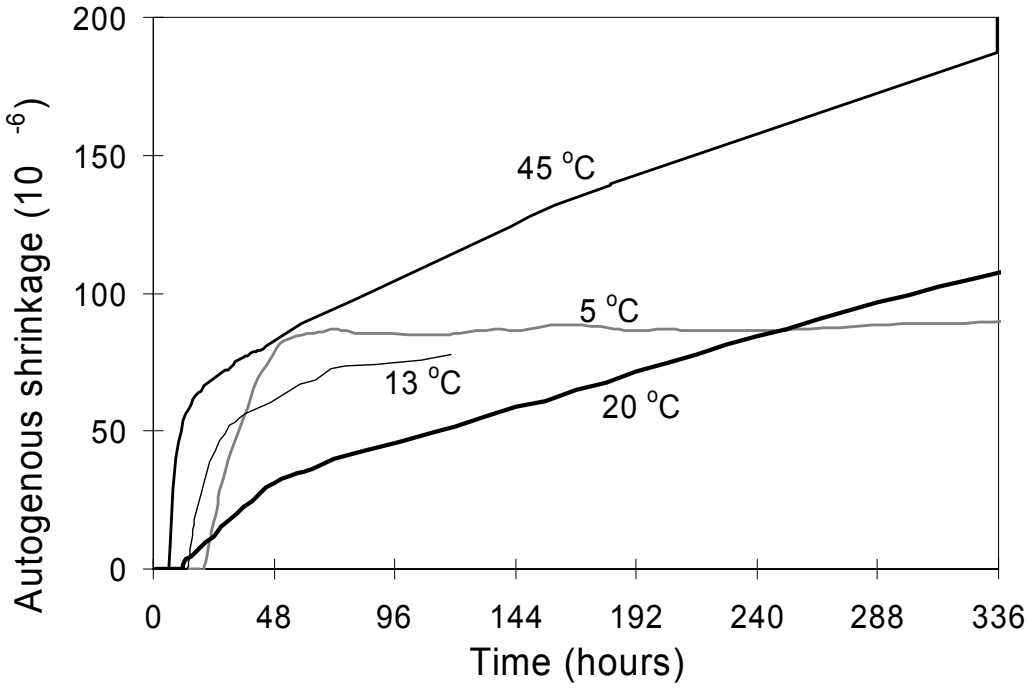

Figure 4: Autogenous deformation over time (from t_0 = 11 maturity hours) for *Concrete 1* during isothermal tests. [4,16]

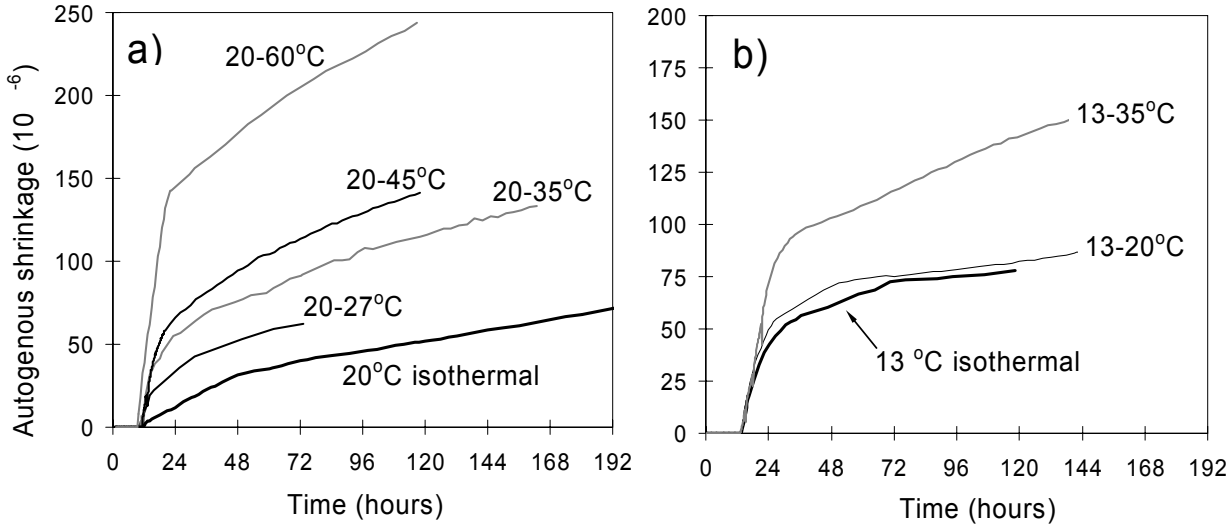

Figure 5: Autogenous deformation over time (from t_0 = 11 maturity hours) for *Concrete 1* in tests with 20 °C (a) and 13 °C (b) initial temperature and different final (isothermal) temperatures. Notation a-b gives initial-final temperature. [4,16]

It is quite easy to measure the sum of thermal and AD under any imposed temperature development. Assuming that CTE depends less on the temperature, it is convenient to obtain AD by subtracting the thermal deformation from the total. Some examples are shown in Figure 6 [16]. The temperature is imposed in steps (Figure 6a), allowing CTE to be calculated at each step, producing the AD curves shown in Figure 6b. Some of the AD-curves are rather surprising compared to the isothermal reference; a fast contraction is followed by an expansion, which in the long term again turns to contraction. Furthermore, the nature of the curves depends strongly on the characteristics of the temperature development imposed on the concrete. We note that AD-developments like the one expressed by the curve "T_{max}=61 °C, *steps*" in Figure 6b have been measured at NTNU in a vast number of tests on different concretes subjected to realistic temperatures with high temperature maxima.

From a practical point of view what is needed for calculations are the total deformations for a given temperature history. However, in a concrete structure each location has its own temperature history – and it would be too cumbersome to do one experiment for each. This is why we need to separate the two types of deformation, and then hopefully to construct a realistic model for each valid over a range of temperature histories. The best approach is clearly to impose realistic stepwise temperature developments such as in Figure 6a, and then calculate CTE and AD. The details and questions raised by this procedure are discussed thoroughly previously [16, 17]. The results presented in the rest of this paper are obtained using this approach.

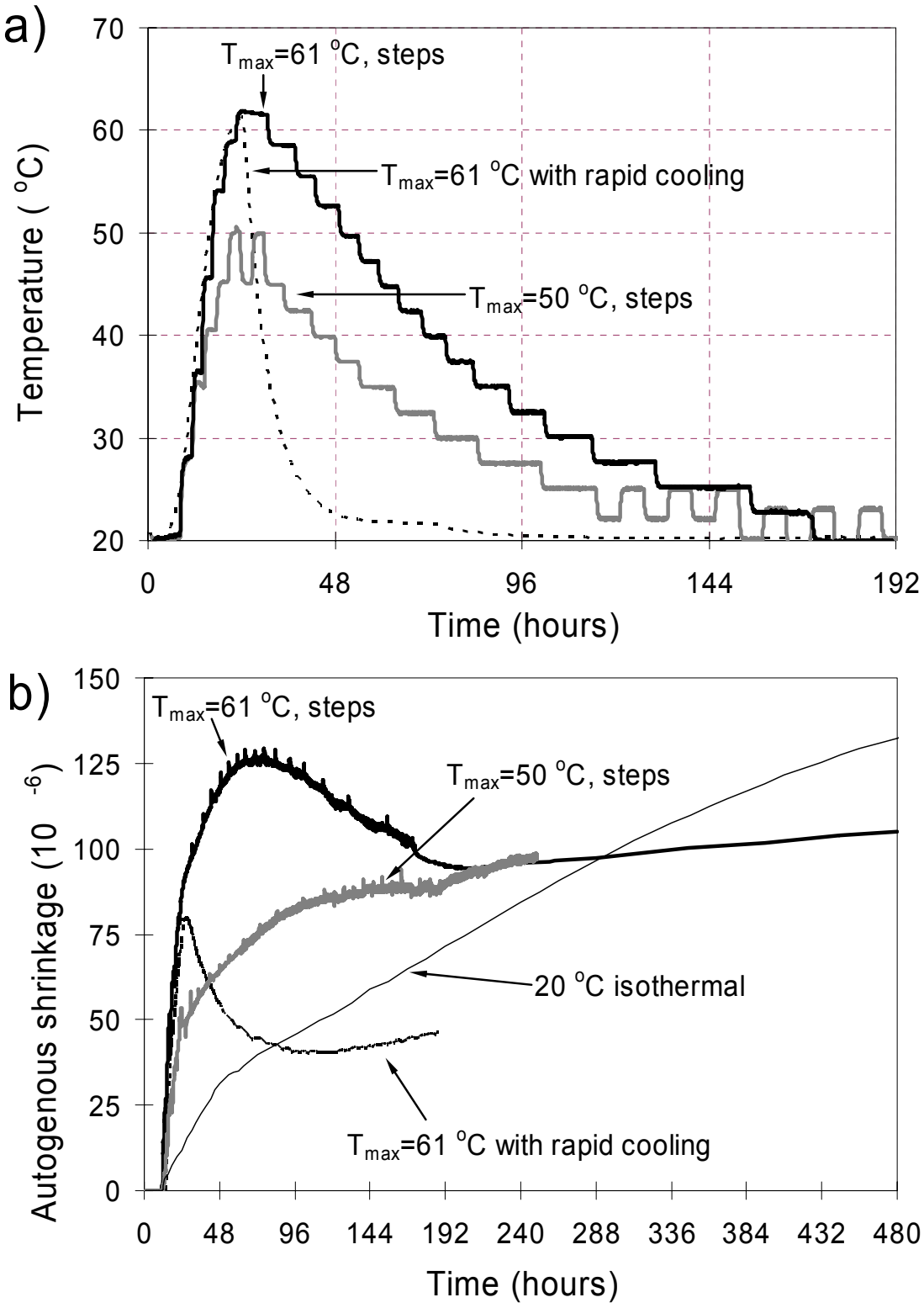

Figure 6: Imposed temperature histories (a), and calculated autogenous deformation from t_0=11 maturity hours (b) for *Concrete 1*. Note that the time scale is different in (a) and (b), and all temperatures are 20 °C isothermal (or isothermal with steps) after 168 hours. [16]

3. CTE RESULTS AND INTERPRETATION

RH-dependence

Figure 7 shows CTE for a cement paste and a concrete (*Concrete 1*) over time for 20°C curing. The early marked drop is a result of the transition from a water suspension to a solid skeleton material. The increase from then on is of practical interest and associated with self-desiccation mainly, since CTE almost returns to the original values after water immersion. This RH dependence has been demonstrated many times for mature cement paste and has been reviewed [16] and analyzed [18,19]. We believe the main reason for the RH dependence (CTE is minimum in 0% and 100% RH state and has a maximum somewhere around 50-70% RH) is the fact that if concrete pore water at a certain temperature exerts a certain RH, then a temperature increase (without loss of water) will lead to increased RH. This again leads to expansion, which adds to the pure thermal expansion, producing an increased CTE compared to a saturated or fully dry concrete where no RH change is possible. On cooling the reverse happens. The phenomenon is caused by the thermodynamic properties of the pore water and has been calculated from such data (enthalpy of adsorption) [18,19].

As Figure 7 shows, the effect is naturally greater in cement paste than in concrete. As we will see below the magnitude of the effect varies, but clearly from a cracking point of view a small CTE is desirable.

Maturity compensation

Figure 8 shows CTE for *Concrete 1* subjected to different temperature histories. There are variations, but clearly the use of the maturity principle with a normal activation energy leads to improved consistency [16]. Note also that there is a basic uncertainly in the separation of AD and CTE from total deformation curves; a rapid temperature change leads to time dependent deformation – it is therefore somewhat arbitrary what one chooses to call thermal deformation, and what AD [16,18].

Effect of concrete composition

Figure 9 shows CTE at 20 °C for different concretes over time. The w/b-ratio has clear effects in line with our expectations considering the RH-effect and the fact that reduced w/b-ratio normally means more binder volume. Self-desiccation is much less at w/b = 0.60 than at 0.23 (this concrete also contains 20% silica fume); the latter super HPC reaches a very high CTE value very fast, and then remains there. One concrete has very low CTE-values the first few days - it consists of limestone aggregate (having low CTE [16]), but we have no explanation for this anomalous behavior.

Different binder compositions are shown in Figure 10, exposed to (stepwise) realistic temperature histories. The early high temperatures lead to fast hydration (and self desiccation) for all the mixes. The high early temperature also appears to eliminate the long term increase seen for the isothermal curing in Figure 9.

It should be kept in mind that accuracy may be a problem in detecting changes in CTE since the imposed T-steps may sometimes be only 2-3°C, but generally the steps are larger than this.

However, changes in CTE are practically important considering that often the cooling contraction is much greater than AD. Note also that when total deformation is measured, whatever is not assigned to thermal causes is counted as AD. This fact may justify the use of a constant CTE – as long as the total deformations are measured.

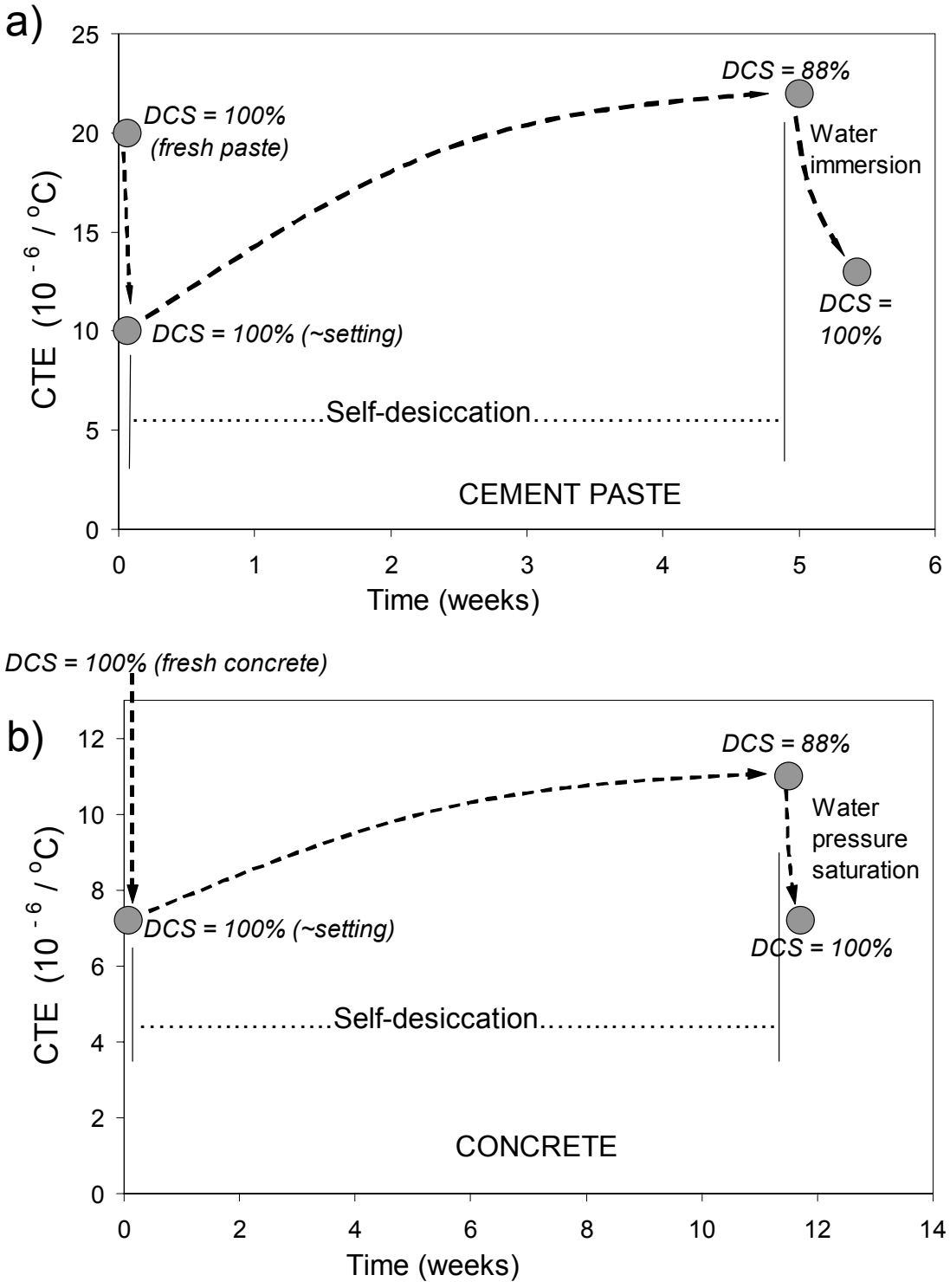

Figure 7: Effect of degree of capillary saturation (DCS) of (a) cement paste and (b) concrete with the same paste as binder (*Concrete 1*). 20 °C isothermal tests (temperature steps between 17 and 23 °C). [18]

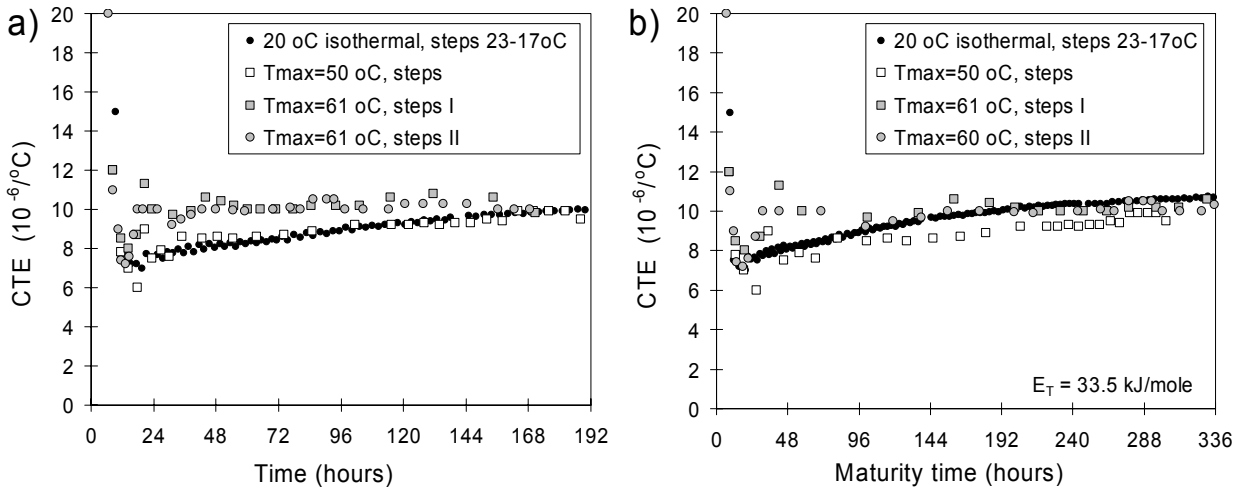

Figure 8 : CTE-development over time (a) and maturity time (b) for *Concrete 1* measured under 20 °C isothermal conditions and realistic temperature histories with 20 °C initial temperature (legend indicates T_{max} at 24 hours). The tests were performed with temperature steps, see Fig.6a, and see Fig.6b for AD. [16]

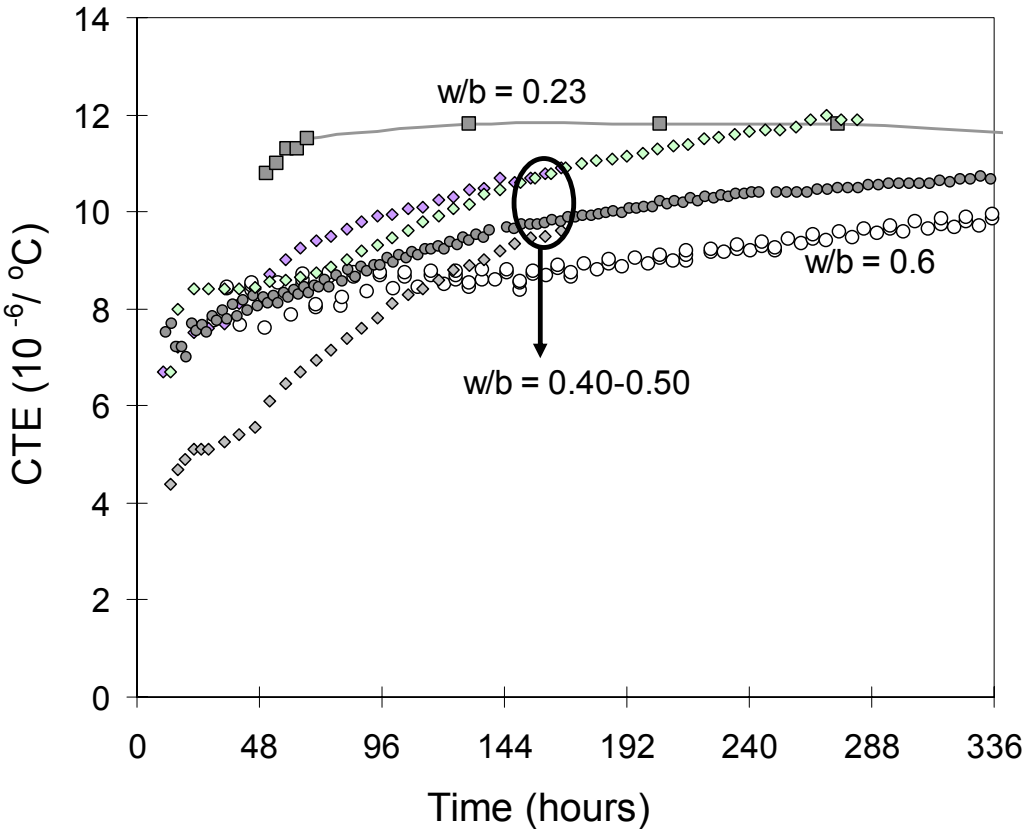

Figure 9: CTE-development at 20 °C conditions (temperature steps between 23 and 17 °C) for concretes with different w/b-ratios. [16]

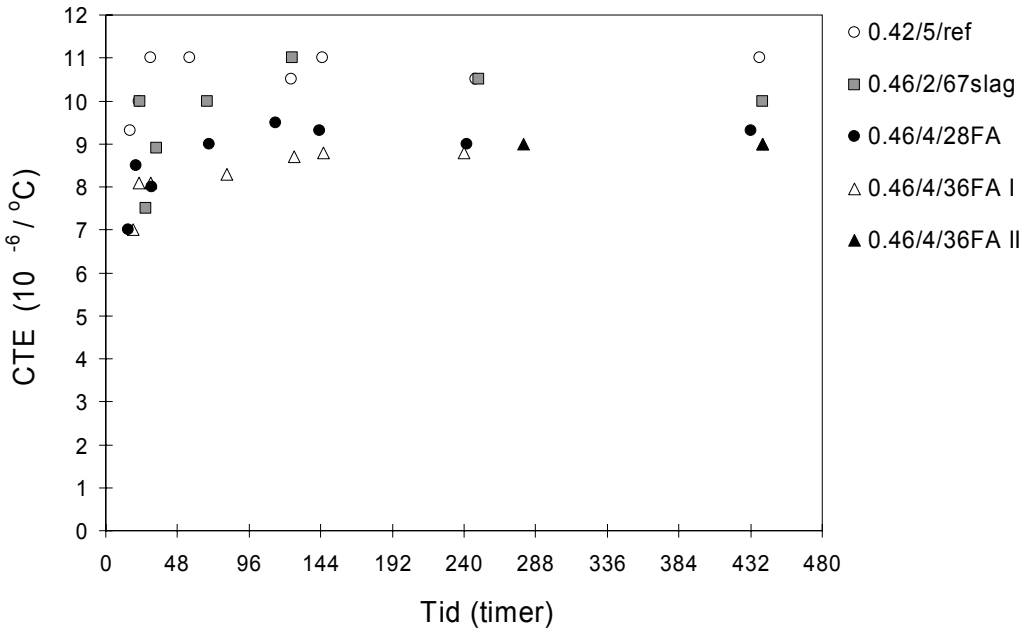

Figure 10: CTE during stepwise realistic temperature histories, CEM I (OPC) with silica fume and fly ash (FA) or slag. Notation a/b/c gives w/b-ratio, silica fume%, and fly ash or slag%. Initial temperature = 20 °C except *046/4/36FA II* with 10 °C. [21]

4. AD RESULTS AND DISCUSSION

Isothermal vs. realistic temperatures

Figure 11 illustrates well different relationships between isothermal and realistic temperature developments, for concretes with various dosages of silica fume [20]. A dosage below 10% has only small influence under isothermal conditions, but more at elevated temperature. At 15% silica fume dosage there is very fast contraction at 20°C, heating increases this strongly. This trend is typical for super HPC [16]. Common for all the concretes at realistic temperatures is the feature also introduced in Figure 6; after about 48 hrs the contraction turns to expansion for a period before resuming the contraction when isothermal conditions are reached (not shown in Figure 10, but in Figure 6). The expansion is most marked for the concrete without silica fume, as noted in several other experimental series. Note particularly from Figure 6 that the expansion only occurs when T_{max} is more than about 30 °C above the starting temperature. This is a general observation in our tests, and explains why the phenomenon has not been observed for tests with moderate temperature increases, 20°C or less. For such conditions several authors have shown that even using the maturity principle on AD can produce acceptable accuracy for calculations on structures.

However, temperature increases of about 40 °C, such as in Figure 10, are by no means unusual in practice. For instance a HPC with 400 kg/m^3 cement, a wall thickness of about 0.5 m is enough to produce this increase using normal formwork and summer conditions (even in Norway!).

The lesson from these observations is that unless the initial temperature calculations indicate very moderate temperature increases in a particular structure, it is necessary to carry out deformation tests at realistic conditions, and not rely on extrapolations from isothermal tests. In fact, our standard minimum procedure for consulting services does not include any isothermal testing at all.

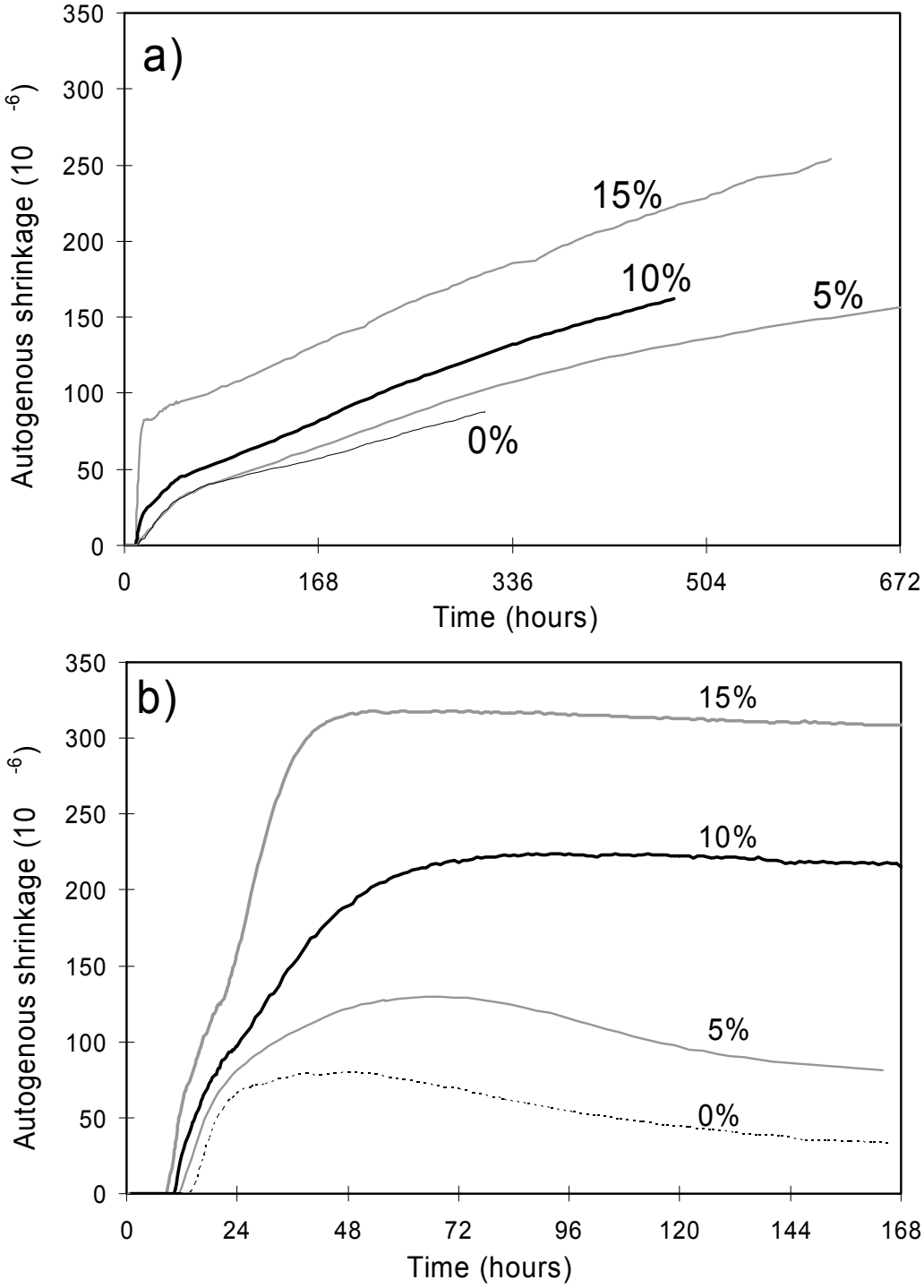

Figure 11: Autogenous deformation from t_0 with various amounts of silica fume, CEM I (OPC) and w/b=0.42. (a) 20 ^{o}C isothermal, (b) realistic temperature history with T_{max} = 61 ^{o}C at 24 hours. *Concrete 1* is the one with 5% silica fume. [11, 20]

Fly ash and slag concretes

For a submerged tunnel project in Oslo, the Road Directorate investigated a number of HPC containing fly ash or slag and small amounts of silica fume [21]. Extensive testing, including durability, was carried out on the concretes. The AD curves under realistic conditions are shown in Figure 12; the CTE-development from the same tests is already presented in Figure 10. Note particularly that there is a different T_{max} for each concrete, namely the one that was

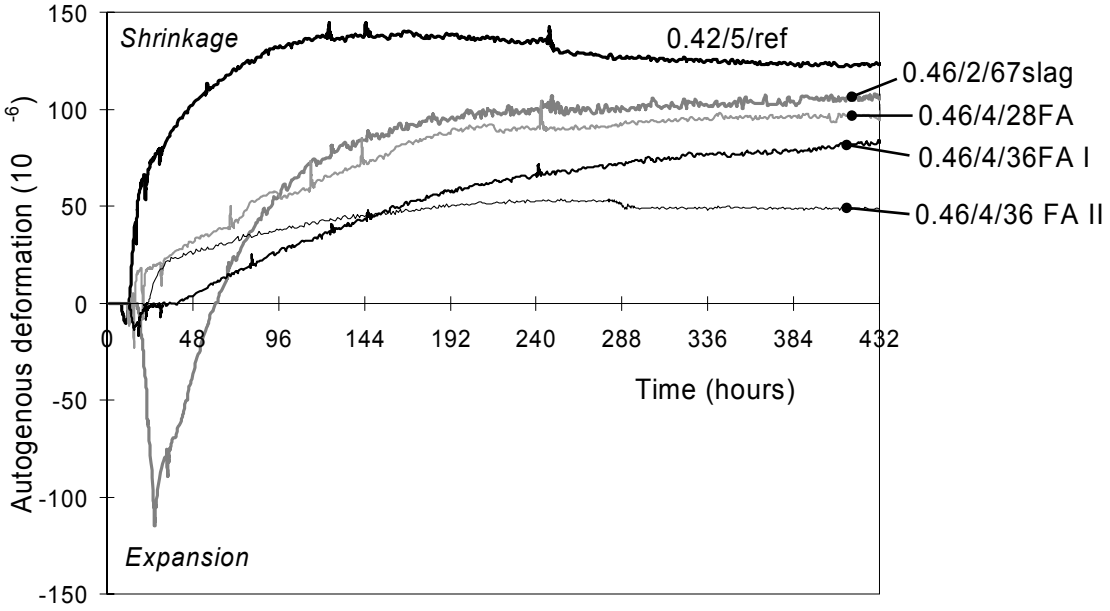

Figure 12: Autogenous deformation from t_0 during realistic temperature histories, CEM I (OPC) with silica fume and fly ash (FA) or slag. Notation a/b/c gives w/b-ratio, silica fume%, and fly ash or slag%. Initial temperature = 20 °C except *046/4/36FA II* with 10 °C [21]. See Figure 10 for CTE-development measured from the same tests.

calculated to occur in the structure based on calorimetric measurements. One major advantage of using fly ash and slag is that the heat development is reduced, and this must of course be taken into account when producing data used for crack risk calculations.

The curves show, as expected, that the reference OPC concrete *042/5/ref* produces high T_{max} (56°C) and also the expansive effect. The fly ash concretes *0.46/4/28FA* and *0.46/4/36FA I* and *0.46/4/36FA II* (two starting temperatures, 20 °C (*I*) and 10 °C (*II*)) show less and more gradual AD than the others. The slag concrete *0.46/2/67slag* has a very special behavior with a strong early expansion followed by strong contraction, before the leveling out after 1 week. Such expansions are found in the literature, our experience with slag is very limited so we cannot say to what extent this behavior is typical.

Again, we conclude that when either unusual (to the laboratory) mixture components and/or elevated temperatures are to be relevant for a particular structure, it is necessary to perform deformation tests as a basis for crack assessment calculations.

5. CONCLUDING REMARKS

Both the thermal contraction and AD generally contribute to tensile stress build up in the cooling period following the initial heating period in a typical concrete structure. The examples shown here illustrate that the relative importance of the two depends strongly on concrete mix constituents and proportions. CTE does vary, but AD can vary much more, in fact it may occur both as contraction and expansion – particularly under realistic temperature conditions.

In general, except for super HPC (i.e. w/b-ratios below 0.30 and for silica fume above 10%); it appears that the thermal deformation is greater than AD. Consequently, it is surprising that so little attention is paid to CTE in the recent literature. The main measures to minimize CTE is to keep the concrete as wet as possible during hydration, and of course to choose aggregate with low CTE, if that is possible. Keeping the concrete wet of course also

minimizes or eliminates AD. Internal curing is a promising possibility currently being considered seriously in the RILEM-committee TC 196-ICC. Performing tests of CTE is important in any case, if calculations to assess crack risk are to be trustworthy.

Regarding AD, testing under realistic temperature conditions is obviously necessary if the expected temperature rise in the structure is calculated to exceed about 20 ^{o}C.

We recommend the type of tests outlined in this paper: The temperature is imposed stepwise, and the total deformation is recorded. CTE is calculated at each step and then the thermal deformation using CTE and the recorded temperature history. Finally the AD is found as the difference between the total- and the thermal deformations.

The literature shows great differences between AD for quite similar concretes and even in Round-Robin tests on the same concrete, particularly in the early period after t_0. We think the work to standardize test principles and methods currently taking place in RILEM TC195-DTD is very important, and will hopefully lead to systematic data collection on different concretes as a basis for construction of useful mathematical models for AD. No such model of general validity exists today.

ACKNOWLEDGEMENTS

The financial contribution of the Norwegian Research Council is gratefully acknowledged. Likewise are the contributions from the partners in the Norwegian NOR-CRACK project. The partners are: Skanska Norge AS, Elkem ASA Materials, Norcem AS, Fesil ASA and The Norwegian Public Roads Directorate. The Norwegian University of Science and Technology was project leader.

Some of the results presented were part of a programme undertaken by the Norwegian Public Roads Administration in the “Bjørvika Immersed Tunnel” project. The use of data is acknowledged.

REFERENCES

[1] Proceedings of the int. conference: Thermal Cracking in Concrete at Early Ages, Ed. by R.Springenschmid, Published 1994 by E & FN Spon, 2 - 6 Boundary Row, London SE1 8HN, UK. ISBN: 0 419 18710 3, pp. 449-456

[2] Proceedings of the int. conference on concrete of early age, RILEM report, Paris, France, 1982, ISBN 2-85978-038-6

[3] Proceedings of the int. NTNU/SINTEF workshop: Early volume change and reactions in paste-mortar-concrete, Trondheim, Norway, 1996

[4] Proceedings of the int. workshop: Autogenous Shrinkage of Concrete. Organized by the Japan Concrete Institute, Hiroshima, Japan, 1998, Ed. by E.Tazawa, © 1999 E & FN Spon, ISBN 0-419-23890-5.

[5] Proceedings of the int. research seminar: Self-desiccation and its importance in concrete technology. Lund, Sweden, 1997, Ed. by B.Persson and G.Fagerlund, ISBN 91-630-5528-7

[6] Proceedings of the second int. research seminar: Self-desiccation and its importance in concrete technology. Lund, Sweden, 1999, Ed. by B.Persson and G.Fagerlund, ISBN 91-630-8230-6

[7] Proceedings of the third int. research seminar: Self-desiccation and its importance in concrete technology. Lund, Sweden, 2002, Ed. by B.Persson and G.Fagerlund, ISBN 91-631-1993-5

[8] Proceedings of the int. RILEM workshop: Shrinkage of Concrete, Shrinkage 2000. Paris, France, 2000, Ed. by V.Baroghel-Bouny and P.-C. Aïtcin, PRO 17

[9] Proceedings of the int. workshop on control of cracking in early-age concrete. Sendai, Japan, 2000

[10] Proceedings of the RILEM int. conference on early age cracking in cementitious systems (EAC'01). Israel, 2001. Ed. by K.Kovler and A.Bentur.

[11] Separate session at ACI Fall Convention 2002, Phoenix, Arizona. Papers were later published in: ACI SP-220: Autogenous deformation of concrete. Ed. by O.M.Jensen, D.P.Bentz and P.Lura, 2004, ISBN 0-87031-143-3

[12] Proceedings of the int. conference: Advances in Cement and Concrete. Copper Mountain, Colorado, 2003. Ed. by D.A.Lange, K.L.Scrivener, J.Marchand, Copyright © 2003 University of Illinois

[13] Proceedings (CD-rom) of the ACBM/RILEM int. symposium: Advances in concrete through science and engineering. Evanston, Illinois, 2004.

[14] Bjøntegaard Ø., Kanstad T., Sellevold E.J. and Hammer T.A. (1999) Stressinducing Deformations and Mechanical Properties of High Performance Concrete at Very Early Ages, In the 5th int. symposium: Utilization of High Strength/ High Performance Concrete, Sandefjord, Norway, Ed. by I.Holand and E.J.Sellevold

[15] Justnes H., Clemments F., Depuydt P., van Gemert D. and Sellevold E.J. (2000) Correlation the deviating point between external and total chemical shrinkage with setting time and other characteristics of hydrating cement paste. Proceedings of the int. RILEM workshop: Shrinkage of Concrete, Shrinkage 2000. Paris, France, Ed. by V.Baroghel-Bouny and P.-C. Aïtcin, PRO 17

[16] Bjøntegaard, Ø. (1999) Thermal Dilation and Autogenous Deformation as Driving Forces to Self-Induced Stresses in High Performance Concrete. Doctoral thesis, NTNU, Dept. of Structural Eng., Dec. 1999, ISBN 82-7984-002-8.

[17] Bjøntegaard Ø., Hammer T.A. and Sellevold E.J. (2004) On the Measurement of Free Deformation of Early Age Cement Paste and Concrete. Cement and Concrete Composites, 26, pp. 427-435.

[18] Sellevold E.J. and Bjøntegaard Ø. (2006) Coefficient of Thermal Expansion of Cement Paste and Concrete: Mechanisms of Moisture Interaction. Materials and Structures, accepted for publication in 2006

[19] Radjy F., Sellevold E.J. and Hansen K.K. (2003) Isosteric Vapor Pressure - Temperature Data for Water Sorption in Hardened Cement Paste: Enthalpy, Entropy and Sorption Isotherms at Different Temperatures. Report BYG-DTU R-057, Techn. Univ. of Denmark, Lyngby. Available at http://www.byg.dtu.dk/publicering/rapporter/R-057.pdf

[20] Bjøntegaard Ø. and Sellevold E.J. (2004) Young high performance concrete with w/b=0.40 and varying silica fume content: Experimental test results and 1-dimensional restraint stress calculations. Evaluation of new results on hot climate conditions and previous results. NOR-CRACK report #3.1, Subtask 3 Parameter studies, STF22 A04616, ISBN 82-14-02588-5

[21] Bjøntegaard Ø. (2004). Bjørvika submerged tunnel, Phase 2: Determination of concrete properties relevant for evaluation of cracking tendency in the hardening phase (in Norwegian). Experimental results for mixture A, B, C and D. NTNU-report R-5-04, Dept. of Structural Eng., 26 pages

[22] Morabito P., Bjøntegaard Ø., van Breugel K., Dalmagioni P., Gram H.-E., Gutsch A., Hedlund H., Jonasson J.-E., Kanstad K., Lura P., Pellegrini R., Rostasy F., Sellevold E. (2001) Round Robin Testing Program. Equipment, testing methods, test results. IPACS report, Ed. by P.Morabito, TU Luleå, Sweden, ISBN 91-89580-42-7, 110 pages

Paper 5 EARLY AGE CRACKING TENDENCY OF LOW-HEAT CONCRETES CONTAINING FLY-ASH AND BLAST FURNACE SLAG

Ø. Bjøntegaard

The Norwegian University of Science and Technology, Department of Structural Engineering, Trondheim, Norway

Abstract

The paper discusses the effect of fly-ash (FA) on the cracking tendency during the hardening phase due to external restraint. The tested concretes had water-to-binder (w/b) ratio of 0.40 and properties such as hydration heat, coefficient of thermal expansion, autogenous deformation mechanical properties and creep have been investigated and reported. Results from semi-adiabatic tests in the Temperature-Stress testing machine and 1D stress calculations show that the FA concrete (35% FA of binder weight in combination with ordinary Portland cement (OPC)) has 25% lower cracking tendency than the reference concrete made only with OPC. The test conditions and evaluation of cracking risk are directly relevant for a 1 m thick concrete structure subjected to external restraint.

Any practically relevant mix-design with FA added directly during the mixing process should however be done with the use of efficiency factors according to the European Standard "EN 206-1". This will require lower w/b-ratios for FA-concretes (or BFS concretes) than a reference without FA (or BFS), which probably will lead both to higher binder contents (i.e. more hydration heat) and possibly more autogenous shrinkage. Hence, a practically relevant comparison using a lower w/b-ratio for the given FA-addition (35% FA requires w/b=0.34) would likely be less favourable than what is found in the present study using w/b=0.4.

Hence, since hydration heat and autogenous shrinkage, as well as all the other involved concrete properties, are altered when changing concrete proportions it is very difficult, if possible at all, to extrapolate results. Any parameter study on FA (or BFS) relevant for practical concreting should therefore be made in accordance with the requirements from the standard. In this regard it is notable that the efficiency factors are 1.0 for FA and BFS if the materials are a part of a certified cement (cement type II and III). For cracking tendency it appears then more favourable to use CEM II and III cements than using the same amount of FA or BFS added separately during mixing in combination with, for instance, OPC.

1. INTRODUCTION

The interest in Norway towards low-heat concretes containing pozzolanic waste material such as fly-ash (FA) or blast furnace slag (BFS) is increasing today both of environmental and technical reasons, and larger infrastructure projects are presently being executed with the use of such concretes /1/. Low-heat concretes develop moderate curing temperatures, which leads to moderate thermal "loads" giving a potential benefit with regard to cracking tendency.

During the last few years research has been carried out in Norway on the effect of FA and BFS with regard to both durability aspects and early age properties - and the associated cracking tendency during the hardening phase. The paper discusses the latter including mix-design aspects with the use of FA and BFS according to the European Standard EN 206-1, which has been mandatory for national requirements since 2003. Properties such as hydration heat, coefficient of thermal expansion, autogenous deformation mechanical properties and creep have been investigated. The total test program has involved high performance concretes (HPC) with various additions of FA or BSF, as well as a BFS-cement /2//3/.

The paper discusses the cracking tendency during the hardening phase due to external restraint of the concrete; a situation that may give serious through-cracking challenging water-tightness and durability, and often leads to costly repair. Results from a concrete made with 35% FA of binder weight is discussed specifically and compared to a reference concrete without FA /**2**/.

2. PROPORTIONING CONCRETE WITH FLY ASH

The European Standard EN 206-1:2000 (Concrete. Part I: Specification, performance, production and conformity) was adopted in the Norwegian Standard NS-EN 206-1 in April 2001. The Norwegian translation was published in Oct. 2003 including a Norwegian National Annex NA (NS-EN 206-1) and the standard was mandatory from that point. The standard specifies, among others, maximum allowable effective w/b-ratios in different exposure- and durability classes. One of the durability classes specified in the standard is denoted "MF40", required when building infrastructures in severe environments (involving high moisture, de-icing/sea-salt, freezing/thawing, chemical attack). The maximum allowable effective w/b-ratio (m) in this class is 0.40 (i.e. $m \leq 0.40$). Another term used for m is *mass ratio.*

Equations for calculating w/b-ratio and m when adding FA and BFS during concrete mixing are given below (Equation (1) and (2)) as well as the relation between the two (Equation (3)). According to NS-EN 206-1 the efficiency factor when calculating m is set to be $k_s = 2.0$ for silica fume (s), $k_{FA} = 0.4$ for FA (for CEM I 42.5 or higher) and $k_{BFS} = 0.6$ for BFS. The consequence is that the w/b-ratio must be lowered to maintain m when replacing cement with FA or BFS. For FA the maximum amount that can be accounted in the calculation of m is 33% of cement weight, hence the excess FA above 33% must be regarded as filler/aggregate. The corresponding number for BFS is 80%. The Norwegian Road Administration uses their own code in specific projects and presently large infrastructure projects are being executed with FA-concrete where $k_{FA} = 0.7$ is specified /1/.

Figure 1 shows the required w/b-ratio to obtain $m = 0.40$ in a concrete with 25% FA of binder content (and 0 and 5% s, respectively) as function of k_{FA}. It is notable that a concrete in the MF40 durability class must contain at least 4% s (and at least 4% air), but the curve representing 0% s is discussed further for simplicity. It can be seen from the figure that m=0.40 for $k_{FA} = 0.4$ and 0% s means w/b = 0.34, while w/b = 0.37 for $k_{FA} = 0.7$ (and naturally w/b = m = 0.45 for $k_{FA} = 1.0$). In this regard it is important to note that low w/b-ratios generally lead to high binder contents which may counteract some of the desired low-heat performance. In addition, low w/b-ratios generally also lead to higher autogenous shrinkage, which definitely contribute negatively with regard to cracking tendency.

Figure 2 gives an example of the consequence of the k_{FA}-factor on the binder content in a 25% FA concrete with m = 0.40 (no s) when assuming either fixed paste volume (283 l/m^3) or fixed water content (150 l/m^3). Compared to k_{FA} = 1.0, for fixed paste volume, a k_{FA} of 0.7 and 0.4 means 4% and 9% more binder, respectively. For fixed water content the corresponding numbers are 8% and 18% more binder. Compared to k_{FA} = 0.7, a k_{FA} of 0.4 means 4% (fixed paste volume) and 9% (fixed water content) more binder. In practical mix-design however the decisive parameter for binder content is the fresh concrete properties, hence the actual required binder content depends on the used concrete part materials (the aggregate in particular).

It is notable that the k-factors are 1.0 for FA and BFS if the materials are a part of a certified cement (cement type II and III), hence when proportioning with such cements the required w/b-ratio will be equal to m (=0.40 in this case). For cracking tendency it appears then more favourable to use CEM II and III cements than using the same amount of FA or BFS added separately during mixing combined with, for instance, an ordinary Portland cement (CEM I).

Water-to-binder-ratio (w/b-ratio):
$$\frac{w}{b} = \frac{w}{c + s + FA + BFS} \tag{1}$$

Effective binder ratio:
$$m = \frac{w}{c + k_s s + k_{FA} \cdot FA + k_{BFS} \cdot BFS} \tag{2}$$

It then follows that:
$$\frac{w}{b} = m \cdot \frac{(1 + \frac{k_s s}{c} + \frac{k_{FA} FA}{c} + \frac{k_{BFS} \cdot BFS}{c})}{1 + \frac{s}{c} + \frac{FA}{c} + \frac{BFS}{c}} \tag{3}$$

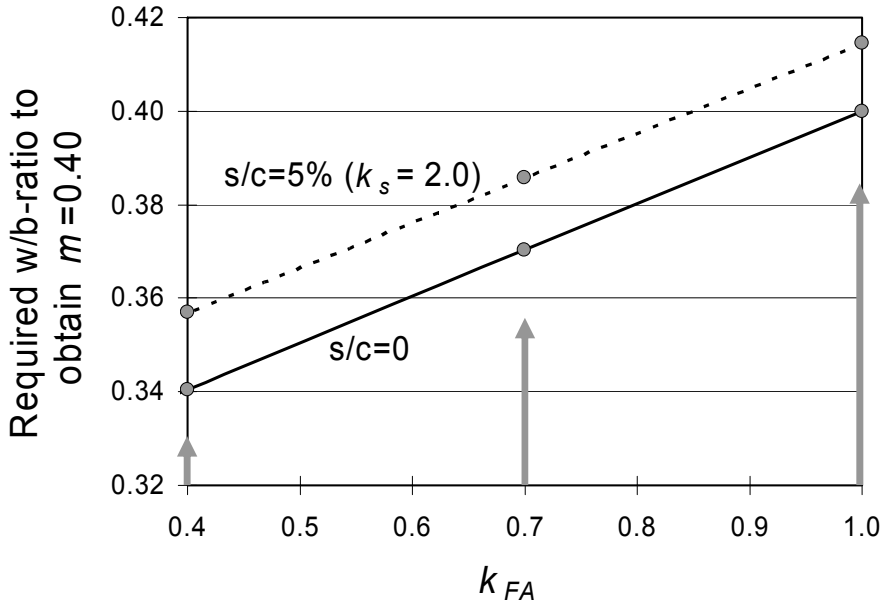

Figure 1: Required w/b-ratio in a 25% FA concrete (FA/b=0.25, no BFS) to obtain m = 0.40 as function of efficiency factor for FA (=k_{FA}). 0 and 5% silica fume (s) content of cement (c) weight and k_s = 2.0.

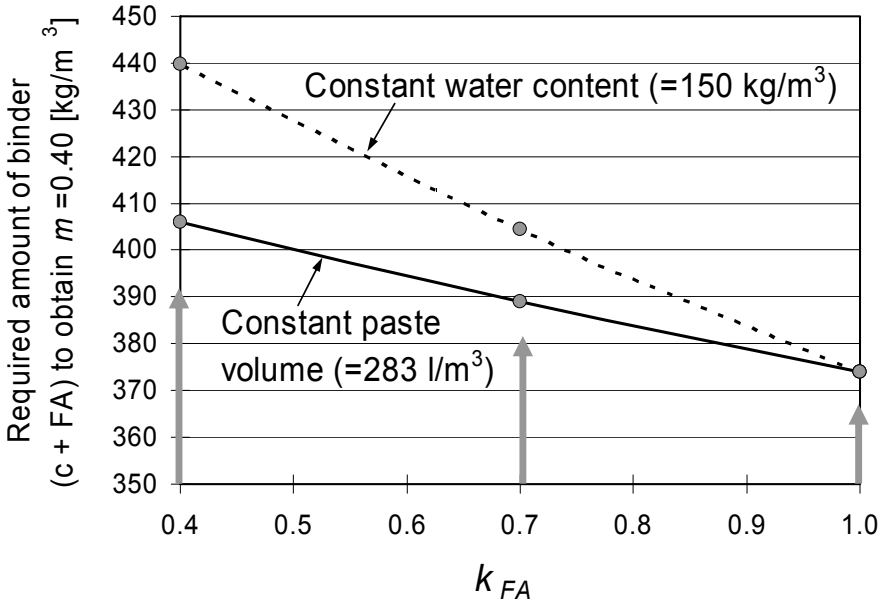

Figure 2: Required binder content in a 25% FA concrete (FA/b=0.25, no BFS, no *s*) to obtain m = 0.40 as function of k_{FA} when keeping a constant water content and constant paste volume, respectively.

3. CONCRETES AND TEST PROGRAM

3.1 Concretes

Concrete compositions of the tested reference (REF) concrete without FA and the concrete with 35% FA (FA concrete) are shown in Table 1. Both concretes are made without *s* and have w/b=0.40. The concretes were a part of parameter study on the effect of 0 - 35% FA, hence the REF and FA concrete shown here are the two extremes /**2**/. The concretes were

designed with k_{FA}=1.0 meaning that w/b was 0.40 for all. The FA concrete (35% FA) shown in Table 1 has therefore an *m* as high as 0.54 when using k_{FA}=0.4 according to NS-EN 206-1 (including only 25% FA in the calculation of *m*, as already discussed), while the REF concrete has *m* = w/b = 0.40. Furthermore, to obtain *m* = 0.40 for the FA concrete it should have been made with w/b = 0.34, leading to (for fixed paste volume) 305 kg cement and 164 kg FA (of which only 101 kg FA is included in the *m*-calculation). This means 28% more cement than the actual tested concrete (and 9% or 27% more total binder dependent on whether only the 25% FA is included as reactive binder or all the FA (35%), respectively). Therefore, a realistic comparison between the REF concrete and a 35% FA concrete (according to the standard) would most likely be less favourable than what is presented in the following chapters.

Table 1: Nominal concrete composition (kg/m^3), fresh concrete measurements and effective w/b-ratios (*m*) with different k_{FA}-factors.

Constituent	**REF concrete (no FA)**	**FA concrete (35% FA)**
CEM I 52.5 LA, Blain = 362 m^2/kg (Norcem)	391	239
Fly ash (Danaske i/s)	-	129
Free water	157	147
Aggregate, sand 0 - 8 mm + stone 8 - 16 mm	1865	1865
Plasticiser (naphthalene)	1.0	0.6
Superplasticiser	3.5	4.3
Slump (mm)	165 mm	145 mm
Air content (%)	0.6	2.0
Density	2450	2420
Binder content	391	368
Paste volume (l/m^3)	283	283
w/b-ratio (k_{FA}=1.0)	0.40	0.40
Effective w/b-ratio (m), incl. all FA		
k_{FA}=0.4	0.40	0.51
k_{FA}=0.7	0.40	0.45
Effective w/b-ratio (m), incl. only 25% FA		
NS-EN 206-1 ⟶ **k_{FA}=0.4**	**0.40**	**0.54**
k_{FA}=0.7	0.40	0.50

3.2 Test programme

The following properties were tested experimentally:
- Temperature sensitivity (activation energy) based on compressive strength tests from setting until 28 days. Curing at 5 °C, 20 °C and 35 °C /4/
- Heat development in a semi-adiabatic calorimeter from casting until 5 days
- Free strain measurements from casting until 2 weeks in a Dilatometer measuring CTE and autogenous deformation.
- 28 days mechanical properties (E-modulus, tensile strength, compressive strength).
- Creep in compression and tension. Loading after around 2 and 7 days. /11/,/12/

- and stress development in a TSTM

3.3 Mode of work and curing conditions

For each concrete the following procedure and test program was performed:

STEP 1	Heat measurement and 2D temperature calculation of a 1 m thick wall structure + The calculated average temperature history for the wall for each concrete were imposed to the specimens in the laboratory - this temperature history is denoted *semi-adiabatic temperature.*
STEP 2	Experimental measurements at 20 ^{o}C isothermal and semi-adiabatic conditions.
STEP 3	Model parameters identification.
STEP 4	1D stress calculation (comparison to the TSTM-test) and crack risk evaluation

In the evaluation of crack risk in STEP 4 (Chapter 6) only the semi-adiabatic TSTM test is considered here (not the isothermal case), hence it is relevant for a 1 m thick structure subjected to external restraint. The semi-adiabatic temperature histories for the REF- and FA-concrete are given in Figure 3. The temperatures were calculated with the use of the Danish finite element program 4C-Temp&Stress /5/ and represent the average temperature history in the wall for initial concrete temperature of 20 ^{o}C, 20 mm plywood formwork and 20 ^{o}C air temperature. The given temperature curves were implemented in a PC controlling the temperature history of the specimens through a heating/cooling water bath unit. The water is pumped through copper tubes fixed to the moulds. The semi-adiabatic temperature rise of the FA-concrete is 33% lower than the REF concrete, which is in line with the fact that the FA-concrete has lower hydration heat pr. kg binder and also the lowest binder content (see Table 1 and 4).

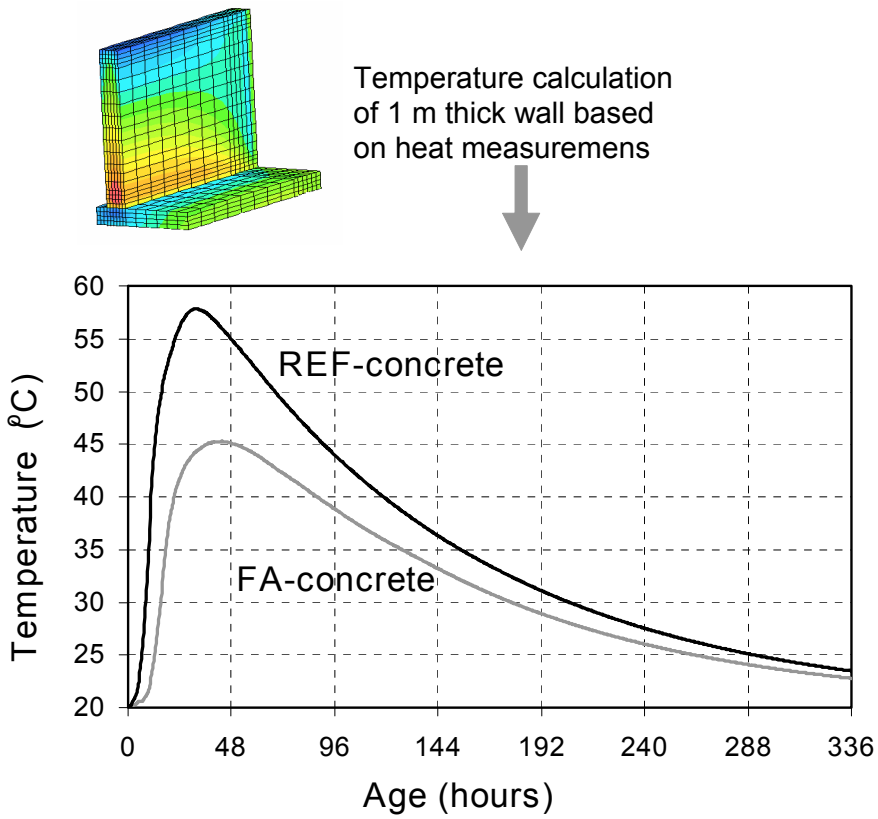

Figure 3: Curing conditions during the tests according to the calculated average semi-adiabatic temperature history for a 1 m thick wall structure

4. EXPERIMENTAL RESULTS

4.1 Thermal dilation and autogenous deformation

Measured temperatures in the core of the specimen in the Dilatometer (free strain) and the TSTM (restraint stress) are shown in Figure 4. Note that it is quite good match between the desired temperatures (Fig.3) and the achieved ones (Fig.4), which indicates a rather good temperature control of the specimens. As can be seen however, the Dilatometer was subjected to a stepwise temperature history. This was done to enable the separation of thermal- and autogenous deformations. The issue is discussed further at this symposium in /6/. Based on this procedure the average coefficient of thermal expansion was found to be $8.4 \cdot 10^{-6}$ for both concretes and autogenous deformation was determined according to Figure 5.

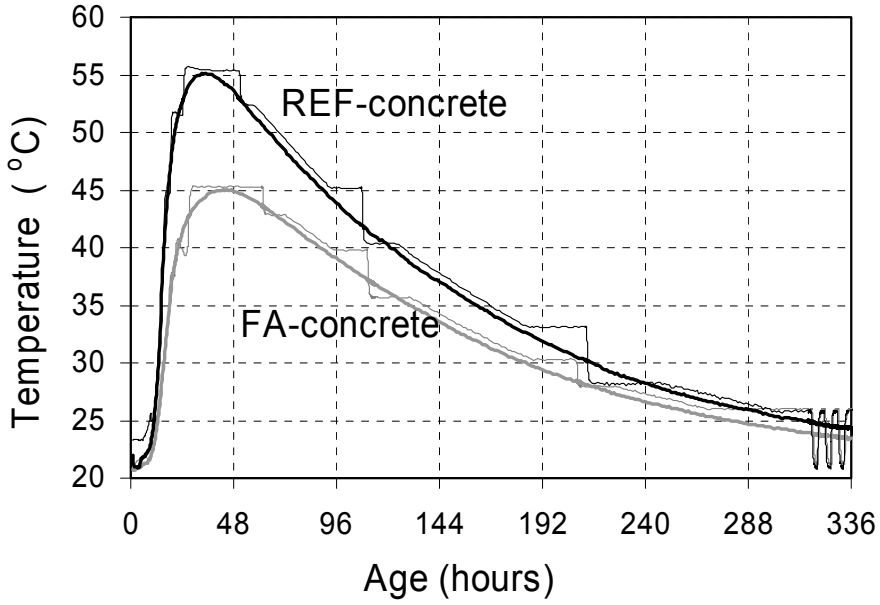

Figure 4: Measured semi-adiabatic temperature in the core of the specimens of the Dilatometer tests (stepwise curves) and the TSTM-tests (smooth curves).

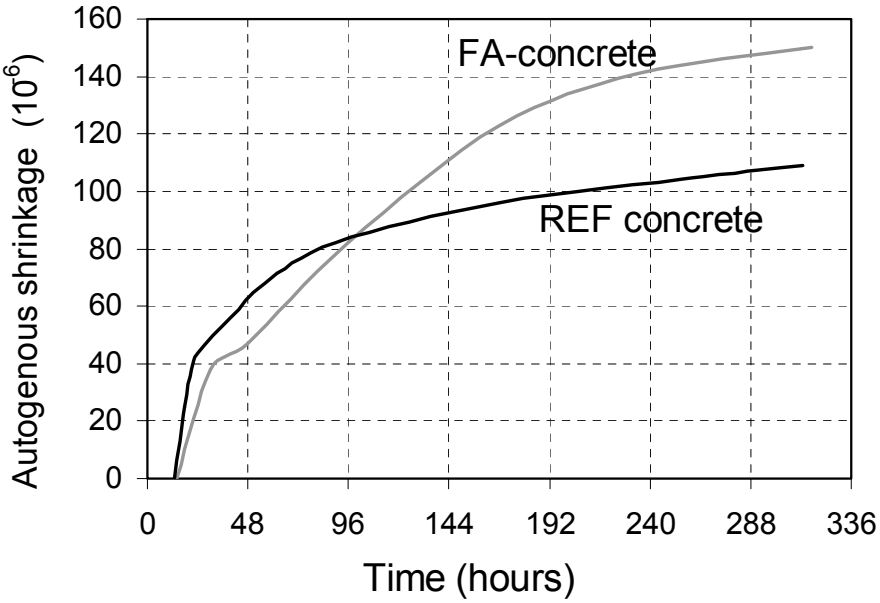

Figure 5: Measured autogenous shrinkage during semi-adiabatic temperature conditions after eliminating the effect of thermal dilation.

4.2 Mechanical properties and creep

Results for 28 days compressive strength (f_{c28}), E-modulus (E_{28}), direct tensile strength (f_{t28}) and splitting tensile strength (f_{ts28}) are shown in Figure 6. The figure contain the two concretes REF and FA (35% FA) as well as two concretes with 10% and 20% FA which also were a part of the program, as already discussed. It is important to note that all concretes have been cured at a "their own" semi-adiabatic temperature history (for REF and 35% FA see Fig.3). This may have contributed to the fact that there seem to be no systematic reduction in the mechanical properties with FA-content, hence indicating a quite high degree of pozzolanic reaction after 28 days. It is notable that the tensile strength tends to increase with FA-content where the splitting strength increases relatively more than the direct tensile strength. The same trend has been found earlier on relatively similar concretes with increasing silica fume content (no FA). /8//9/

Creep was measured as a part of an on-going Ph.D-project /11//12/, showing increasing creep with FA-content, see next chapter.

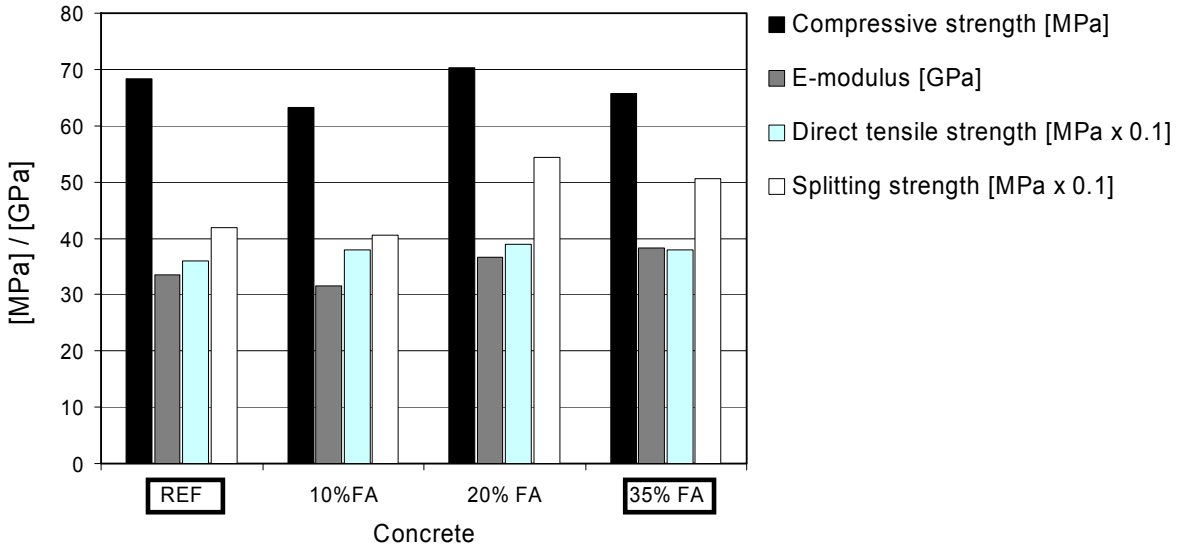

Figure 6: 28-days mechanical test results after curing at semi-adiabatic temperatures for the REF concrete and the FA concrete (35% FA) as well as two concretes with 10% and 20% FA, respectively /7/.

5. MATERIALS MODELLING

Concrete maturity t_{eq} (equivalent time) is calculated according to Equation (4), whereas the formula in Equation (5) was used to express the mechanical properties development. The formula (modified Model code equation) contains an X_{28}-parameter which is the 28-days compressive strength (f_{c28}), E-modulus (E_{28}) or tensile strength (f_{t28}). A basic idea behind this formula /8//9/ is that the curvature parameters s_c and the starting point parameter t_0 are set to be the same for all the properties and, thus, can be identified from simple compressive strength tests. The curvature parameter n is set to be 1.0 for the compressive strength, while n-parameters for the E-modulus (n_E) and tensile strength (n_t) were not determined during the present test program (only 28-days testing) as the identification of n requires testing over time. Default n-parameters have however been identified from a number of previous tests /8//9/ and used here. Hence, when the curvature parameter s_c is determined for compressive strength our impression is that the default parameters n_E and n_t give sufficient accuracy. The time parameter t_0 is the starting (maturity) time for the property development (when stresses

are starting to develop in the TSTM-test), whereas t_{eq} is the concrete maturity. The compressive strength model parameters were determined by fitting the formula to the experimental tests by least square sum iteration. This holds also for heat development, which is expressed by Equation (6). The formula was originally proposed by Freiesleben-Hansen /10/. The tables 3 and 4 gives complete materials data for the concretes giving, together with the autogenous deformation developments in Figure 5, the necessary input for 2D and 3D temperature- and stress calculations of any given structure. Such calculations are not performed here (only 1D calculations, see next chapter), but such calculations would be a natural next step in the evaluation of the performance of the concretes.

$$t_{eq} = \sum_{t} \exp(E_r(\frac{1}{293} - \frac{1}{273 + T_i})) \times \Delta t_i \tag{4}$$

Where E_r [K] (the activation energy divided by the gas constant R=8.314 J/(mole K)) is the temperature sensitivity parameter. $E_r = A$ for T>20 °C and $E_r = A+B$ for T<20 °C, see Table 2.

$$X(t_e) = X_{28} \cdot \left\{ \exp\left[s_c \cdot \left(1 - \sqrt{\frac{28}{t_{eq} - t_0}} \right) \right] \right\}^n \tag{5}$$

$$Q(t_{eq}) = Q_\infty \cdot \exp\left(-\frac{\tau}{t_{eq}} \right)^\alpha \tag{6}$$

where Q_∞, τ and α are model parameters and t_{eq} is the maturity.

Table 3: Model parameters for activation energy and mechanical properties

	Activation energy		Mechanical properties						
Concrete	***A*** [K]	***B*** [-]	t_0 [h]	f_{c28} [MPa]	***s*** [-]	f_{t28} [MPa]	n_t *) [-]	E_{28} [MPa]	n_E *) [-]
REF-concrete	3400	150	13	64	0.176	3.6	0.59	34500	0.37
FA-concrete	4300	0	15	66	0.310	3.7	0.59	35300	0.37

*) Default parameters /9/

Table 4: Parameters for heat development and thermal dilation

	Heat development					Thermal dilation
Concrete	Q_∞ [kJ/kg *b*]	τ [h]	α [-]	c_p [kJ/(kg *b* x °C]	ρ [kg/m^3]	*CTE* [10^{-6}/°C]
REF-concrete	313	17.40	1.73	1.03	2450	8.4
FA-concrete	250	21.19	1.37	1.03	2420	8.4

6. 1D STRESS CALCULATIONS

6.1 Calculation principle

The stress calculations are based on linear visco-elasticity for aging materials. The calculations were performed incrementally in an Excel spreadsheet. For a general stress history in the TSTM, the strains are in principle determined as:

$$\varepsilon_{TSTM}(t) \;=\; \int_0^t J(t_e^{'},t,t') \cdot d\sigma(t') \;+\; \varepsilon_{Tot}(t) \qquad (7)$$

ε_{Tot} is the total free strain (thermal dilation + autogenous deformation) measured during the Dilation Rig test and ε_{TSTM} is the strain measured in the parallel TSTM-test. ε_{TSTM}=0 during full restraint and $\varepsilon_{TSTM} \neq 0$ during partial restraint. The compliance function *J(t,t')* and the creep ratio $\varphi(t,t')$ is defined as:

$$J(t,t') = \frac{1}{E(t_e^{'})}(1+\varphi(t,t')) \quad \text{and} \quad \varphi(t,t^{'}) = \varphi_o t_e^{'^{-d}} \cdot (t-t')^p \qquad (8)$$

In these equations t is the actual time (concrete age in days), t' the time when a stress increment ($d\sigma$) is applied, and t_e' is the maturity at t'.

The creep measurements are presently being analyzed in an on-going Ph.D-study /11/12/, and preliminary model parameters for the FA-concrete are identified to be φ_o=1.80, d=0.26 and p=0.20. In earlier creep tests /13/ on concretes with m = 0.40 and no FA (quite similar to the REF concrete) the creep parameters φ_o=0.75, d=0.20 and p=0.21 were identified; these values are used here for the REF concrete. A high φ_o-parameter for the FA concrete indicates high creep.

6.2 1D Calculation results

For the REF- and FA concrete the measurements of restraint stress over time from the TSTM-test are shown in Figure 7 together with the calculation results as well as the direct tensile strength development. It is notable that the measured stresses "bends off" after around 4 days (96 h) because of a sudden and deliberate decrease in the degree of restraint in the TSTM-test from that time. The restraint is 100% up till 4 days. The restraint reduction after 4 days was done in order to avoid early tensile failure of the specimen and, thus, to provide stress results throughout the whole testing period and thereby "calibration curves" for stress calculations. The calculating procedure was as follows:

Calculation (1): The strains occurring in the TSTM after 4 days are included in the calculation in addition to those from the parallel Dilatometer test - this calculation (denoted "calculated stress" in the figure) represents the test situation and calculated stresses over time should therefore be quite similar to the one from the TSTM. It can be seen that the match between measured and calculated stresses are rather good.

Calculation (2): The strains from the TSTM after 4 days are not included in the calculation. This calculation then represents the stress development in the TSTM if it had been run with 100% restraint the whole test (denoted "calculated stress 100% restraint" in the figure). Stresses above tensile strength are of course fictitious, but still meaningful for comparison reasons. This calculation shows for the REF concrete that the final stress is 50% higher than the tensile strength and for the FA concrete 13% higher, hence the final crack index (concrete stress divided by the strength) is 1.5 and 1.13 for the two concretes, respectively, which

means a 25% lower crack index for the FA-concrete compared to REF at the end of the cooling phase after around 2 weeks. The crack index over time for each concrete is plotted in Figure 8. The results then also indicate that in order to keep the crack index below 1.0 (indicates no cracking in theory) the restraint can maximum be (1/1.5=) 66% for the REF concrete and (1/1.13=) 88% for the FA concrete. Figure 8 is based on the direct tensile strength data, as already stated, but if the splitting strength data were used instead the FA concrete would come out even more favourable than REF: the final crack index for the FA concrete would then be 29% lower for REF.

The stresses are expected to fall after 2 weeks (336 h) for the given cases due to relaxation dominance since the cooling (thermal contraction) of the concretes is completed.

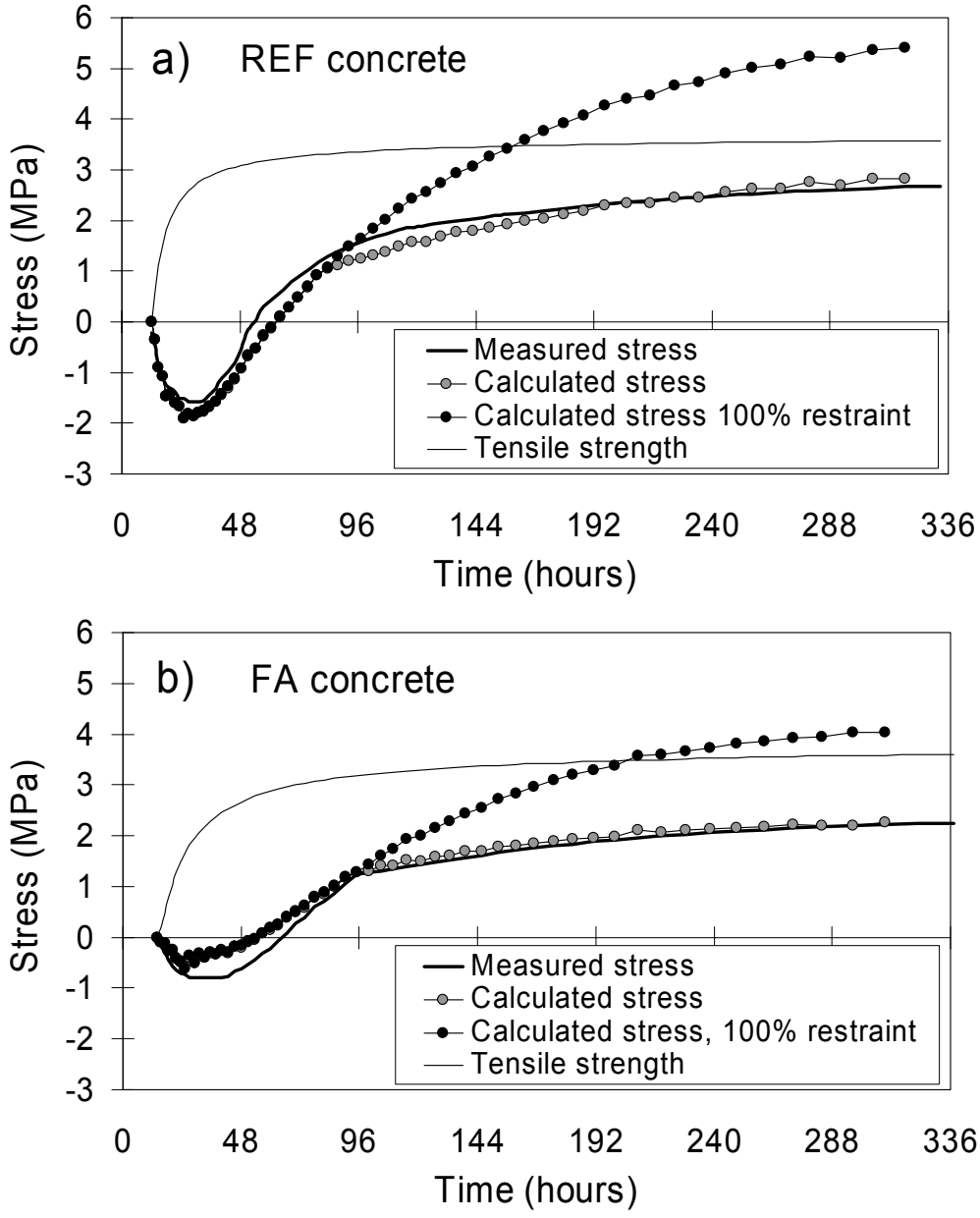

Figure 7: Measured stress in the TSTM (partial restraint) during semi-adiabatic temperature, direct tensile strength and 1D stress calculations. REF- (a) and FA-concrete (b)

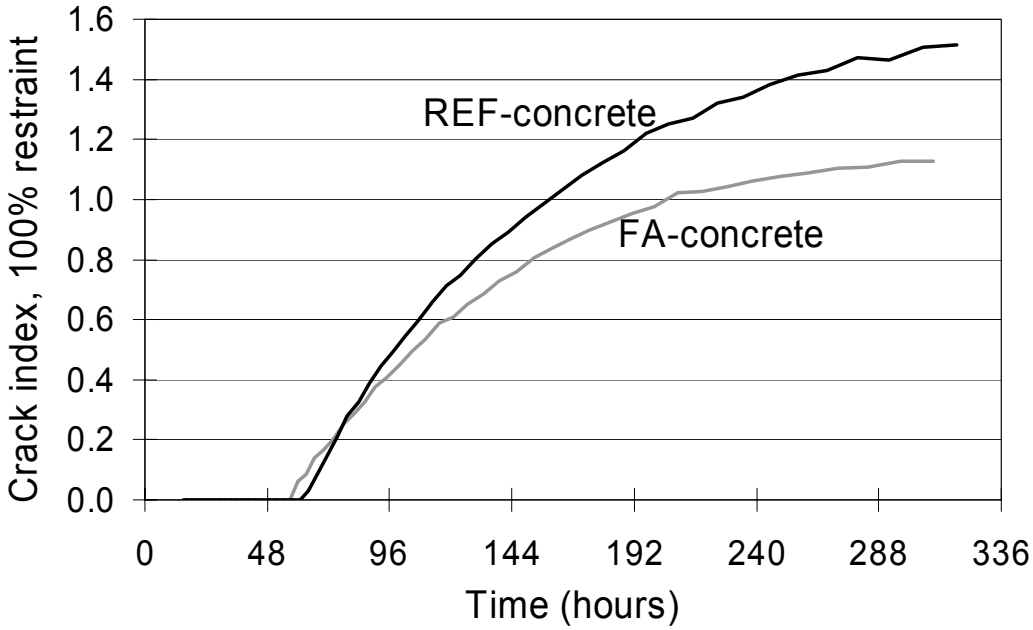

Figure 8: Crack index, i.e. ratio (calculated) concrete stress at 100% restraint - tensile strength over time

7. CONCLUSIONS

The reported parameter study on the effect of fly-ash (FA) was conducted with a constant water-to-binder (w/b) ratio of 0.40, and, hence, with an efficiency factor for FA of 1.0. All involved properties relevant for early age stress development were measured and the tendency of through-cracking during the hardening phase due to external restraint evaluated. The results show that the FA concrete (35% FA of binder weight in combination with ordinary Portland cement (OPC)) has 25% lower cracking tendency than the reference concrete made only with OPC. The test conditions and evaluation of cracking risk are directly relevant for a 1 m thick concrete structure subjected to external restraint.

Any practically relevant mix-design with FA added directly during the mixing process should therefore be done with the use of an efficiency factor of 0.4 according to the European Standard “EN 206-1”. This will require a w/b=0.34 for a concrete with the given FA-content to be within the same durability class as the reference concrete, which most likely leads both to a higher binder content (i.e. more hydration heat) and more autogenous shrinkage than what was measured for the tested FA (having w/b=0.40). The consequence in terms of early age cracking tendency is not clear, but a w/b=0.34 is likely to be far less favourable than w/b=0.40. This should be explored in the future. In principle, the same is valid also when using blast furnace slag (BFS), but here the efficiency factor is 0.6.

Since hydration heat and autogenous shrinkage, as well as all the other involved concrete properties, are altered when changing concrete proportions it is very difficult, if possible at all, to extrapolate results to other concrete compositions. Hence, any parameter study on FA (or BFS) relevant for practical concreting should be made in accordance with the requirements from the standard. In this regard it is notable that the efficiency factors are 1.0 for FA and BFS if the materials are a part of a certified cement (cement type II and III). For cracking tendency it appears then more favourable to use CEM II and III cements than using the same amount of FA or BFS added separately during mixing in combination with, for instance, OPC.

ACKNOWLEDGEMENTS

The financial contribution of the Norwegian Research Council is gratefully acknowledged. So are the contributions from the partners in the Norwegian NOR-CRACK project. The partners are: Skanska Norge ASA, Elkem ASA Materials, Norcem AS, Fesil ASA and The Norwegian Public Roads Directorate. The Norwegian University of Science and Technology was project leader.

NOTATIONS

w = free water
c = cement
b = binder
s = silica fume
FA = fly-ash
BFS = blast furnace slag
m = effective w/b-ratio
k_s = efficiency factor for silica fume
k_{FA} = efficiency factor for fly-ash
k_{BFS} = efficiency factor for blast furnace slag
CTE = Coefficient of Thermal Expansion
TSTM = Temperature-Stress testing machine
f_c = compressive strength
f_t = direct tensile strength
f_{ts} = splitting strength
E = E-modulus

REFERENCES

/1/ See: http://www.vegvesen.no/region_ost/prosjekter/bjorvika/index.stm

/2/ Bjøntegaard Ø. and Kjellsen K.O (2006) Experimental tests and 1D stress calculations on young HPC with w/b=0.40: Effect of cement type and fly-ash. NOR-CRACK report 3.2, to be published in 2006

/3/ Research programmes undertaken by the Norwegian Public Roads Administration in connection with the "Bjørvika Immersed Tunnel" project.

/4/ Tests performed by K.O.Kjellsen at Norcem AS, Brevik, Norway and submitted for use in reference /2/

/5/ Danish Technological Institute: http://www.danishtechnology.dk/building/13585

/6/ Sellevold E.J. and Bjøntegaard Ø. (2006) Driving forces to cracking in hardening concrete: Thermal and autogenous deformations. Proc. of the second int. symp.: Advances in Concrete through Science and Engineering, Sept. 11-13, Quebec City, Canada.

/7/ Bjøntegaard Ø. and Sellevold E.J. (2003) Bjørvika submerged tunnel - Determination of concrete properties relevant for evaluation of cracking tendency in the hardening phase (in Norwegian). NTNU-report R-9-03, Department of Structural Engineering, June 2003, 37 pages

/8/ Kanstad T., Hammer T.A., Bjøntegaard Ø. and Sellevold E.J. (2003) Mechanical Properties of Young Concrete: Part I - Experimental Results related to Test Methods and Temperature Effects, Materials and Structures, Vol. 36, May 2003, pp 218-225

/9/ Kanstad T., Hammer T.A., Bjøntegaard Ø. and Sellevold E.J. (2003) Mechanical Properties of Young Concrete: Part II - Determination of Model Parameters and Test Programme Proposals, Materials and Structures, Vol. 36, May 2003, pp 226-230

/10/ Freisleben Hansen, P., "Hærdeteknologi-2, Dekrementmetoden", BKF-centralen 1978 (in Danish)

/11/ Ji G. (2006) Self-induced stresses in hardening concrete: Experimental tests, materials modelling and 3D stress calculations of structures (working title). Doctoral thesis, NTNU, Dept. of Structural Eng., to be completed in 2006

/12/ Ji G., Bjøntegaard Ø. Atrushi D., Sellevold E.J. and Kanstad T. (2005) Compressive and tensile creep of early age concrete with mineral additives. Concreep7: Int. conf. on creep, shrinkage and durability of concrete and concrete structures, Nantes, France, pp. 369-374

/13/ Atrushi D. (2003) Tensile and Compressive Creep of Early Age Concrete: Testing and Modelling. Doctoral thesis, NTNU, Dept. of Structural Eng., March 2003, ISBN 82-471-5565-6.

Statens vegvesen

Norwegian Public Roads Administration

Norwegian Public Roads Administration
Directorate of Public Roads
P.O.Box 8142 Dep
N-0033 Oslo
Telephone +47 915 02030
E-mail: publvd@vegvesen.no

ISSN 1504-5005